1996

# A diagnostic study of stratospheric/tropospheric mass exchange

Timothy Allen Haddix
*San Jose State University*

# INFORMATION TO USERS

This manuscript has been reproduced from the microfilm master. UMI films the text directly from the original or copy submitted. Thus, some thesis and dissertation copies are in typewriter face, while others may be from any type of computer printer.

**The quality of this reproduction is dependent upon the quality of the copy submitted.** Broken or indistinct print, colored or poor quality illustrations and photographs, print bleedthrough, substandard margins, and improper alignment can adversely affect reproduction.

In the unlikely event that the author did not send UMI a complete manuscript and there are missing pages, these will be noted. Also, if unauthorized copyright material had to be removed, a note will indicate the deletion.

Oversize materials (e.g., maps, drawings, charts) are reproduced by sectioning the original, beginning at the upper left-hand corner and continuing from left to right in equal sections with small overlaps. Each original is also photographed in one exposure and is included in reduced form at the back of the book.

Photographs included in the original manuscript have been reproduced xerographically in this copy. Higher quality 6" x 9" black and white photographic prints are available for any photographs or illustrations appearing in this copy for an additional charge. Contact UMI directly to order.

**UMI**

A Bell & Howell Information Company
300 North Zeeb Road, Ann Arbor MI 48106-1346 USA
313/761-4700 800/521-0600

# A DIAGNOSTIC STUDY OF

# STRATOSPHERIC/TROPOSPHERIC MASS EXCHANGE

A Thesis

Presented to

The Faculty of the Department of Meteorology

San Jose State University

In Partial Fulfillment

of the Requirements for the Degree

Master of Science

by

Timothy Allen Haddix

August, 1996

APPROVED FOR THE DEPARTMENT OF METEOROLOGY

Dr. Douglas L. Westphal, Naval Research Laboratory, Monterey, CA

Dr. Douglas M. Sinton

Dr. Alison F. C. Bridger

APPROVED FOR THE UNIVERSITY

## ABSTRACT

## A DIAGNOSTIC STUDY OF STRATOSPHERIC/TROPOSPHERIC MASS EXCHANGE

by Timothy Allen Haddix

Stratosphere-to-troposphere mass exchange is estimated for a weak tropopause fold event near Coffeyville, KS during early December, 1991. A thermal tropopause boundary (8 K $km^{-1}$) is used to derive the instantaneous mass flux from MM4 model data initialized with MAPS data. Mass exchange is 1.13 X $10^{14}$ kg over a 12-hour period. This mass exchange is multiplied by an estimated 1500 - 2500 weak tropopause fold events per year over the Northern Hemisphere yielding a range of annual mass exchange of 1.7 - 2.8 X $10^{17}$ kg. These values are within the range of other recent studies (1.0 - 4.0 X $10^{17}$ kg). Dynamics of the case study are investigated through a diagnostic inspection of potential vorticity, vertical velocity, jet streaks, and the divergence of geostrophic **Q**-vector. Mass exchange occurs upstream of the actual fold, and then over time downward vertical motions extrude the stratospheric air further into the troposphere.

## ACKNOWLEDGMENTS

As I reflect on the past six years it's hard to realize just how much effort has gone into this thesis. As my mentor so eloquently put it, "This is your independent study for your master's degree." Had I known in the beginning, how much work was involved I probably would have been more apprehensive about meeting the challenge. As I have found during my 34 years, most things in life that really count do not come easily. I look at this project as one of those. Doug, as I have already said to you in person, your guidance and meteorological expertise have been crucial to my completion of this thesis. "Thanks," seems just too little to say, but I am not a millionaire. Although this thesis has been the result of many grueling hours in front of the PC, on my part, there are several other people that commend my thanks. I have had the pleasure of getting to know Bill Mckie, a system's programmer at NASA. He is the man responsible for writing the graphics software which enabled me to produce the many figures seen in this thesis. Bill is not only a great programmer but a very genuinely nice guy. Thanks Bill!

I remember when I started at SJSU some 4 years ago not knowing what lay ahead for me. Each of the professors I had for my coursework provided me with a piece of the puzzle that I needed to produce this finished product. All I had to do was put them together. I will remember Dr. Goodman for two very different reasons. First, she was the person who got me my first graduate assistantship at NASA. Second, I can remember many times when she would turn around from the board and say, "Come on guys, this is easy."

For any of you who ever have taken a physical meteorology class you would know that this is a dream. I know this was her way of saying, "With some hard work, you guys can figure this out." Thanks, Dr. Goodman. I will remember Dr. Bridger, my dynamics professor, for her attention to detail. Dynamics is pure mathematics and requires a step-by-step process to really understand what you are doing. She was the best lecturer I ever had during all of my education. She also performed the official "hooding" for my graduation and was a reviewer of this thesis. Thanks Dr. Bridger. I cannot forget my synoptics professor, Dr. Sinton. To his credit, he never really seemed like a professor to me. His method of teaching combined both testing and practical application of meteorology. Thanks for your unique style and for being a reviewer of this thesis, Dr. Sinton. I, too, think that college should be more about learning and less about testing.

There are many ingredients that go into making a master's degree. Some of those that have been especially important to me consist of my family and friends. To my parents, I thank them for their endless love and support through this effort. They will never know just how much this has meant to me. I have been blessed with many friends, both prior and during this endeavor. There are five people that I owe special thanks to. Smitty was the first person who told me that I should go for my dreams. Although Smitty is a very bright, accomplished businessman, he has a problem with numbers. Sorry Smitty, you would not make a good meteorologist. That aside, he is the epitome of a friend for life. Thanks Smitty! To my roommate, Seanly, I only ask that I can continue to pay cheap rent

until I find a good paying job. Although, I have two brothers, I look at Seanly as my adopted brother and very good friend. Janie was first my boss and subsequently a very good friend. Although Janie has a propensity for asking for free meals, she has done without for a long time during my journey. Janie thanks for your support over the years. We can now resume eating. Friends number four and five are Ali and Jorge. I have gotten to know many people during my life but these two Physics buddies of mine are special in that they offer a different perspective on life. Ali is from Iran and Jorge is from Nicaragua. The stories of their journeys to this country gave me a larger perspective of the world and have made me realize that as time consuming and difficult this thesis has been for me, it really is insignificant when compared to other things. I could never have made it through the pre-requisite Physics classes if it were not for the two of you. Thanks Ali and Jorge.

# CONTENTS

# List of Tables

# List of Figures

# Chapter 1

# Introduction

## 1.1 Case Study Description

Sassen *et al.* (1995) claim that several tropopause fold events occurred during 5 - 6 December 1991 over the Coffeyville, KS (COF) area. Their case study hypothesized that these fold events introduced stratospheric aerosols from the 1991 Mt. Pinatubo eruption into the troposphere, and that these aerosols subsequently influenced the formation and enhancement of cirrus clouds. They cite anecdotal evidence which supports their theory of tropopause folds, including: the high radioactivity in the fold area, the high concentration of ozone in the fold area, and the signature of high potential vorticity extrusions into the troposphere. These are consistent with the concept of a tropopause fold presented by Danielsen (1964).

The specific goals of this research are to: more carefully document the existence and origin of a tropopause fold event over the COF area; diagnose the dynamics associated with the tropopause fold event; and make a quantitative estimate of the stratosphere-to-troposphere (ST) mass exchange during the tropopause fold event. The data used in support of this thesis was collected during Project FIRE [First ISCCP (International Satellite Cloud Climatology Project) Regional Experiment] with COF being the primary data collection site.

## 1.2 Case Study Synoptics

The synoptic case study to be investigated with this research can be summarized as follows. The upper-tropospheric flow pattern over North America at 0000 UTC on 3 December 1991 was dominated by a single high-amplitude trough-ridge system, as shown in the National Meteorological Center (NMC) 250-mb analysis (Fig. 1a). Hereafter in the text, time and date are denoted by hh/dd, e.g., 00/03 represents 0000 UTC on 3 December 1991. The polar jet stream had a NW-SE tilt extending from western Canada through the Rocky Mountains and down to Arizona. The sub-tropical jet stream was situated from Baja California northeastward towards the New England states. At 00/04 the trough-ridge system had moved eastward while leaving a zonal flow pattern over the west coast of North America, as shown in Fig. 1b. By 00/05 an upper-level closed low-pressure system had developed west of Baja California as exhibited in Fig. 1c. This low pressure

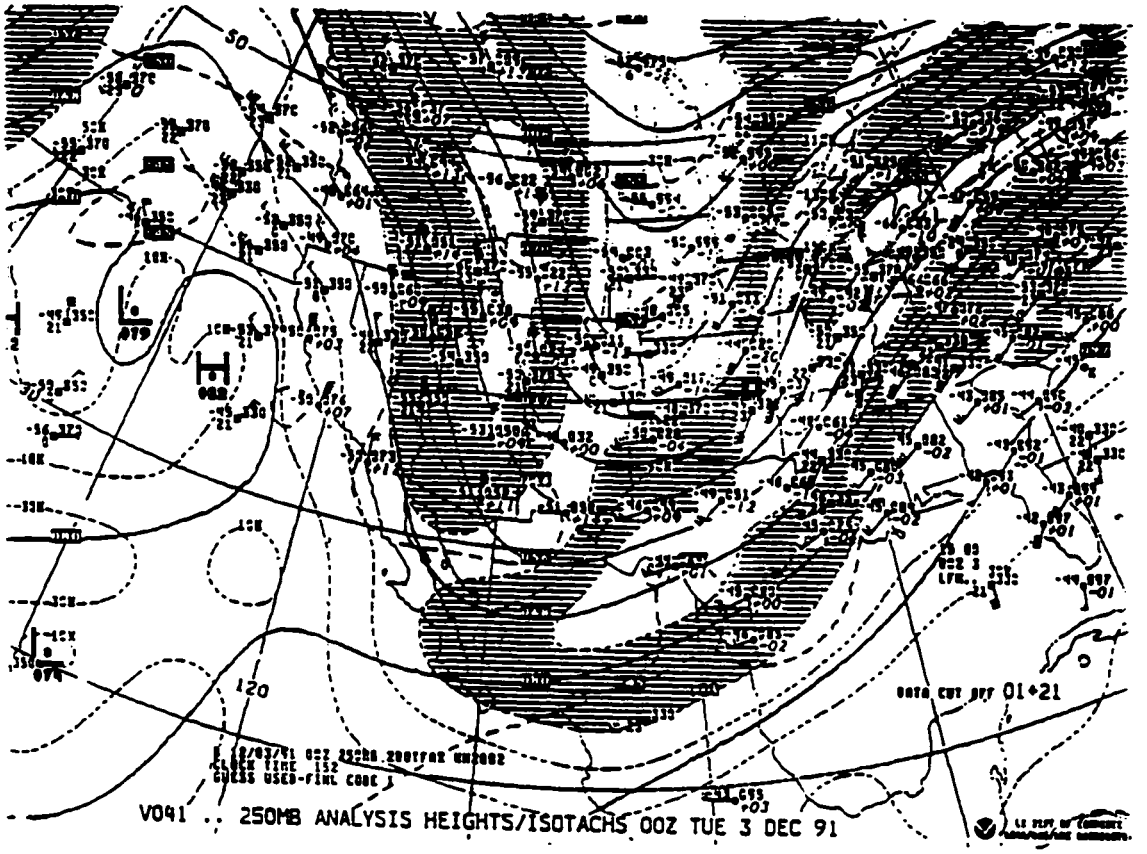


**Fig. 1a:** NMC analysis of 250-mb geopotential heights (dam; solid lines), temperatures (°C; thick dashed lines), and horizontal winds for 00/03. Isotachs (thin dashed lines) are at 20-kt intervals, beginning with 10 kts. Winds representing 70 - 110 kts (36.0 - 56.6 m $s^{-1}$) are shaded. COF is denoted by a white box with a thick black border.

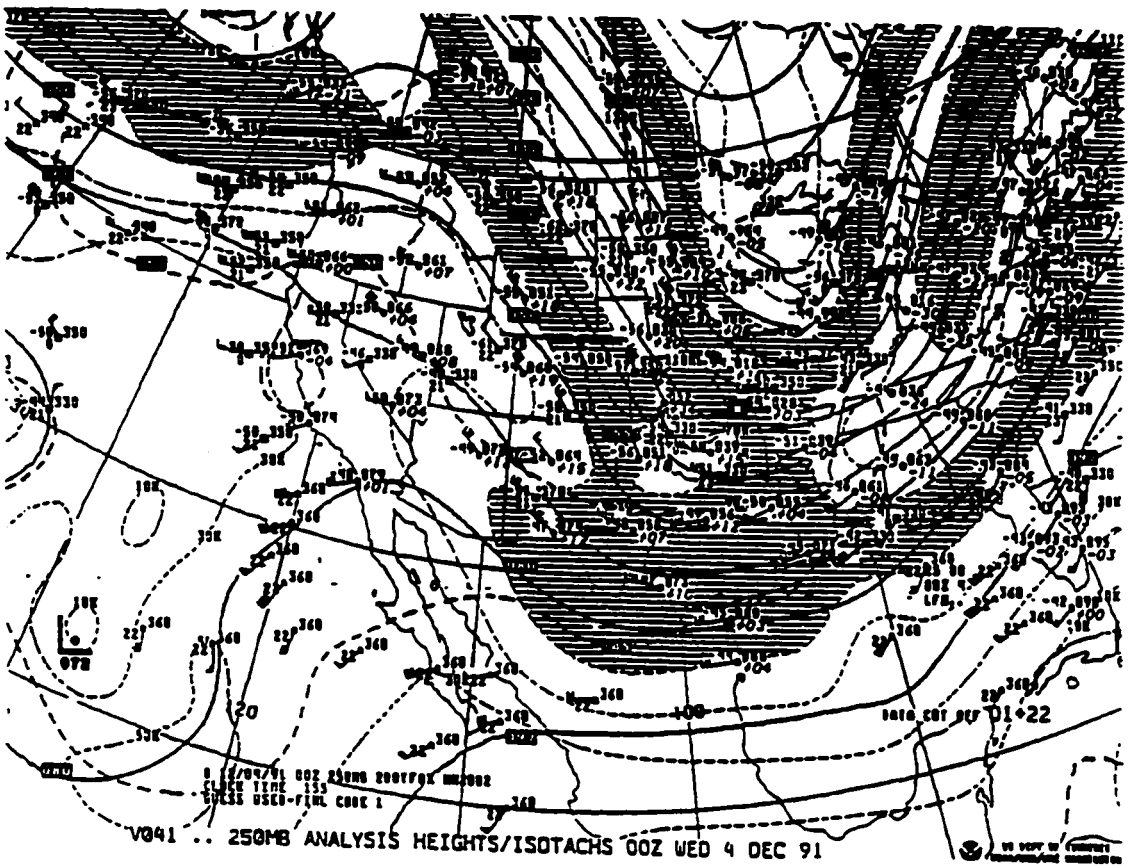


**Fig. 1 (cont.) b:** Same as in Fig. 1a except for 00/04.

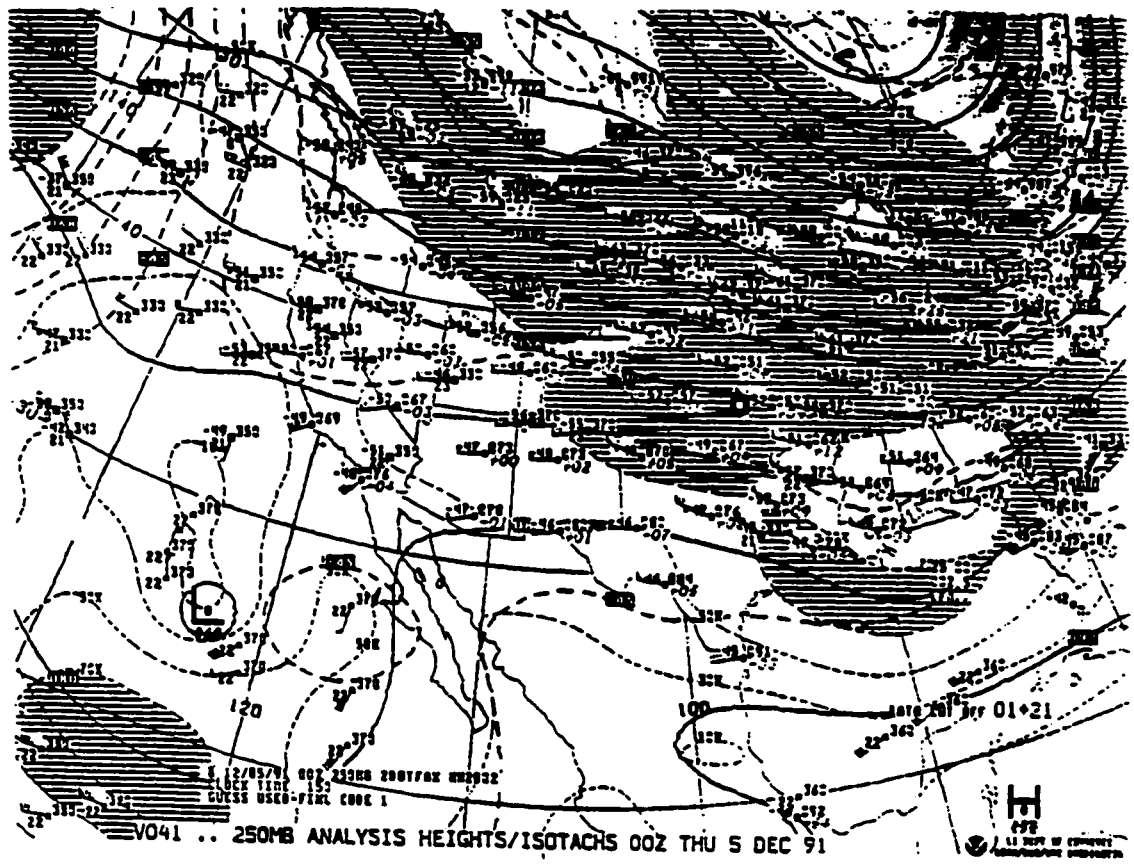


**Fig. 1 (cont.) c:** Same as in Fig. 1a except for 00/05.

system intensified and moved eastward during 5 - 6 December 1991 to Baja California, as shown in Fig. 1d. According to Sassen *et al.* (1995), this low pressure system played a significant role in providing the upper-level moisture needed to produce high-level cirrus on 5 December 1991 (Figs. 2a, 2b, and 2c) over the southern Great Plains area and more specifically, over COF (37.1° N, 95.6° W).

## 1.3 Preliminary Analysis

The zonal flow pattern shown in Fig. 1c is unlike the more classical tropopause fold case with a large trough-ridge system and an intense jet associated with the folding process, such as at 00/03 (Fig. 1a). Preliminary analysis by Sassen *et al.* (1995) does however suggest that several weak tropopause fold events occurred near the COF area during 5 - 6 December 1991. The Wind Profiler Network (WPN) data from Neodesha, KS (NDS), located a few miles northeast of COF, shows the passage of two weak jet streaks of 50 - 60 m $s^{-1}$ between 200 and 350 mb around 05/05 and 21/05 (Fig. 3). Figure 4 shows the proximity between NDS and COF. Sassen *et al.* (1995) also reported that high concentrations of ozone, indicative of stratospheric air, were found deep in the troposphere during this case study period. Their results show two peaks of ozone concentration near 250 and 400 mb around the time of the first jet streak passage over NDS at 03/05 in between a ozone deplete layer at 300 mb, as shown in Fig. 5. These

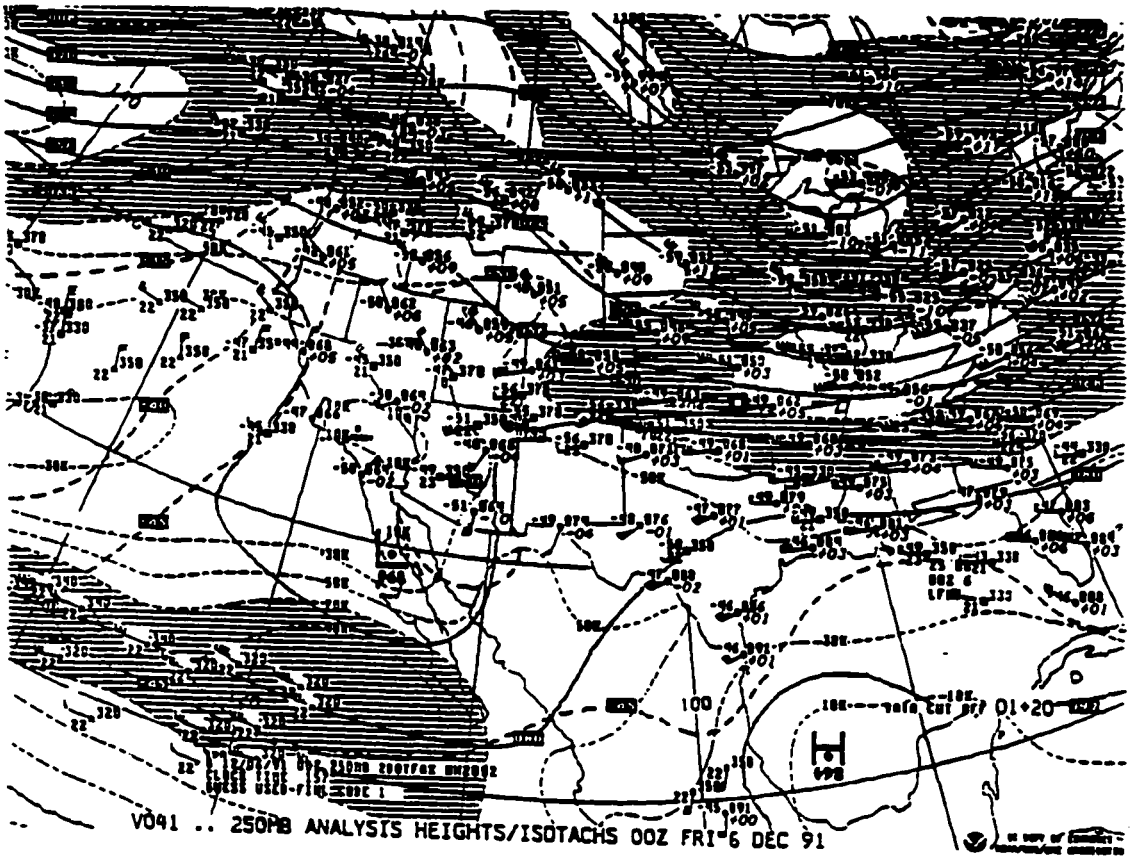


**Fig. 1 (cont.) d:** Same as in Fig. 1a except for 00/06.

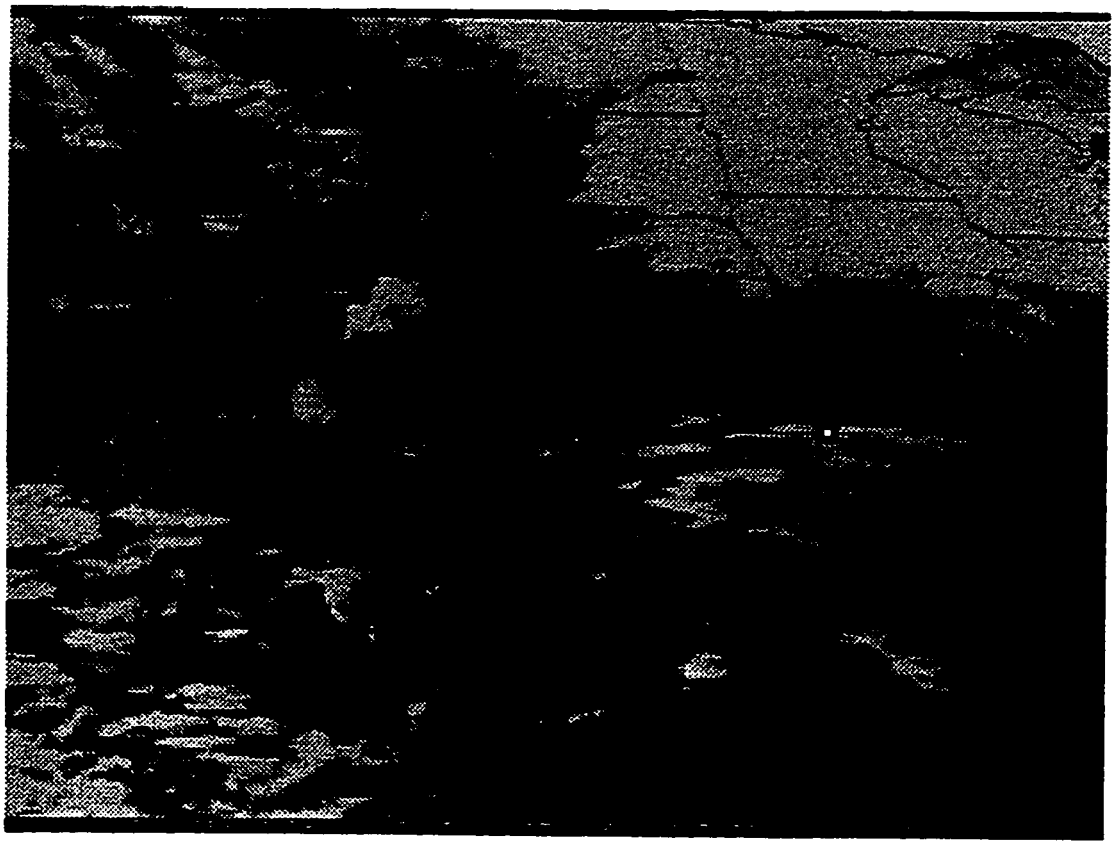

**Fig. 2a:** GOES (Geostationary Operational Environmental Satellite) infrared imagery for 06/05.

**Fig. 2 (cont.) b:** Same as in Fig. 2a except for 17/05.

**Fig. 2 (cont.) c:** Same as in Fig. 2a except for 21/05.

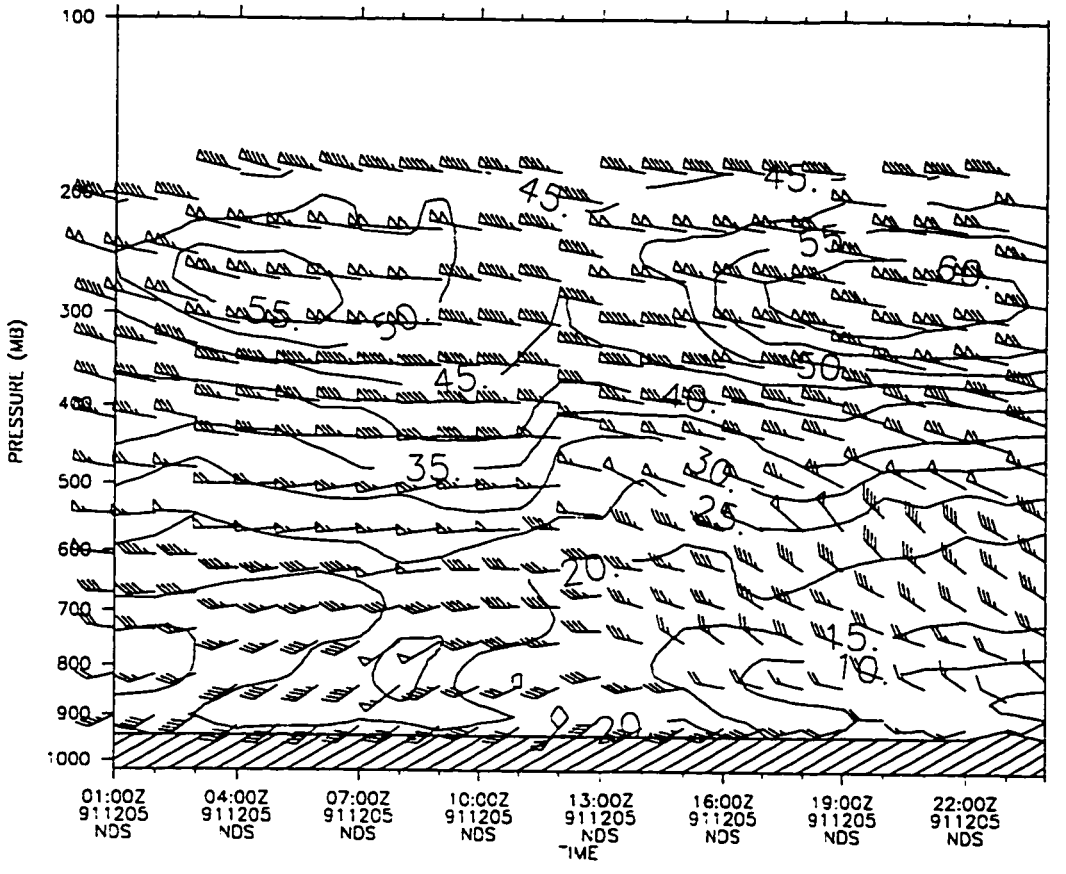


**Fig. 3:** WPN time-height series of horizontal winds (m $s^{-1}$; solid lines, kts; wind barbs) for NDS between 01/05 - 00/06.

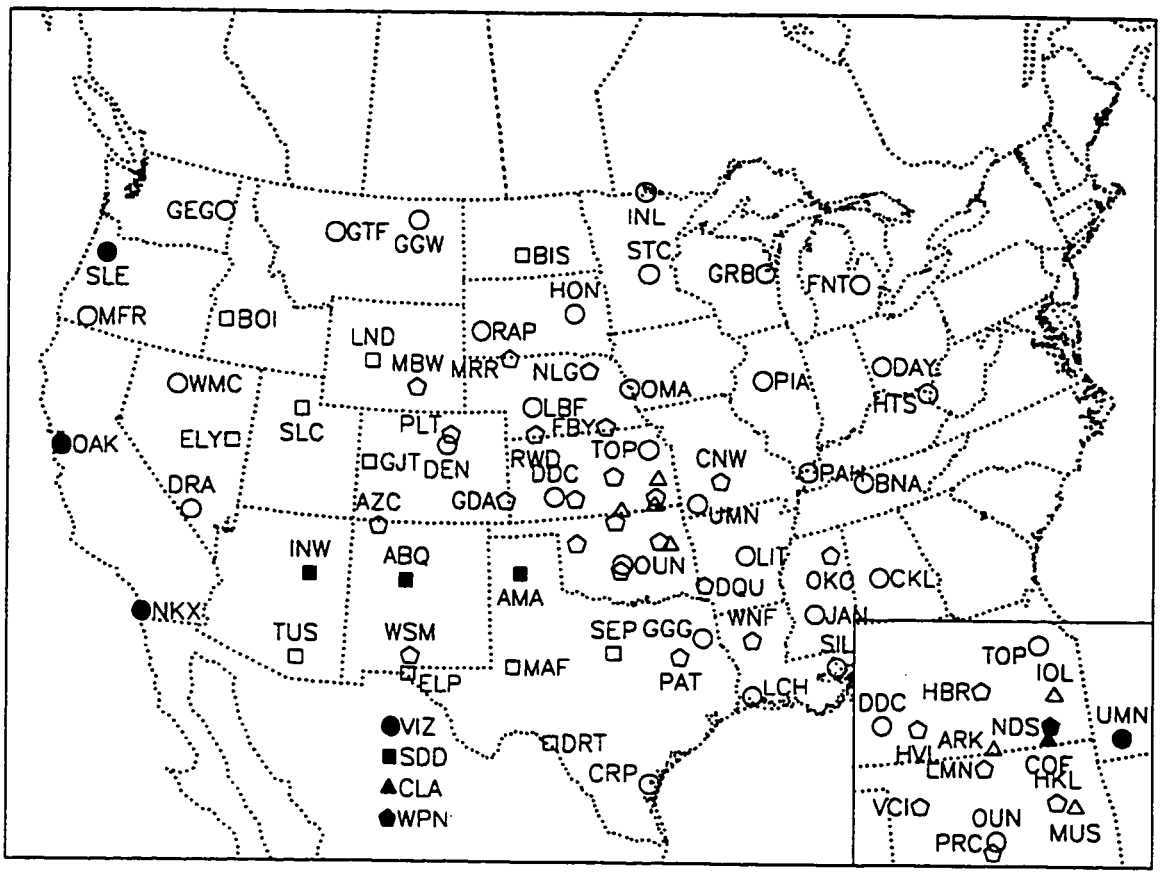


**Fig. 4:** Data observation sites used in this paper (dark center symbols) and used during Project FIRE (dark and clear center symbols). Observation sites referenced in the text are labeled with their 3-letter identifier. The lower right-hand corner of the map is an enlargement of the Kansas/Oklahoma area around COF. The legend in the lower left area of the map indicates the instrument type used at the observation site, i.e. VIZ (radiosonde manufactured by VIZ Manufacturing Company), SDD (Space Data Division) radiosonde, CLA (CLASS [Cross-chain Loran Atmospheric Sounding System] radiosonde), and WPN.

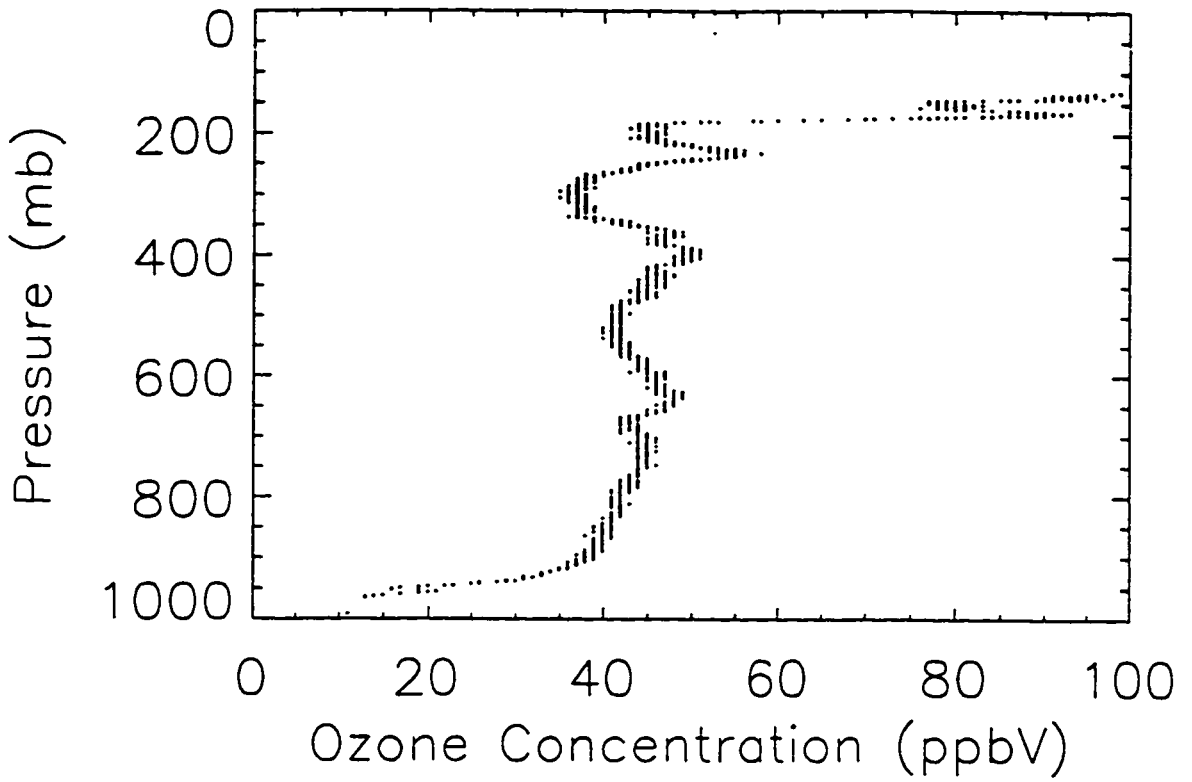


**Fig. 5:** Ozonesonde-derived vertical ozone profile (ppbv [parts per billion by volume]) at COF for 03/05.

results suggest that ozone rich stratospheric air was extruded down to 400 mb, while ozone deplete tropospheric air bounded it above and below this level.

The standard approach to ST studies involves performing a cross sectional analysis of potential vorticity. Sassen *et al.* (1995) were unable to do this with conventional radar observations and profiler data. Access to gridded analyses and model simulations allows us to analyze this particular fold event with greater accuracy. For example, just after the passage of the second jet streak, data from the Mesoscale Analysis Prediction System (MAPS) shows a weak signature of a fold event with an extrusion of high potential vorticity around a 60 m $s^{-1}$ jet streak extending down into the troposphere between 200 and 400 mb along a weak upper-tropospheric front diagnosed between the 324 and 328 K isentropic surfaces (Fig. 6). This tongue-like feature of potential vorticity is the primary signature of a tropopause fold according to Danielsen (1964). In combination, these preliminary diagnostics of ozone rich areas at levels down to 400 mb, high potential vorticity and concentrated potential temperature gradients, indicate that tropospheric folds took place over COF in association with the weak jet streaks during the case study period.

## 1.4 Justification

Although Sassen *et al.* (1995) claimed that stratospheric aerosols combined with the effects of tropopause fold events led to the unusual cirrus cloud formations over the COF

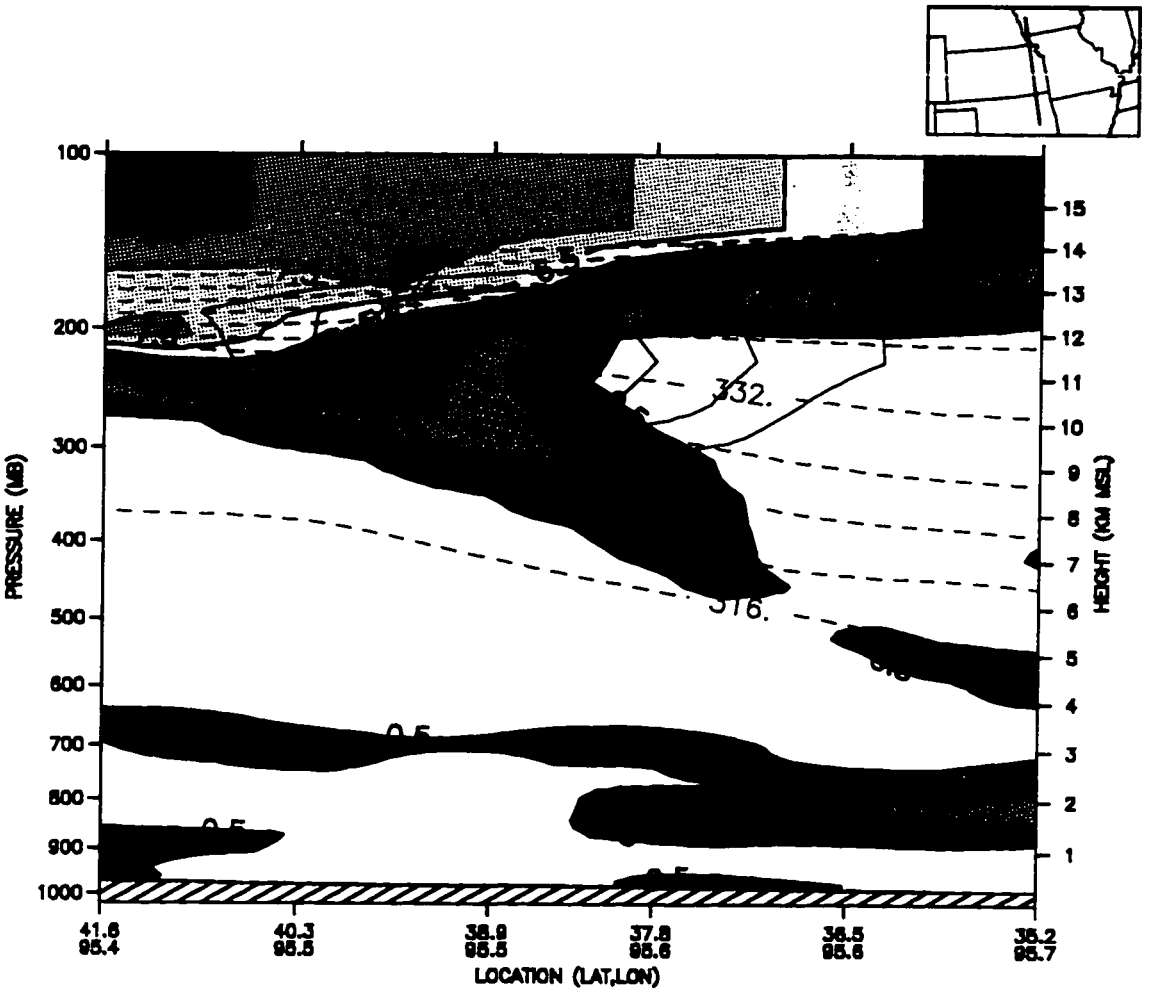


**Fig. 6:** N-S cross section of MAPS potential vorticity ($m^2$ K $s^{-1}$ $kg^{-1}$; solid black lines separated by shaded areas), potential temperature (K; dashed red lines), and horizontal winds (m $s^{-1}$; solid red lines) at 00/06 along the line depicted in the upper right-hand map.

area, their research did not address the specific evolution, dynamics, and magnitude of these tropopause fold events. The strongest of the several tropopause fold events identified by Sassen *et al.* (1995) during the case study period occurred around 21/05. This particular tropopause fold is the primary focus of this research. In particular, the following questions need to be answered: Where did the fold originate? What was the dynamical forcing that led to the fold? What was the magnitude of the fold? Sassen *et al. 's* (1995) microphysical study of the cirrus cloud properties leaves little doubt that a tropopause fold occurred near the COF area around 21/05. Determining the origin, forcing, and extent of the tropopause fold event over the COF area will further our understanding of the dynamics associated with weak tropopause folds, enable us to quantify the amount of ST mass exchange during a weak tropopause fold event, and provide the background for validating the initial conditions for, and simulations from, future numerical modeling research in the area of microphysical cloud processes. Expanding our knowledge of the dynamics behind weak tropopause fold events will facilitate improvements in numerical weather prediction and will ultimately lead to better meteorological forecasts.

Chapter 2 addresses the background theory for this research. Chapter 3 outlines the data available to diagnose the origin, dynamics, and mass exchange associated with this particular fold over the COF area in early December 1991. Chapter 4 addresses the results of this research and Chapter 5 addresses the conclusions.

# Chapter 2

# Background

## 2.1 Tropopause Folds

Tropopause fold events have been widely studied during the past several decades in the meteorological community (e.g., Reed 1955; Danielsen 1968; Danielsen and Hipskind 1980). Essentially, a tropopause fold can be described as a thin tongue-shaped extrusion of stratospheric air into the troposphere. The extent of the extrusion varies depending upon the amount of dynamic forcing. The extruded stratospheric air consists of laminae of high stability and/or strong gradients of potential temperature. This air typically lies above the jet stream; however, it can be redistributed via upper-level fronts (Keyser and Shapiro 1986). Tropopause folds have played an important part in our understanding of ST mass exchanges as they pertain to the continuity of mass within our atmosphere. It has been hypothesized that upper-level frontal systems have resulted from tropopause folding, in

which upper- and mid-tropospheric subsidence transports stratospheric air deep into the troposphere, occasionally reaching 700 to 800 mb in particularly intense cases (Reed and Danielsen 1959).

## 2.2 Diagnosis of Potential Vorticity

Diagnosed values of potential vorticity have been used in the past to determine regions of stratospheric air within the troposphere (Reed and Danielsen 1959; Barnes and Colman 1993). Potential vorticity is conserved following the movement of an air parcel in adiabatic flow, making it an excellent tracer under adiabatic conditions. Potential vorticity, $P_\theta$ ($m^2$ K $s^{-1}$ $kg^{-1}$), defined in isentropic coordinates, can be described as the product of two stabilities: inertial stability and static stability,

$$P_\theta = -(\zeta_\theta + f)(g\frac{\partial\theta}{\partial p}), \tag{2.1}$$

where relative vorticity, $\zeta_\theta$ ($s^{-1}$), is measured on isentropic surfaces, $f$ ($s^{-1}$) is the Coriolis parameter which is dependent on latitude, $g$ (m $s^{-2}$) is the gravitational constant, $\theta$ (K) is the potential temperature, and $p$ (Pa) is the pressure. The first term on the right hand side of Eq. (2.1) represents inertial stability and is often referred to as absolute vorticity. It is a measure of the resistance to horizontal displacements at constant potential temperature (Danielsen *et al.*, 1987). The second term represents static stability, and is a measure of

resistance to vertical displacements (Danielsen *et al.*, 1987). If both terms in Eq. (2.1) are positive, a vertically or horizontally displaced parcel is forced back to its equilibrium position; if either is negative, the displacement is amplified and mixing develops (Danielsen, 1964). Holton (1992) adds that potential vorticity is in some sense a measure of the ratio of absolute vorticity, $(\zeta_\theta + f)$, to the effective depth of the vortex. This depth is the distance between potential temperature surfaces measured in pressure units. In summary, potential vorticity describes a potential for creating vorticity by changing latitude, or by adiabatically changing the separation of isentropic layers (Hoskins *et al.*, 1985).

Large potential vorticity values, greater than 4 Potential Vorticity Units (1 PVU = $10^{-6}$ $m^2$ K $s^{-1}$ $kg^{-1}$), are generally assumed to indicate air of stratospheric origin (Hoskins *et al.*, 1985). Alternative definitions and units are sometimes used for measuring potential vorticity. Keyser and Shapiro (1986) used $10^{-7}$ K $mb^{-1}$ $s^{-1}$ for potential vorticity units. After proper unit conversions have been made, this selection differs by a factor of "$g$" and is thus 10 times larger than the aforementioned PVU. The PVU described above is used in this thesis. Potential vorticity values below 1.0 PVU and above 4.0 PVU indicate air of tropospheric/stratospheric origin, respectively. Additionally, an air mass with potential vorticity values between 1.0 and 4.0 PVU is considered to be in a transition mode. Recall, Fig. 6 shows potential vorticity values within this transition mode in the tropopause fold area.

## 2.3 Origin of Air Within Tropopause Folds

According to Danielsen (1964), the ageostrophic components of the wind field are frequently too small to be measured, but their integrated effects can be graphically determined through an isentropic trajectory analysis. He showed that trajectories computed on conventional constant pressure surfaces are subject to extremely large errors when vertical motions are large. Danielsen explains that vertical motions in the atmosphere correlate positively with temperature advection. Subsequently, temperature advection causes changes in wind and pressure gradients which lead parcel trajectories to turn more anticyclonically than trajectories on a purely isobaric surface. Ultimately, unless vertical motions are negligibly small, isobaric parcel trajectories do not remain in vertical alignment making it difficult to track air parcel origin. Assuming adiabatic conditions, this problem is corrected by using an isentropic trajectory analysis, thus making it easier to track air parcel origin.

A method similar to Danielsen's isentropic trajectory analysis is used in this thesis to determine the origin of the weak tropopause fold depicted in Fig. 6. By taking the horizontal and vertical components of the wind field and integrating back through time, air parcel origin is determined. This approach takes into account diabatic effects over time, unlike Danielsen's isentropic trajectory analysis. As will be discussed in Chapter 3, several

model simulations are analyzed to see if the mass and wind fields are well correlated with the observations near the COF area. From this, it is determined that the best method of showing the origin is to use back-trajectories from two consecutive simulations initialized at different times. The results of these two simulations are then meshed together giving a final back-trajectory.

## 2.4 Dynamics Contributing to Tropopause Folds

In order to facilitate the study of the dynamics associated with tropopause folds, this research uses two theoretical techniques. Holton's Q-vector theory (1992) is used to detect rising and sinking atmospheric motions, and Danielsen's theory (1968) is used to discern the actual structure of a tropopause fold.

In order to better explain each of these theories, it is necessary to understand atmospheric motions in and around the jet stream. The jet stream is the region in the troposphere, typically found between 200 and 300 mb, where winds are strongest and where baroclinic disturbances get their energy. Jet streaks are smaller regions of maximum wind speed within a jet stream, and are important because this is where tropopause folding is likely to occur (Mattocks and Bleck, 1986). The wind speed within a jet streak is generally faster than the speed of the jet stream itself because the air is being forced through a convergent region. This is analogous to water being constricted through

a garden hose. If the opening of the garden hose is shrunk, the water is forced through a smaller area increasing the speed at which the water is released from the hose. Figure 7 shows a schematic of a straight jet streak where the jet entrance (exit) region is on the left (right) of the diagram. Within the entrance (exit) region, horizontal winds blow across the geopotential height contours to lower (higher) heights and pressures due to imbalances in the pressure gradient and the Coriolis force. As a result of these imbalances, vertical motions are produced yielding rising and sinking of air parcels around the jet streak. This movement causes air to converge and diverge in areas around the jet streak as depicted in Fig. 7.

In analyzing the relationship between jet streaks and tropopause folds, it is useful to decompose the total horizontal wind, $\tilde{V}_H$, into its geostrophic and ageostrophic components. The total horizontal wind vector is defined by

$$\tilde{V}_H = \tilde{V}_g + \tilde{V}_{ag}. \tag{2.2}$$

The geostrophic wind is defined by

$$\tilde{V}_g = \frac{1}{\rho f} \tilde{k} \times \nabla\, p, \tag{2.3}$$

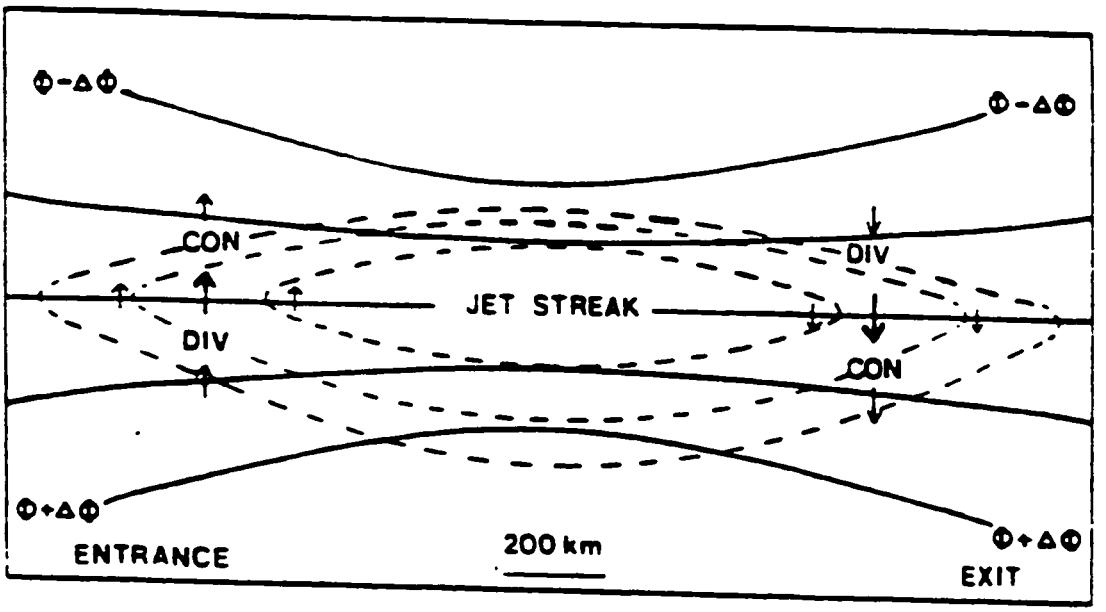


**Fig. 7:** Schematic illustration of ageostrophic motions (arrows), geopotential heights (solid black lines) and associated convergence (CON) and divergence (DIV) patterns in the vicinity of a straight jet streak (dashed black lines). (From Shapiro and Kennedy, 1981).

and relates the wind to the pressure field. It represents completely unaccelerated flow where the horizontal pressure gradient and the Coriolis force are in balance. Although the real wind is not purely geostrophic, the large-scale quasi-horizontal flow is nearly geostrophic over large portions of the atmosphere. The ageostrophic wind, $\tilde{V}_{ag}$, is directly proportional to the acceleration of the actual horizontal wind, i.e., it is a measure of the acceleration of the fluid parcel (Riegel, 1992). The ageostrophic wind is defined by

$$\tilde{V}_{ag} = \tilde{V}_{H} - \tilde{V}_{g} = \frac{1}{f}\tilde{k} \times \frac{d\tilde{V}_{H}}{dt}, \tag{2.4}$$

and is generally an order of magnitude weaker than the geostrophic wind. When examining synoptic scale systems, the thermal wind is used to detect where jet streaks occur in the atmosphere. The thermal wind is actually a geostrophic wind shear, defined by

$$\tilde{V}_{T} = \frac{\partial \tilde{V}_{g}}{\partial z}. \tag{2.5}$$

From Eq. (2.3) it can be seen that $\tilde{V}_{T}$ is a direct result of horizontal temperature gradients and the distribution of mass within a layer of the atmosphere.

By using the aforementioned theories combined with analyzing the geostrophic, ageostrophic and thermal winds, we are able to diagnose the atmospheric forcing associated with tropopause folds around a jet streak . Each of the two theories is now reviewed to see how they can be used to diagnose the dynamics of tropopause folds.

### 2.4.1 Q-vector Theory

Vertical motions can be attributed to geostrophic and ageostrophic forcing, gravity and mountain waves, convective activity, and other atmospheric forcing. Barnes and Colman (1993) claim that given a mid-latitude synoptic event where the jet streak is essentially straight, as is nearly the case at 00/06 (Fig. 1d), the **Q**-vector can be an effective diagnostic tool to determine rising and sinking motions around the jet level. Usage of the **Q**-vector is a quasi-geostrophic (QG) approach to isolating the vertical motion associated with geostrophic forcing. The **Q**-vector as defined by Holton (1992) is

$$\tilde{Q} = (\tilde{Q}_1, \tilde{Q}_2) = (-\frac{R}{p}\frac{\partial \tilde{V}_g}{\partial x} \bullet \nabla T, -\frac{R}{p}\frac{\partial \tilde{V}_g}{\partial y} \bullet \nabla T). \qquad (2.6)$$

It represents the advection of horizontal temperature gradient by the geostrophic wind. The convergence (divergence) of the **Q**-vector indicates rising (sinking) motions in the atmosphere due to geostrophic forcing. Below the tropopause and looking downstream,

this requires that the divergence of the geostrophic **Q**-vector be negative (positive) on the right hand side (left hand side) of the jet entrance region. In summary, the **Q**-vector is an effective tool in diagnosing vertical motions around jet streaks, and plays an important role in understanding the tropopause fold process.

In basic fluid dynamics, there are primary circulations associated with the geostrophic wind (those associated with vorticity and temperature advection), and secondary circulations associated with rising and sinking motions and the divergence of the ageostrophic wind. These secondary circulations are typically an order of magnitude weaker than the primary circulations and are often hard to detect. In combination, these two circulations allow for thermal wind balance to be maintained. According to Bluestein (1986), geostrophic deformation acts to increase the horizontal temperature gradient. When this gradient becomes too large for the vertical shear, the atmosphere is forced from thermal wind balance. As a result of this imbalance, a secondary circulation of rising and sinking motion develops. The rising (sinking) of the air parcel causes adiabatic cooling (heating) reducing the horizontal temperature gradient, thus restoring thermal wind balance. Through this process of rising and sinking motions near the tropopause boundary, ST mass exchanges take place giving rise to what are called tropopause folds.

### 2.4.2 Danielsen's Theory

According to Danielsen (1968), the folding process is initiated by the QG shears in the baroclinic atmosphere west of developing troughs or ridges. He indicates that stratospheric air moves diabatically down through the stratosphere on the cyclonic side of the jet. It is then extruded from the lower stratosphere and into the troposphere where it passes beneath the jet as it descends and moves to lower latitudes. The typical schematic of a tropopause fold according to Danielsen (1968) is shown in Fig. 8, where the jet (J) is directed into the page. The folding develops along the axis of confluence between direct and indirect circulation cells beneath the core of the jets (Danielsen, 1968). Figure 8 closely resembles the cross section shown in Fig. 6. His theory plays an important part in diagnosing the tropopause fold signature in this thesis.

## 2.5 ST Mass Exchange

Tropopause folding is now believed to be the main process by which ST mass exchange occurs in the mid-latitudes, and is perhaps the primary mechanism for the transport of mass from the stratosphere to the troposphere (Andrews *et al.*, 1987). Vaughan *et al.* (1994) found that ST mass exchange effects can be found to last 1-2 days in duration per fold event. In various studies by Reiter (1975), Danielsen and Mohnen (1977), and

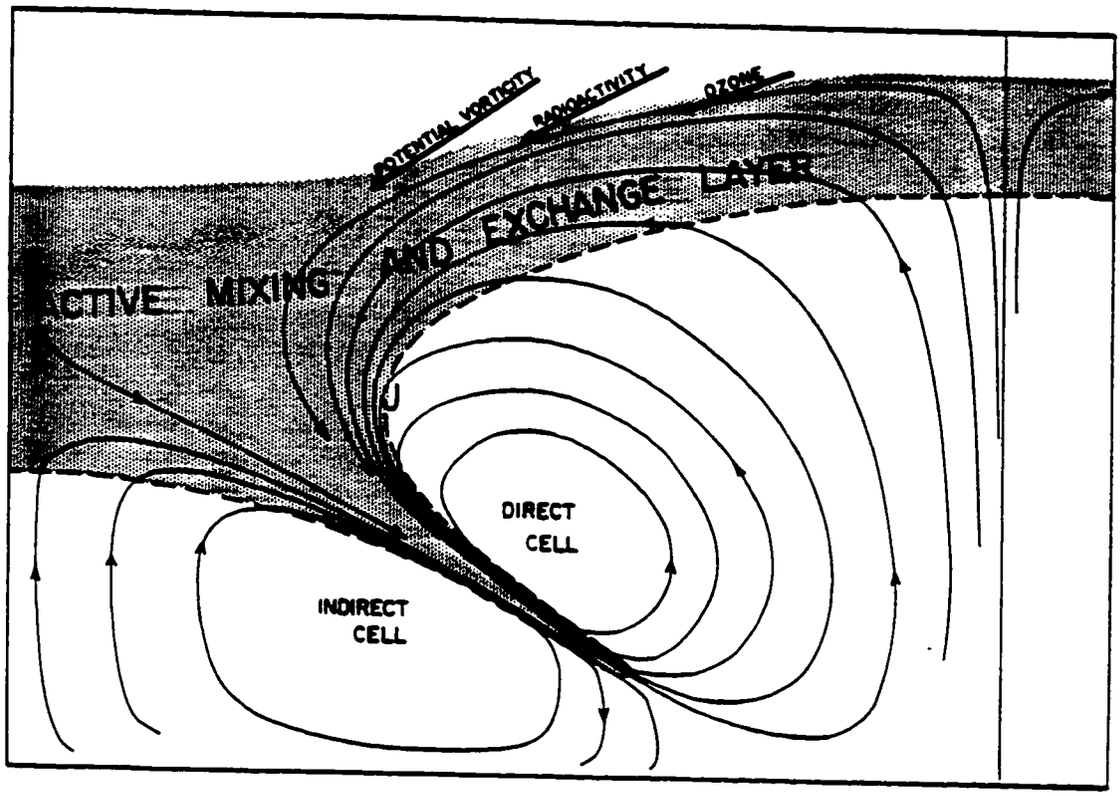


**Fig. 8:** Schematic illustration of a cross section of a tropopause fold and its relation to the jet streak (J). (From Danielsen, 1968).

Holton (1990), the annual transport of ST mass exchange has been estimated to be between 1.0 - 4.0 X $10^{17}$ kg over the Northern Hemisphere. A second set of mass exchange estimates were obtained from regional case studies where radioactive fallouts and ozone concentrations were examined (Reiter and Mahlman, 1965; Ancellet *et al.*, 1991; Ebel *et al.*, 1991). Ozone is produced in the stratosphere from photochemical processes and is known to be extruded down into the troposphere during fold events. Mass exchange results from Ebel *et al.*, (1991) were based upon a linear relationship between ozone concentration (ppb [parts per billion]) and potential vorticity. The ozone concentration was then used to calculate mass exchange.

Absent from all of these studies was an explicit mathematical formulation of the cross-tropopause mass exchange. In order to determine mass exchange, a tropopause boundary must be determined. There are two definitions widely accepted in identifying the tropopause boundary. The first, a thermal definition of the tropopause boundary, is marked by a prominent change or a reversal in sign of the atmospheric lapse rate (Danielsen, 1959). With this, one would see a concentration of isentropes at the tropopause boundary separating a region of stable air above the boundary from unstable air below. The second, a dynamic definition of the tropopause boundary, is marked by a prominent change in potential vorticity thought to be caused by diabatic or dissipative processes. Expanding upon these definitions, Wei (1987) claimed that the physical mechanisms responsible for the exchange of mass and trace constituents between the

stratosphere and the troposphere were due to diabatic processes, temporal movement of the tropopause, and transport along isentropic surfaces which intersect the tropopause. According to Wei (1987), the cross-tropopause mass flux, $F(\rho)$, in isentropic coordinates is defined by

$$F(\rho) = [\rho J_\theta (\frac{d\theta}{dt} - \frac{\partial \theta}{\partial t_{Z_0}} - \tilde{U}_\theta \bullet \nabla_{Z_0} \theta)]_{\theta_s}, \tag{2.7}$$

where

$$J_\theta = \left|\frac{\partial z}{\partial \theta}\right|, \tag{2.8}$$

$\rho$ is density, $\theta$ is potential temperature, $t$ is time, $z$ is height, $Z_0$ denotes the critical stability threshold, and $\tilde{U}_\theta$ is the horizontal wind. The first term on the right hand side represents the mass flux due to diabatic processes, the second term represents the cross-tropopause mass flux resulting from the temporal change of the tropopause potential temperature, and the last term represents the mass flux due to the potential temperature gradient along the tropopause boundary. According to Wei (1987), tropopause folding is primarily associated with the magnitude of the third term on the right hand side of Eq. (2.7). Wirth (1995) challenged Wei's thermal tropopause definition. He claimed that in certain situations, terms in Eq. (2.7) tend to cancel each other out making it difficult to discern the physical mechanisms of ST mass flux. Wirth (1995) preferred using the

dynamical definition for the tropopause boundary, noting that there is no problem with cancellation of any terms.

In contrast, Hoerling *et al.* (1993) used both a thermal and dynamic tropopause definition, as well as Wei's theory, to assess the global cross-tropopause mass exchange from twice-daily European Centre for Medium-Range Weather Forecasting (ECMWF) Global Weather Experiment (GWE) final level IIIb uninitialized analyses for January 1979. The thermal tropopause boundary was defined as the height where the temperature lapse rate became less than a critical value of 2 K $km^{-1}$ for a depth of at least 2 km. The dynamic tropopause boundary was defined at 3.5 PVU. Their Northern Hemispheric mid-latitude results indicated that from 25-50°N, January ST mass exchange was roughly 6.0 X $10^{16}$ kg using either the thermal or dynamic tropopause definition.

Wei (1987) also stated that Eq. (2.7) could be transformed into any coordinate system for purposes of interpreting mass flux; however, it should be noted that each term loses its original meaning. Eq. 2.7 modified to sigma coordinates is the basis for the mass exchange calculations with this research. Converting Eq. (2.7) to sigma coordinates yields

$$F(\rho) = \frac{p_*}{g}[\dot{\sigma} - \frac{\partial \sigma}{\partial t_{z_0}} - \tilde{U}_\sigma \bullet \nabla_{z_0}\sigma)]_{\sigma_s}, \tag{2.9}$$

where

$$\sigma = \frac{p - p_t}{p_*}, \tag{2.10}$$

and

$$p_* = p_s - p_t. \tag{2.11}$$

The sigma coordinate system in our case is a normalized pressure system where $p$ is pressure, $p_t$ is pressure at the model top (100 mb), $p_s$ is surface pressure, $\dot{\sigma}$ is vertical velocity, $t$ is time, $g$ is gravity, $Z_0$ is the critical stability threshold and $\tilde{U}_\sigma$ is the horizontal wind. The three terms in Eq. (2.9) no longer have the same straight-forward physical meaning as Wei's Eq. (2.7) in isentropic coordinates, making it difficult to discern diabatic and adiabatic terms, though recall that Wirth (1995) questioned that approach. Nevertheless, the terms do have physical meanings. Combined with $\frac{p_*}{g}$, the 1st term within parentheses represents the vertical flux across the tropopause. The second term represents the flux due to the movement of the tropopause boundary. The third term represents the horizontal flux across a sloping tropopause. Through scale analysis, term 1 is roughly $O(10^2)$ larger than the remaining two terms, signifying that vertical velocity should drive the mass exchange calculation.

For this thesis, a thermal definition of the tropopause surface is used. Though Hoerling *et al.* (1993) used a lapse rate of 2 K $km^{-1}$, for a depth of at least 2 km, the critical stability is determined in this thesis by analyzing various cross sections and soundings, and then selecting a value that captures the transition from stratosphere to troposphere near the vicinity of COF during the time of the tropopause fold. A lapse rate of 8 K $km^{-1}$ is found to adequately identify the tropopause boundary. The 2-km-deep restriction is not applied since the laminae are so thin in this study (Fig. 6). The search is done from the top of the model downward in order to avoid erroneously locating temperature inversions commonly found in the lower layers of the atmosphere.

Estimated total mass exchange (kg) during the lifetime of the tropopause fold is given by

$$TME = \int_{T_L} \int_{A} F(\rho) da dt , \tag{2.12}$$

where, $F(\rho)$ (kg $m^{-2}$ $s^{-1}$) is the cross-tropopause mass flux, $A$ ($m^2$) is the area of integration, and $T_L$ (s) is the duration of time for the tropopause fold event. In a way similar to Ancellet *et al.* (1991), we can extrapolate from Eq. (2.12) a yearly value of mass exchange associated with weak tropopause folds by multiplying the total mass exchange associated with this tropopause fold by the estimated number of yearly mid-latitude baroclinic waves. The number of baroclinic waves, similar in size to Fig. 1a, is estimated

to be 1460 per year in the Northern Hemisphere (Danielsen and Mohnen 1977). Research to date has not quantified the number of weak mid-latitude baroclinic waves occurring at any one time over the Northern Hemisphere. In this thesis we assume that there are many, if not more, relatively weak baroclinic waves. Hence, we estimate that over the Northern Hemisphere there are $2000 \pm 500$ weak baroclinic waves per year. Using this estimate, mass exchange results associated with this tropopause fold can be compared with the other previously mentioned studies.

# Chapter 3

# Data

Data used in this thesis are separated into two categories: ungridded and gridded. All data that are used in this research are listed in Table 1. The data are now explained in detail.

## 3.1 Ungridded Data

Several types of ungridded data are used for this research. One of the most important types of data comes from a wind profiler network. The wind profiler is a vertically pointing microwave radar that measures horizontal wind speed and direction between about 1,500 and 53,000 feet above ground level (Lester, 1993). The WPN for this case study is particularly valuable as it consists of wind data with 250-m vertical resolution

**Table 1:** Case study data available for 3 - 6 December 1991.

| |
|---|
| **Synoptic Analyses** |
| NMC significant level geopotential height, temperature, and wind analyses |
| NMC North American surface analyses |
| **MAPS Analyses** |
| Combination of aircraft, wind profiler, surface observation, and radiosonde data |
| **MM4 Model Analyses** |
| Model runs initialized with MAPS data |
| **Miscellaneous** |
| VIZ, SDD, and CLASS radiosonde data |
| Wind Profiler Network data |
| Infrared, visible, and water vapor satellite imagery |
| Ozonesonde data |

collected at 6-s intervals and averaged to 1-hourly values (Mace *et al.*, 1995). A sample of the profiler data collected during Project FIRE is depicted in Fig. 3 and is used to locate jet streaks in and around the COF area. Radiosonde data are available at 3-h intervals at the stations depicted in Fig. 4. The radiosonde station density and release frequency are insufficient for studying the dynamics of this tropopause fold (Sassen *et al.*, 1995), but are valuable in validating the MAPS analyses and the MM4 (Mesoscale Model, Version 4) simulations. The observations from WPN, radiosonde, and CLASS radiosonde data are used to evaluate the reliability of mass and wind fields from MAPS and NMC analyses and MM4 simulations. Ozonesonde data is available for this case study and is valuable since ozone acts as a tracer of stratospheric air. Water vapor satellite imagery provided by Soden (1991) is used to diagnose dry and moist atmospheric areas and is very helpful in tracking tropospheric folds (Barnes and Colman, 1993). Infrared satellite imagery provides insight into the cirrus bands propagating through the COF area during the case study period. Synoptic charts and upper-level jet analyses during the case study period are used to analyze the movement of the frontal systems and the jet stream.

## 3.2 Gridded Data

The gridded data available for this case study comes from MAPS analyses and MM4 simulations initialized with MAPS data. MAPS is a mesoscale data assimilation system which uses a hybrid isentropic-sigma coordinate system (Benjamin *et al.*, 1991). It

incorporates data from rawinsondes, surface-based wind profilers, aircraft reports, surface observations, and satellite radiance (Benjamin, 1989). Rossby (1937) first summarized the advantages of viewing weather features on isentropic surfaces: isentropic surfaces act like material surfaces, flow patterns on them are spatially and temporally coherent, and frontal discontinuities are virtually nonexistent. According to Benjamin (1989), an isentropic analysis is advantageous on the mesoscale since it enlarges the apparent scale of frontal features of advective origin (e.g. dry tongues, moist plumes or conveyor belts, and stratospheric intrusions). MAPS data is available every 3 hours during the case study, and is essential both in identifying the origin of the air parcels found around the tropopause fold area, and in initializing the MM4 model.

MM4 is a hydrostatic, three-dimensional, primitive-equation model with a terrain-following vertical coordinate (Anthes *et al.*, 1987). The model domain is shown in Fig. 4; however, many of the results in this thesis are shown for various sub-domains of the overall domain around the tropopause fold. The horizontal model grid is 76 X 57 with a 60-km grid spacing. The top of the model is at 100 mb and there are 26 vertical levels. The main advantages of MM4 versus MAPS are that model output is available on an hourly basis and that the data are dynamically consistent. This model is only used as a diagnostic tool for this tropopause fold case study, as opposed to using it for a sensitivity study of the fold dynamics.

### 3.2.1 MAPS Analyses

To assess the validity of our analysis of the origin, dynamics, and mass exchange associated with the weak tropopause fold around 21/05, it is necessary to determine the accuracy of the data. First, a detailed comparison of geopotential height and wind fields at 275 mb (middle of the jet level) at various times is made between the MAPS analyses, radiosonde observations, and NMC analyses. Second, an intercomparison of the 500-mb MAPS geopotential height fields at successive 3-h intervals is performed. Each of these comparisons is now looked at in detail.

#### 3.2.1.1 Differences between Analyses and Observations

Figure 9a compares the wind and mass fields at 275 mb between the observations and the MAPS analyses at 12/05. It shows that MAPS geopotential heights are 60 - 80 m greater than those obtained from radiosonde data. Wind direction is comparable between the two sets of data; however, MAPS winds are generally 5 - 10 m $s^{-1}$ less than the observed winds. In contrast, Fig. 9b shows how closely the MAPS data and the observations matched at 12/04. MAPS mass field errors are 20 m or less. This analysis shows that at 12/04 there is good data correlation between the MAPS data and the observations; however at 12/05, the MAPS mass field is very suspect, leading to a further look at the data.

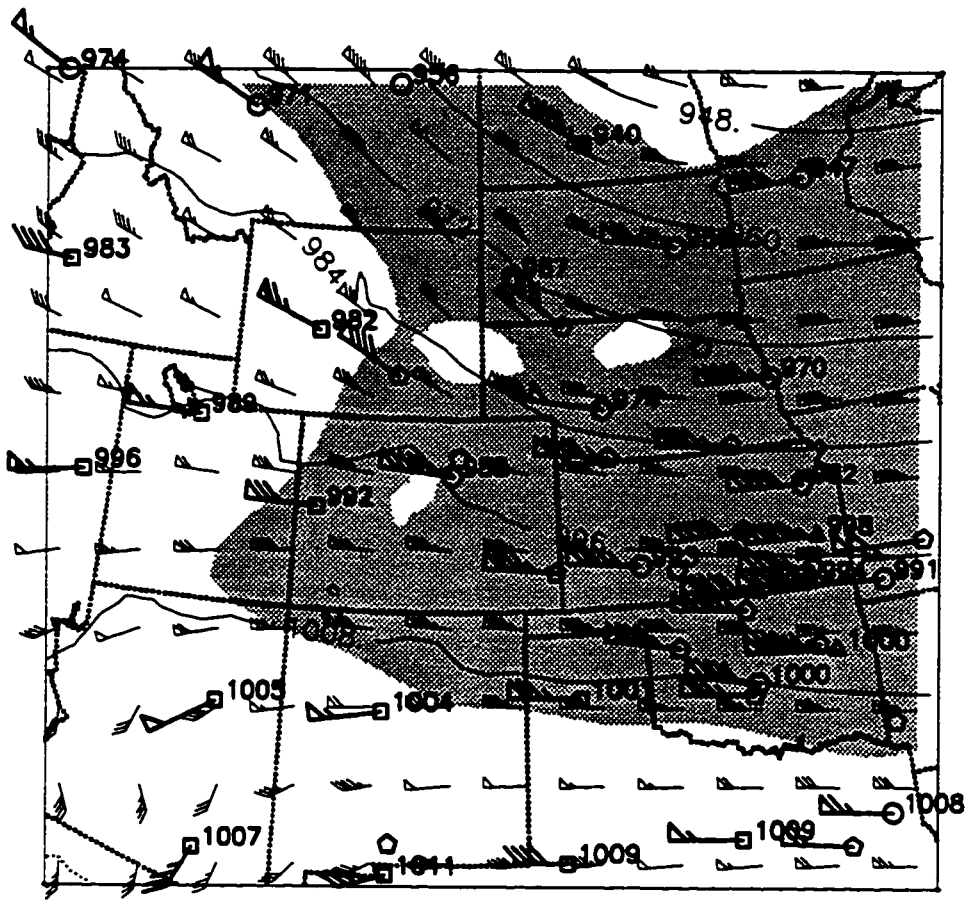


**Fig. 9a:** 275-mb geopotential heights (dam) and horizontal winds (kts; wind barbs) for 12/05. Radiosonde data (bold print) and MAPS analysis (light print). Areas with MAPS winds of 70 - 110 kts (36.0 - 56.6 m $s^{-1}$) are shaded. Refer to Fig. 4 for the station symbol identifiers.

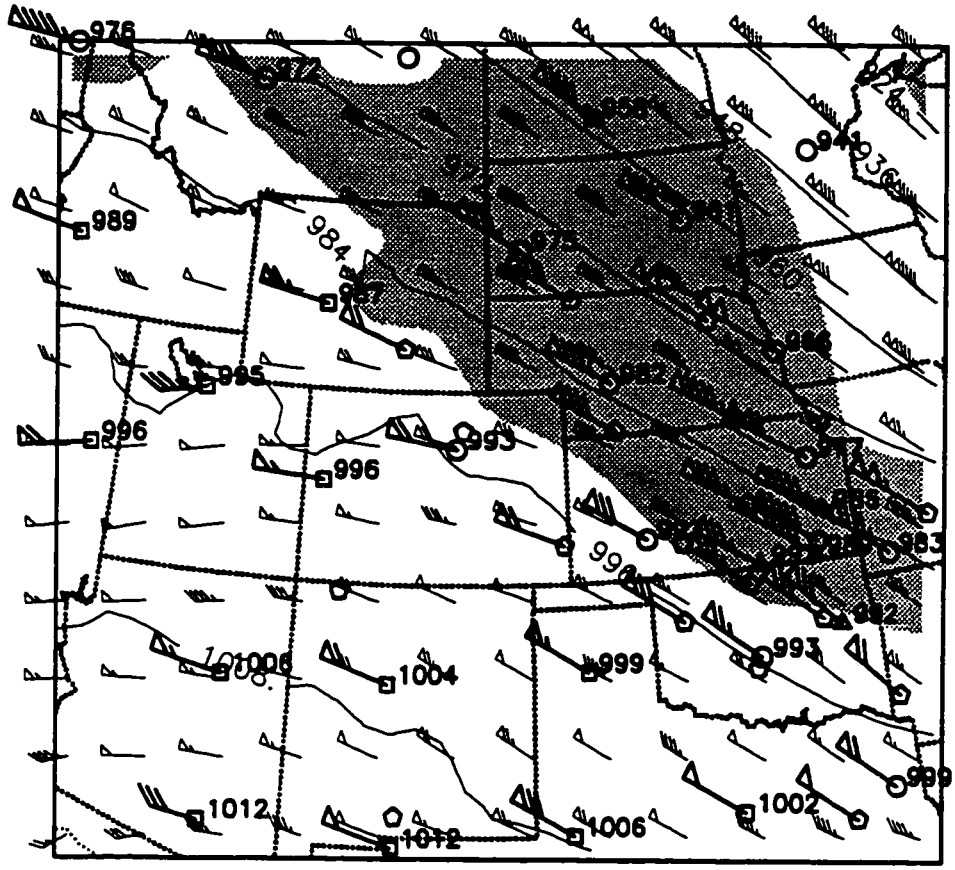


**Fig. 9 (cont.) b:** Same as in Fig. 9a except for 12/04.

Figure 10 shows a comparison of the 500-mb geopotential height field at COF at 3-h intervals on 5 December 1991 between CLASS radiosonde data, MAPS analyses, and the NMC analyses. The 500-mb level has been chosen since this a preferred level for analyzing short waves and associated tropopause folds in the upper levels of the atmosphere. It should be noted that any differences found at 500 mb are possibly due to errors at lower levels and will propagate up through the atmosphere. The comparison between NMC analyses and CLASS radiosonde data available at 00/05, 12/05, and 00/06 show 500-mb geopotential height differences of less than 5 m. The MAPS analyses and the CLASS radiosonde data show differences of up to 20 m except at 12/05 and 21/05 when geopotential height differences are greater than 30 m. These larger differences prompted yet a further look into the MAPS data.

#### 3.2.1.2 Anomalies with the MAPS data

MAPS analyses at some successive 3-h intervals on 5 December 1991 show 40 - 50 m differences in the mass field. Figure 11 shows the extent of the differences at each successive 3-h period by looking at the profile of MAPS geopotential heights averaged over the model domain. Figure 11 shows a typical synoptic scale difference (in the absence of a large-scale upper-level disturbance) of less than 10 m at 500 mb over each 3-h period between 00/05 and 09/05, and the 6-h period 18/05 - 00/06. Note that between

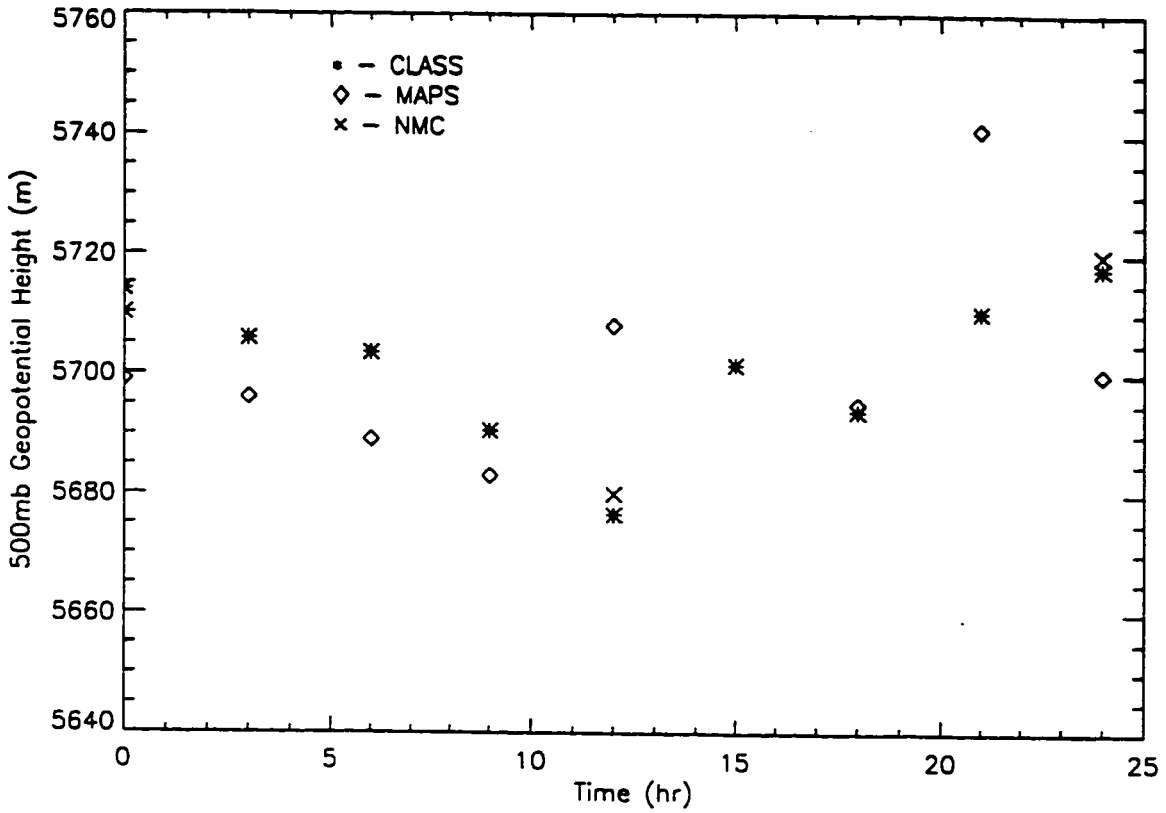


**Fig. 10:** Time series comparison of 500-mb geopotential heights (m) for CLASS radiosonde data, MAPS analyses and NMC analyses at COF between 00/05 and 00/06. NMC analyses are available every 12 hours. CLASS radiosonde data are available every 3 hours. MAPS analyses are available every 3 hours, except 15/05.

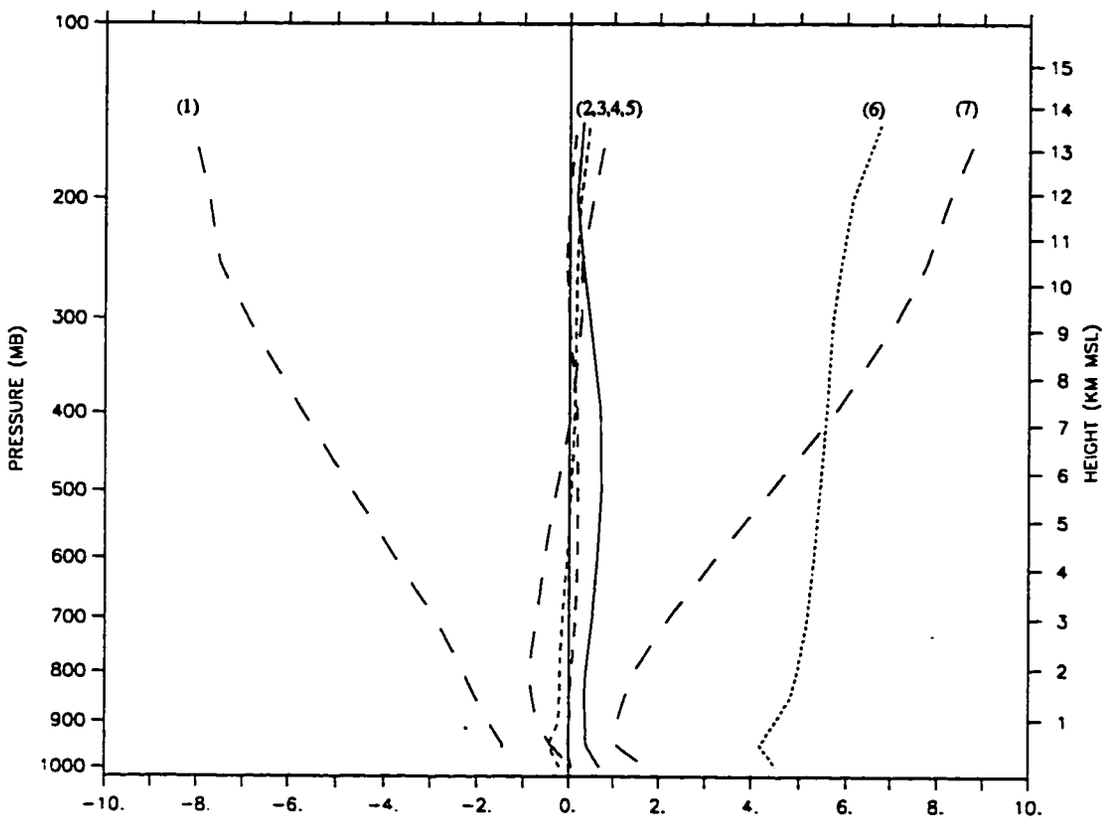


**Fig. 11:** Vertical profiles of the differences in the domain-averaged MAPS 3-h geopotential height (dam) data. Refer to Fig. 4 for the domain. Group 1 differences are considered anomalies and consist of lines: (1) 00/06 - 21/05, (6) 12/05 - 09/05, and (7) 21/05 - 18/05. Group 2 differences are considered normal and consist of lines: (2) 06/05 - 03/05, (3) 03/05 - 00/05, (4) 09/05 - 06/05, and (5) 00/06 - 18/05 (a 6-h difference).

12/05 - 09/05, 21/05 - 18/05, and 00/06 - 21/05 differences of 40 - 55 m at 500 mb are found. These errors are found at all heights up to the top of the model. This 40 - 55 m difference during any 3-h period is atypical given the near zonal upper-level flow over the central U.S. (Figs. 1c, 1d), and is much larger than any of the other 3-h changes. Figures 12a, 12b show a dramatic difference in geopotential heights of nearly 60 m between 21/05 and 00/06, especially over the southwestern part of the domain. Anomalies in this region are of particular interest since the cirrus clouds over the COF area are suspected to have been enhanced by the southwesterly flow from the low centered over the Baja California area during the case study period.

Since geopotential height differences are positively correlated with changes in temperature, we would also expect to see large temperature differences around 21/05. The vertical profile of 500-mb MAPS temperature differences surrounding 21/05 over the domain are roughly 1.6 - 2.2°C as can be seen in Fig. 13. In contrast, the 6-h difference between 00/06 - 18/05 is only 0.5°C. It is important to remember that 21/05 is near the time of the tropopause fold event, so any anomalous data at this time would lead to uncertainties in the diagnosis of the fold event.

The positive correlation between greater geopotential heights and temperature is explained by integrating the hydrostatic equation,

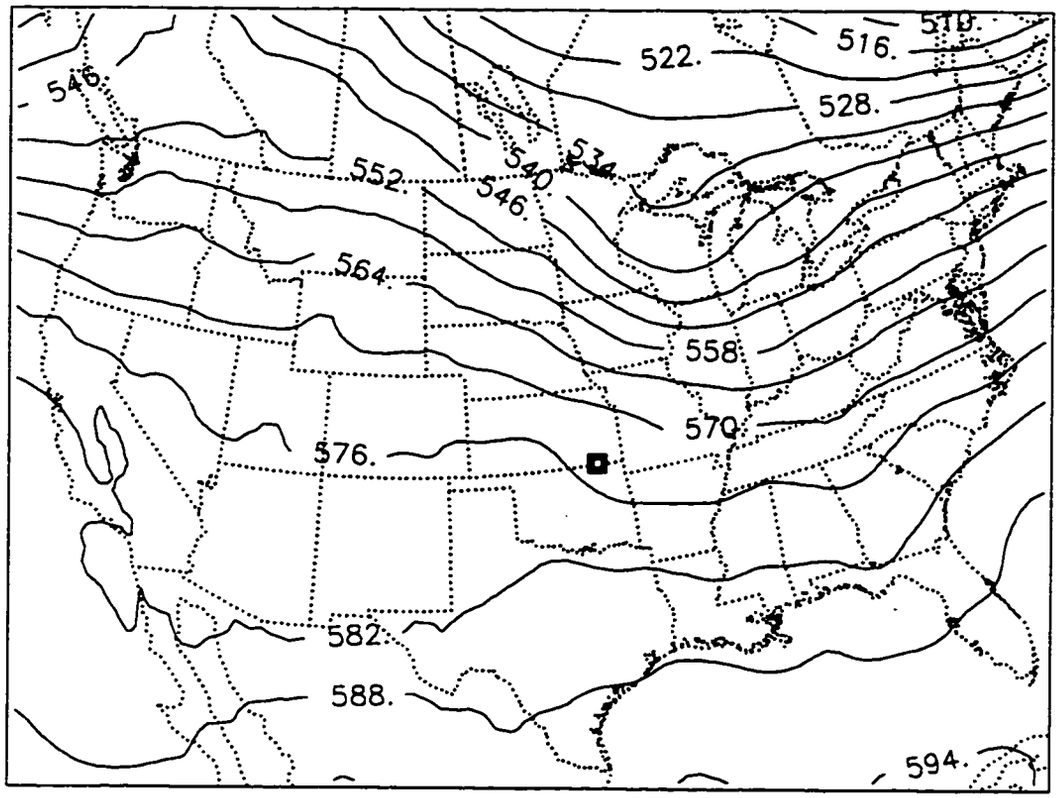


**Fig. 12a:** MAPS 500-mb geopotential heights (dam; thin black lines) for 21/05.

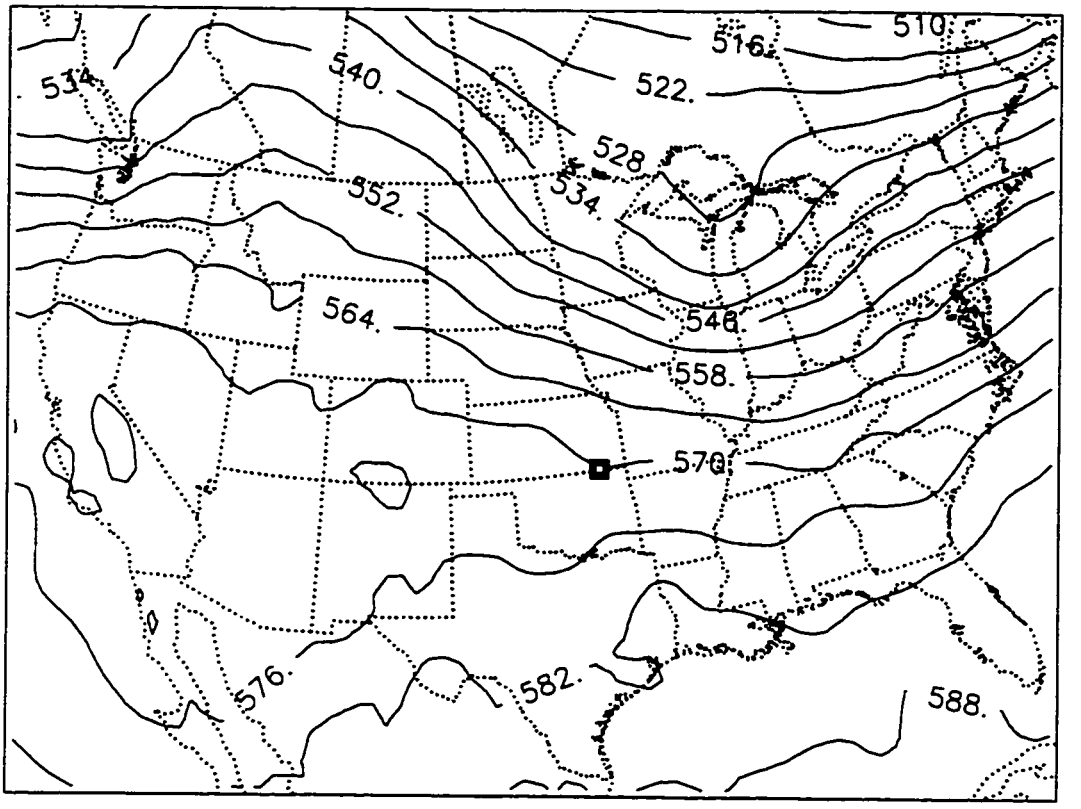


**Fig. 12 (cont.) b:** Same as in Fig. 12a except for 00/06.

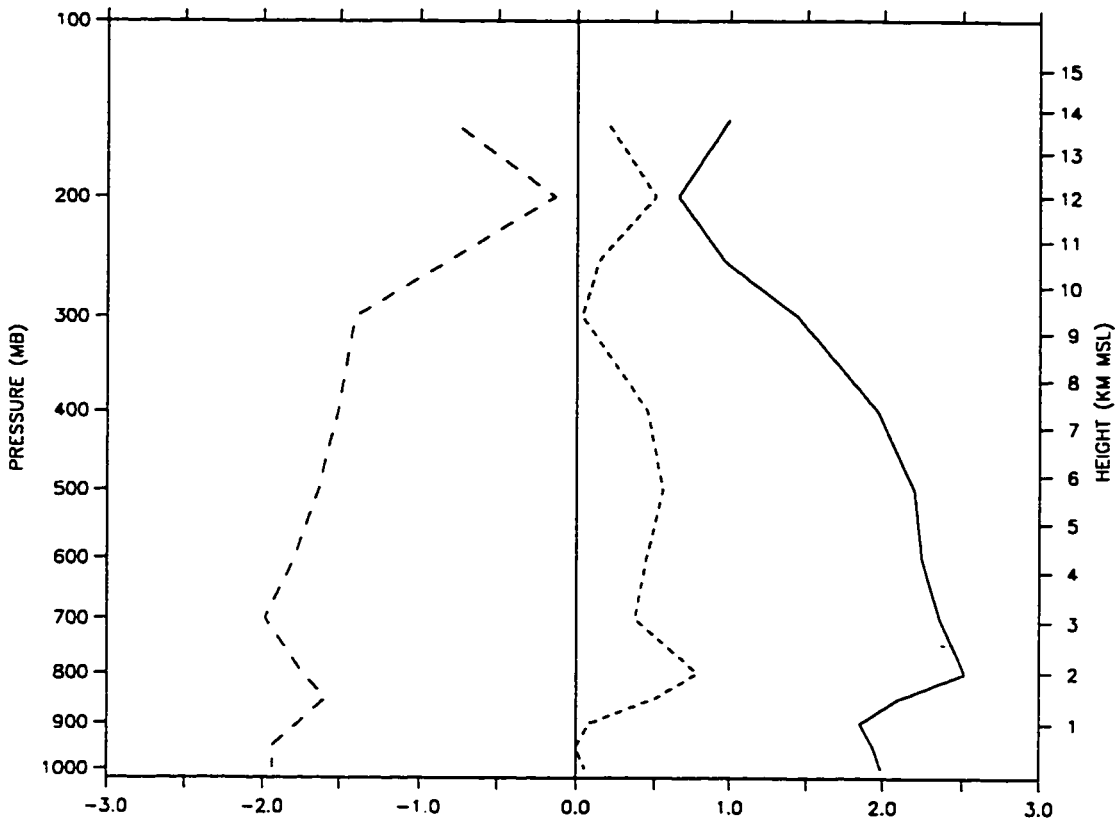


**Fig. 13:** Vertical profiles of the differences in the domain-averaged MAPS 3-h temperature (°C) data: 00/06 - 21/05 (long dash), 00/06 - 18/05 (short dash), and 21/05 - 18/05 (solid line). Refer to Fig. 4 for the domain.

$$\frac{\partial p}{\partial z} = -\rho g, \tag{3.1}$$

and computing the 500-mb geopotential height change for a 2.0 K temperature difference. After integration, Eq. (3.1) is approximated by

$$\frac{T}{T+\Delta T} = \frac{z}{z+\Delta z}. \tag{3.2}$$

For a mean temperature T of 258.15 K, $\Delta$T of 2.0 K, and geopotential height z of 5640 m, the geopotential height difference $\Delta$z is approximately 43.7 m. This large geopotential height difference is within the range shown in Fig. 11 for the MAPS analyses 21/05 - 18/05 and 00/06 - 21/05. This 2.0 K increase shows that the anomalously warm temperatures in the 21/05 MAPS analysis are sufficient to explain the height differences. More importantly, this conclusion is probably applicable to all atmospheric levels. Thus, the MAPS analysis at 21/05 is shown to have large mass field errors. It is therefore excluded from the dynamical analysis of this tropopause fold event.

The 12/05 MAPS analysis is also found to have large mass field errors. Since the 15/05 MAPS analysis is missing, a MAPS intercomparison is impossible. Instead, a comparison is made directly with radar observations along a SW-NE path from San Diego, CA (NKX) to Monet, MO (UMN) at 00/05, 12/05, and 00/06. This cross section

is chosen since it is along the path of some of the suspected air parcel trajectories ending at COF at 21/05. Table 2 shows almost a 50-m difference between the radiosonde observations and the MAPS analyses at 12/05, but only near a 10-m difference at 00/05 and at 00/06. This shows a large discrepancy between the MAPS analysis and the radiosonde observations at 12/05, which is unexpected given the near zonal upper-level flow during this time frame shown in Figs. 1c, 1d. This mean geopotential height difference of approximately 50 m at 12/05 is similar to the difference with the MAPS analysis at 21/05 and is therefore excluded from the analysis of the dynamics of this tropopause fold case study.

### 3.2.2 Model Analyses

Realizing that MAPS geopotential height fields analyzed at 12/05 and 21/05 were much different than the actual observations at these times, we turned to a numerical model, MM4, for additional gridded analyses. This first simulation is initialized with MAPS data at 12/04 and then run through 00/06. The MAPS analysis at 12/04 is a good initialization for the simulation since the wind and mass fields vary by small amounts between the radiosonde and MAPS data at this time, as shown in Fig. 9b. For example, across the sub-domain, the MAPS geopotential height fields differ by only a few meters, the winds differ by 5 m $s^{-1}$ or less and the wind direction is nearly the same. A baseline time of 12/05 at a jet stream level of 275 mb is chosen to compare the MM4 simulation and the observations.

**Table 2:** Absolute value of geopotential height differences (m) between radiosonde data and MAPS analyses taken along a SW-NE path represented by stations identifiers in Fig. 4.

| | TIME | | |
|---|---|---|---|
| STATION | 00/05 | 12/05 | 00/06 |
| NKX | 1 | 68 | 4 |
| INW | 25 | 57 | 12 |
| ABQ | 4 | 54 | * |
| AMA | 4 | 55 | 2 |
| COF | 15 | 31 | 18 |
| UMN | 8 | 29 | 15 |
| Average Difference | 9.5 | 49.1 | 10.2 |

* Data not available

Figure 14 shows that the MM4 simulated mass field in the southern portion of the sub-domain is well correlated with the observations. MM4 simulated winds are approximately 5 - 10 m $s^{-1}$ greater than the observations. Differences in wind speed and direction on 12/05 are negligible between MAPS, MM4 simulation, and observations. Figure 15 shows that the difference between the mass field in the MM4 simulation, CLASS and NMC data is approximately 10 m at COF for 12/05, whereas the difference between the MAPS data, CLASS and NMC data is approximately 40 m. Although this simulation showed dynamically consistent results with the observations at 12/05, it did not show a well defined jet streak and potential vorticity extrusion over the COF area at 21/05. Hence, a second MM4 model was initialized with MAPS data from 09/05 and run through 00/06. This simulation is the primary one used to assess the dynamics and mass exchange associated with the weak tropopause fold; however, both simulations are used to assess the origin of the air parcels ending at COF at 21/05.

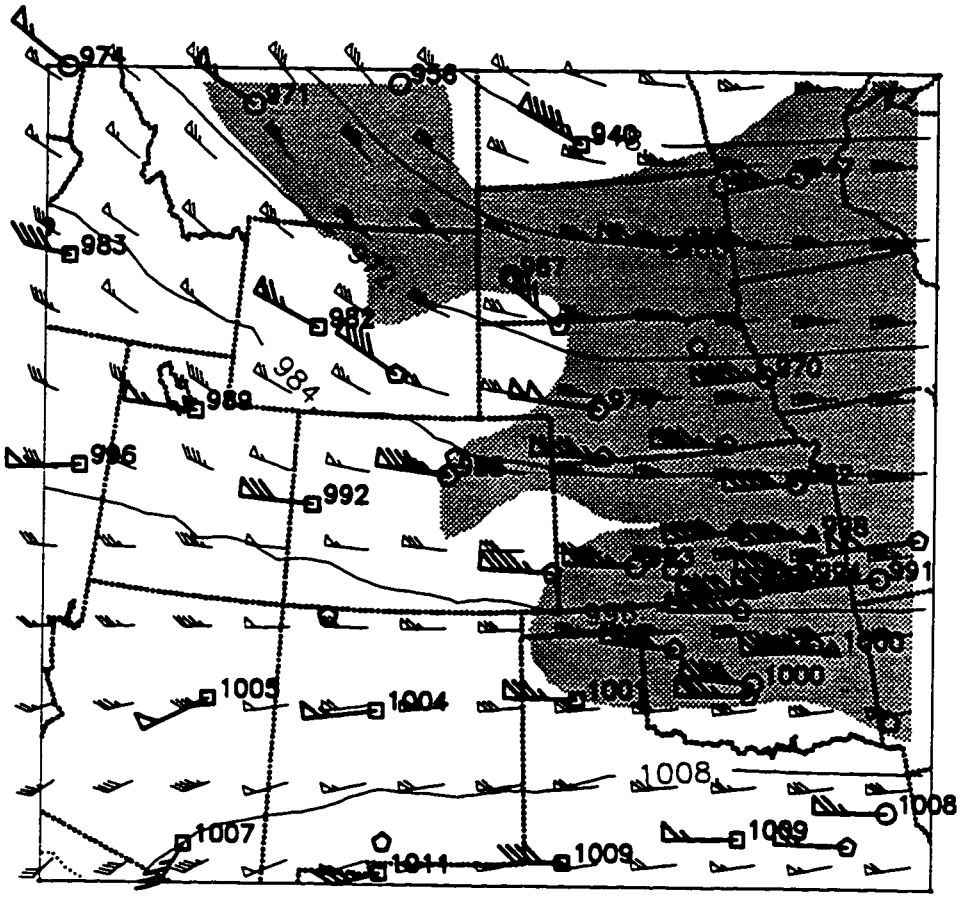


**Fig. 14:** 275-mb geopotential heights (dam) and horizontal winds (kts; wind barbs) for 12/05. Radiosonde data (bold print) and MM4 simulation (light print). Areas with MM4 winds 70 - 110 kts (36.0 - 56.6 m $s^{-1}$) are shaded. Refer to Fig. 4 for the station symbol identifiers.

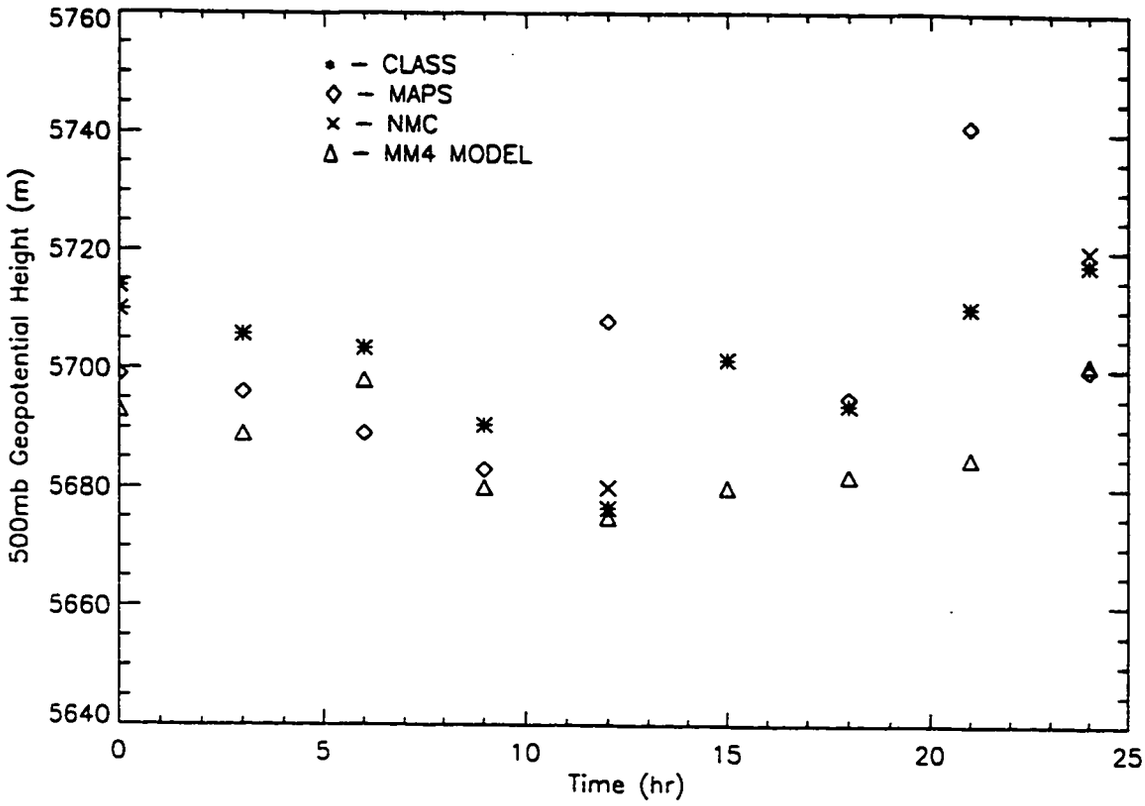


**Fig. 15:** Same as in Fig. 10 except for the addition of MM4 data.

# Chapter 4

# Results

## 4.1 Origin

Sassen *et al.* (1995) claim unusual cirrus were found above a frontal zone with a top of 350 mb. Thus, the 250 and 400 mb levels are used to track the air associated with this weak tropopause fold event. We expect that the air parcels ending at COF at 21/05 at 400 mb in the troposphere originated upstream in the stratosphere, and those ending at 250 mb originated upstream in the upper-troposphere.

Looking first at the parcels that ended over COF at 400 mb, Fig. 16 shows a series of back-trajectories with 5 release points from the KS, OK area at 21/05. A slight discontinuity between the back-trajectories is due to the use of the two consecutive MM4

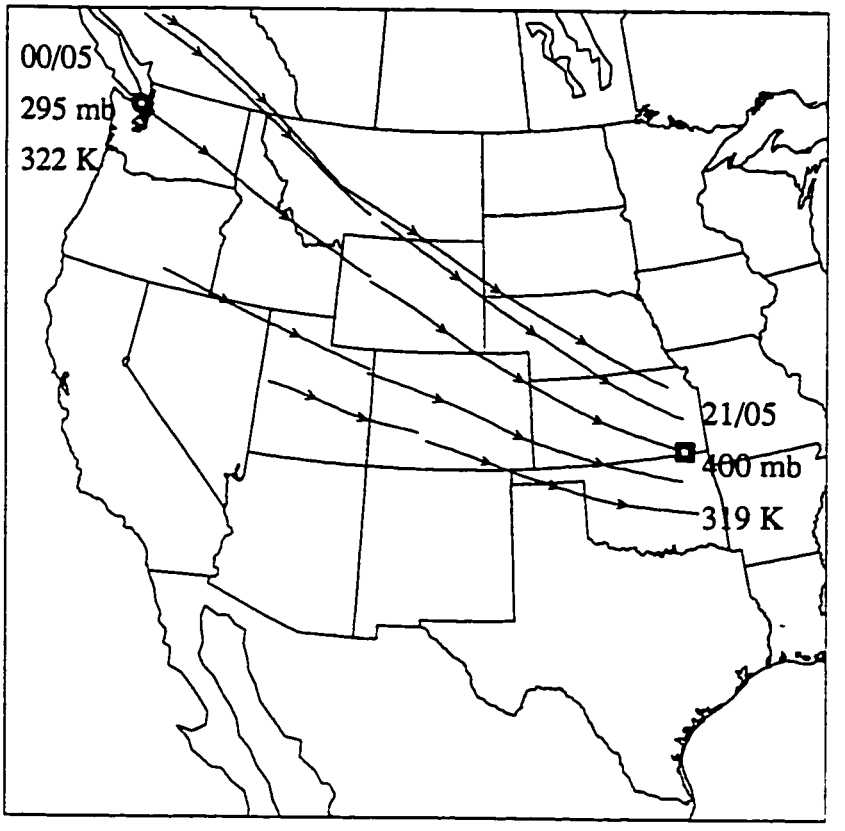


**Fig. 16:** Simulated MM4 21-h back-trajectories for parcels arriving at 21/05 in the vicinity of COF at 400 mb. COF is denoted by the white box with the thick black border. The trajectory origin at 00/05 is denoted by the white circle with the thick black border. The length between the arrows represents 3 hours. The trajectory arriving at COF at 400 mb and 319 K, descended from an original height of 295 mb and 322 K.

simulations, 00/05 - 09/05 and 09/05 - 21/05. Depending upon the release point, the origin varies by 13° latitude and 69 mb yielding an end result difference of 5° latitude and 0 mb surrounding the stations near COF. The 400-mb parcel ending at COF at 21/05 began in northwestern WA at 295 mb. Figures 17a, 17b show cross sections of wind and potential temperature along the approximate path of the trajectory ending at COF at 00/05 and 21/05, respectively. Figure 17a shows that the potential temperature of the 295-mb air parcel over northwest WA at 00/05 is approximately 322 K and is located near the tropopause at approximately 9.5 km. Figure 17b shows that by 21/05, the parcel has descended approximately 2.5 km to 400 mb at COF. The potential temperature is virtually conserved, cooling by approximately 3° to 319 K. The parcel is now clearly within the troposphere. This MM4 simulation shows that the parcel originated upstream from the COF area 21 hours earlier near the stratosphere and descended into the troposphere during its journey.

To validate the MM4 simulation results, a comparison is made with the trajectory endpoints using radiosonde data. Figure 18 shows a stuve diagram of two soundings, one at Salem, OR (SLE) at approximately 00/05 and the other at COF at around 21/05. SLE is the closest radiosonde location to northwest WA corresponding to the origin of the 400-mb back-trajectory. At SLE, the potential temperature at 295 mb is 322 K, and the tropopause is located directly above, in agreement with the MM4 simulation. At COF, the 322 K isentrope is found at 400 mb, also in fair agreement with the MM4 simulation.

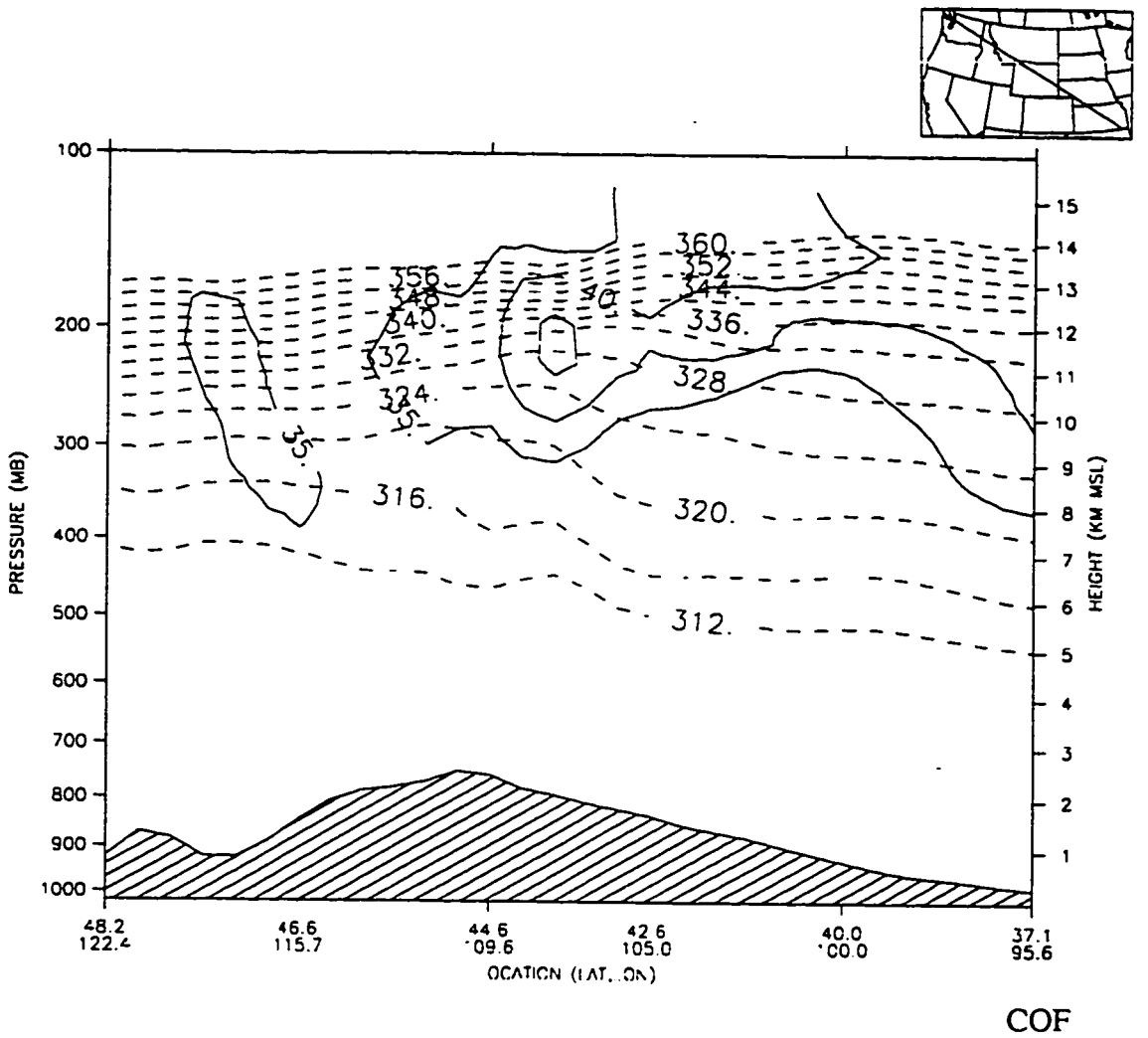


**Fig. 17a:** NW-SE cross section of MM4 horizontal winds (m $s^{-1}$; solid black lines) and potential temperature (K; dashed black lines contoured only from 312 to 360 K) at 00/05 along the line depicted in the upper right-hand map. This cross section approximates the path of the trajectory ending at COF, shown in Fig. 16.

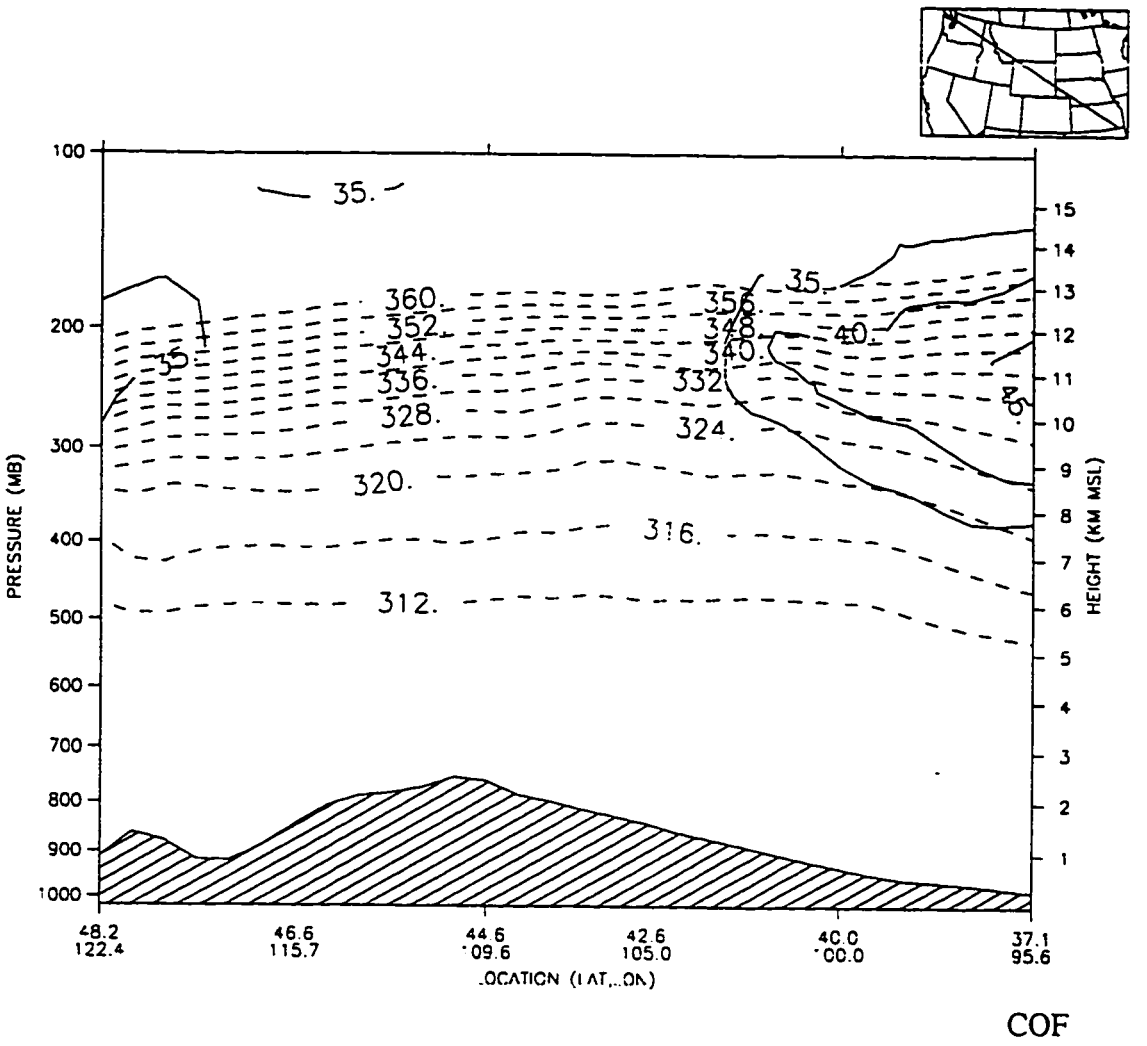


**Fig. 17 (cont.) b:** Same as in Fig. 17a except for 21/05.

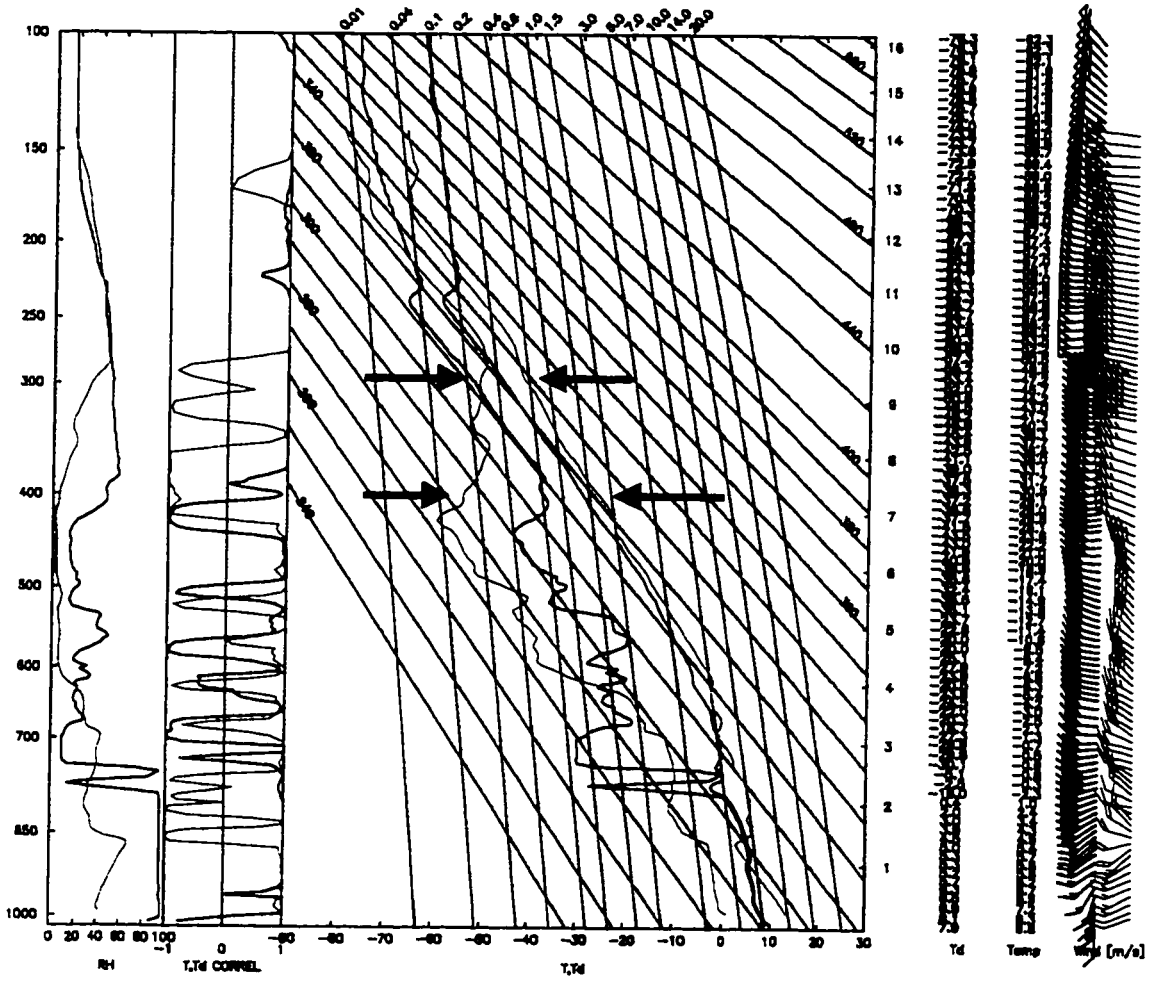

**Fig. 18:** Stuve diagram of radiosonde data at Salem, OR (SLE) for 2301 UTC 4 December 1991 (bold black lines) and at COF for 2045 UTC 5 December 1991 (magenta lines). SLE represents the approximate origin of the 21-h, 400-mb COF trajectory. The layer between the thick black arrows represents the region of air descending, WNW-ESE from 295 - 400 mb.

The moist layer at COF where Sassen *et al.* (1995) observed cirrus, namely 8.5 - 13 km, is seen on the stuve diagram as the area with a small dew point depression of 10 - 20°C. A stable layer is seen between 400 and 440 mb at COF, which is likely to be the upper-level frontal zone that Sassen *et al.* (1995) saw just beneath the cirrus layer. The radiosonde data and the MM4 simulation confirm the hypothesis that the parcel originated near the stratosphere and subsequently was transported further downward into the troposphere.

Next, looking at the parcels that arrived over COF at 250 mb, Fig. 19 shows a series of back-trajectories with 5 release points from the KS, OK area at 21/05. Depending on where the back-trajectory was initially released, the origin varies by 18° latitude and 18 mb yielding an end result difference of 5° latitude and 0 mb surrounding the stations near COF. The 250-mb parcel ending at COF at 21/05 began in central CA at 241 mb. Figures 20a, 20b show cross sections of wind and potential temperature along the approximate path of the trajectory ending at COF at 00/05 and 21/05, respectively. Figure 20a shows that the potential temperature of the 241-mb air parcel over central CA at 00/05 is approximately 334 K and is located near the tropopause. Figure 20b shows that by 21/05 at COF, the parcel descends minimally to 250 mb while the potential temperature remains steady. This MM4 simulation shows that the parcel originated

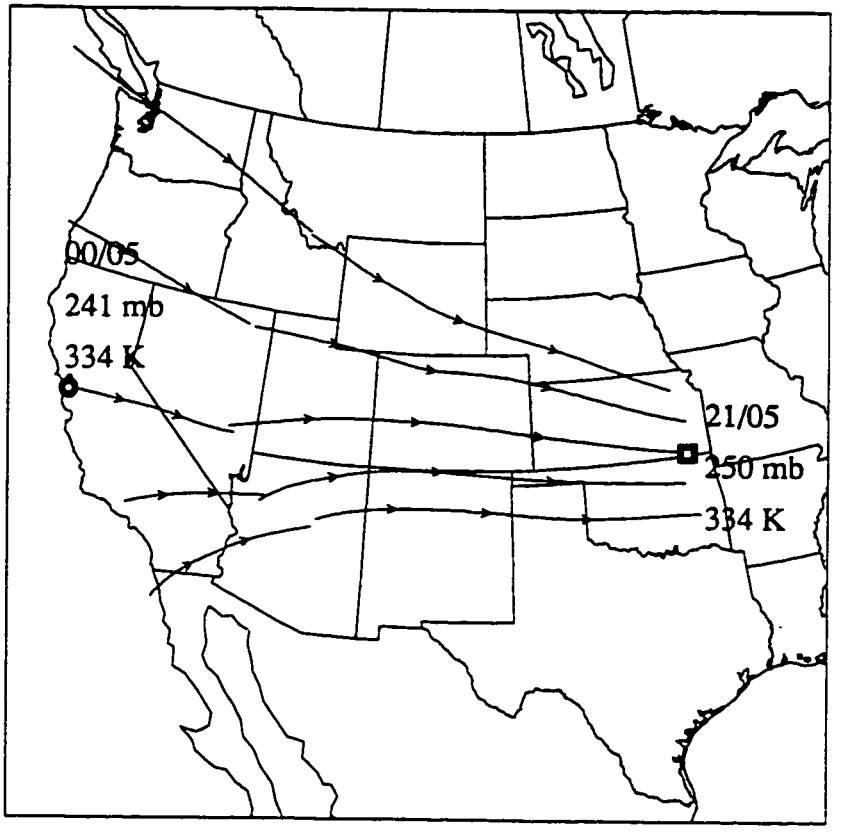


**Fig. 19:** Same as in Fig. 16 except for 250 mb. The trajectory arriving at COF at 250 mb and 334 K, nearly maintained its original pressure and temperature of 241 mb and 334 K.

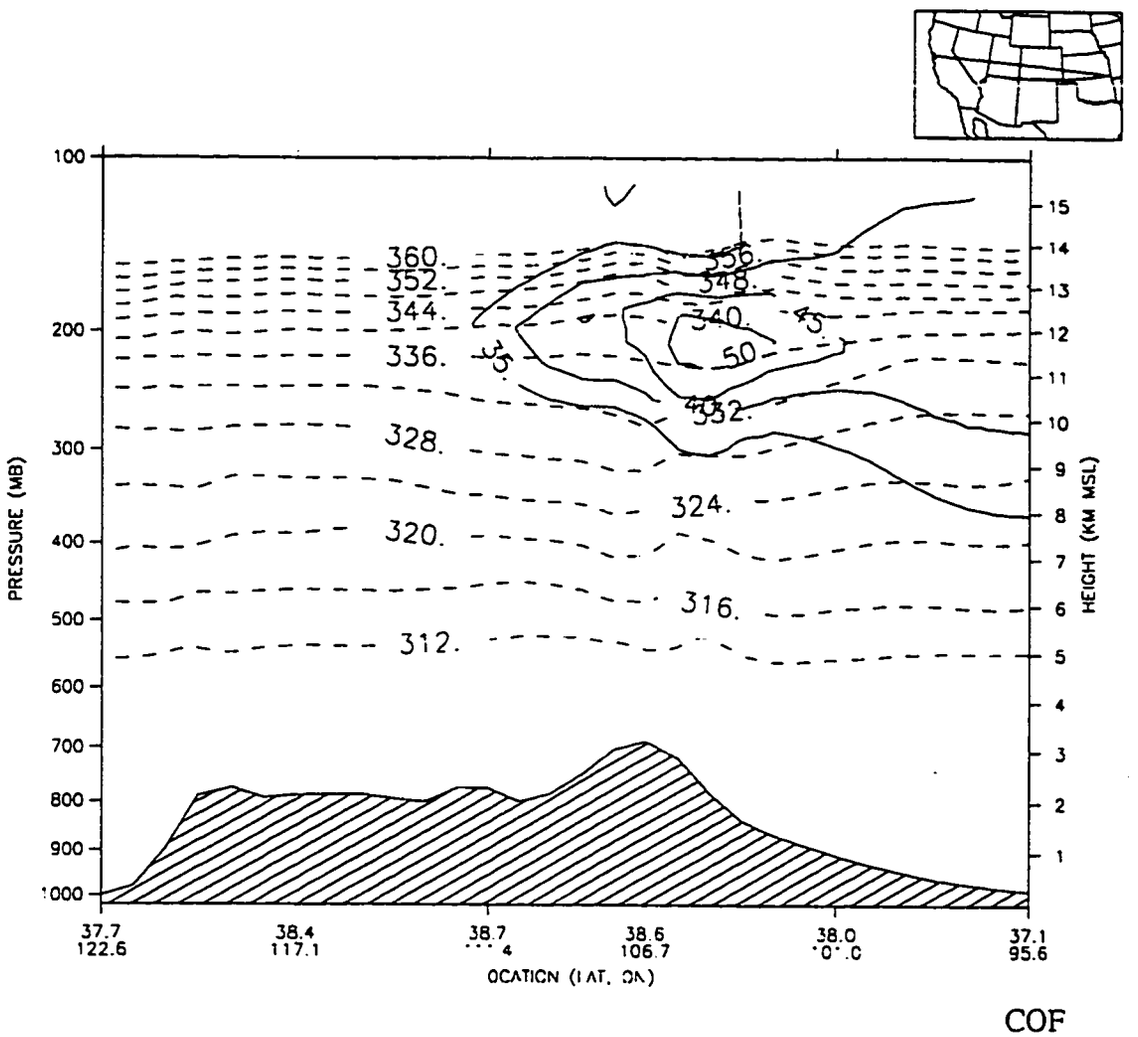


**Fig. 20a:** W-E cross section of MM4 horizontal winds (m $s^{-1}$; solid black lines) and potential temperature (K; dashed black lines contoured only from 312 to 360 K) at 00/05 along the line depicted in the upper right-hand map. This cross section approximates the path of the trajectory ending at COF, shown in Fig. 19.

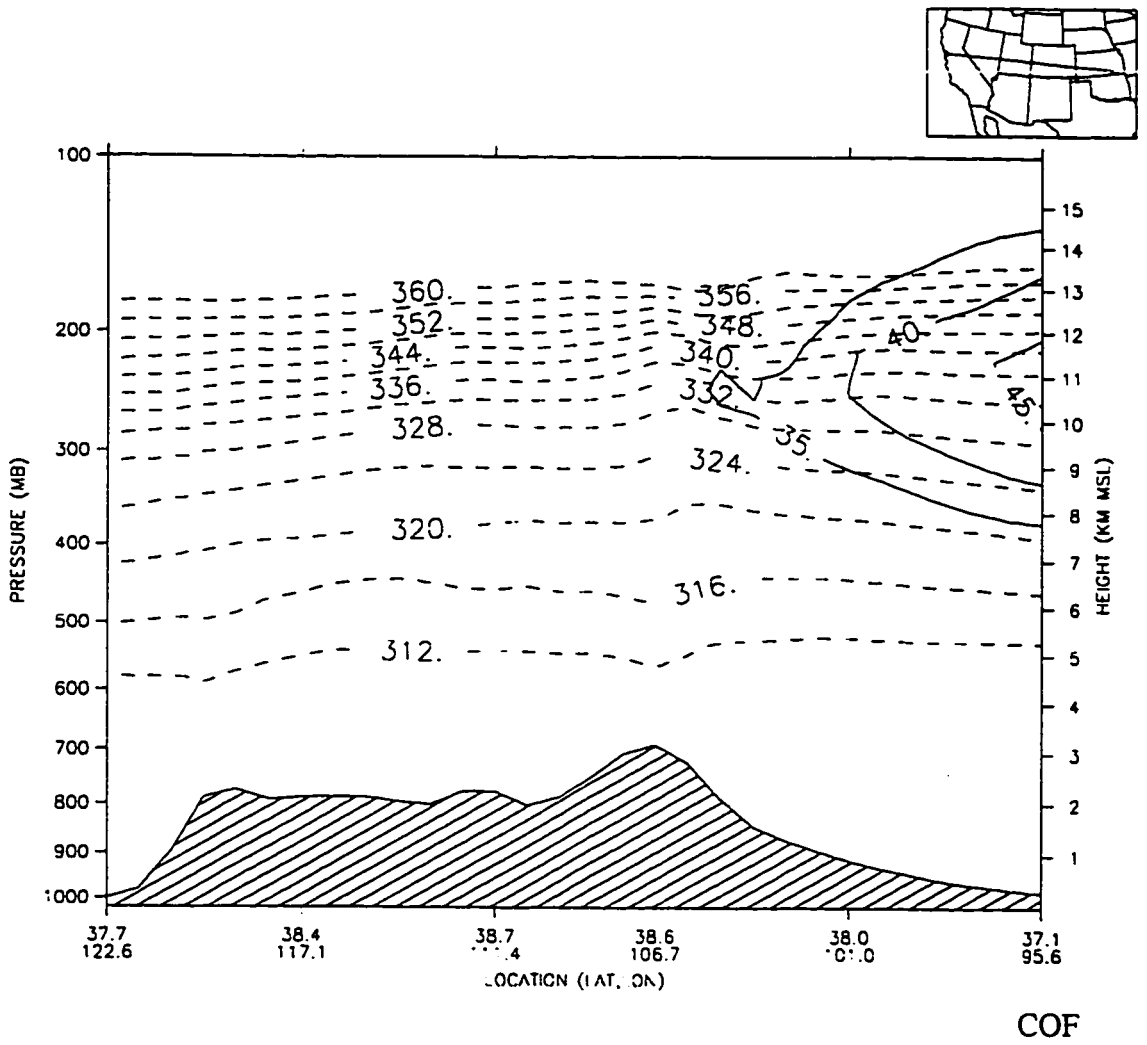


**Fig. 20 (cont.) b:** Same as in Fig. 20a except for 21/05.

upstream from the COF area 21 hours earlier near the stratosphere and made a general west to east trajectory during its journey to COF with little vertical movement.

To validate the MM4 simulation results, a comparison is again made with the trajectory endpoints using radiosonde data. Figure 21 shows a stuve diagram of two soundings, one at Oakland, CA (OAK) at approximately 00/05 and the other at COF at around 21/05. OAK is the closest radiosonde location in central CA that corresponds to the origin of the 250-mb back-trajectory. At OAK, the potential temperature at 241 mb is 334 K, and the tropopause is located directly above, in agreement with the MM4 simulation. At COF, the 334 K isentrope is found near 250 mb, also in fair agreement with the MM4 simulation.

Note, from Fig. 19, that parcels to the south of COF have a much more WSW-ENE trajectory. It is possible that some of the air parcels at levels near 250 mb over COF at 21/05 originated from a more WSW trajectory rather than just a W-E trajectory. Satellite and water vapor images, Fig. 2c and Fig. 22 respectively, support the fact that sub-tropical moisture encroached the COF area from the southwest U.S. during the time frame of this case study. It is likely that the core part of this moisture advected at high levels in the atmosphere over COF with the flow from the northwest sinking below it.

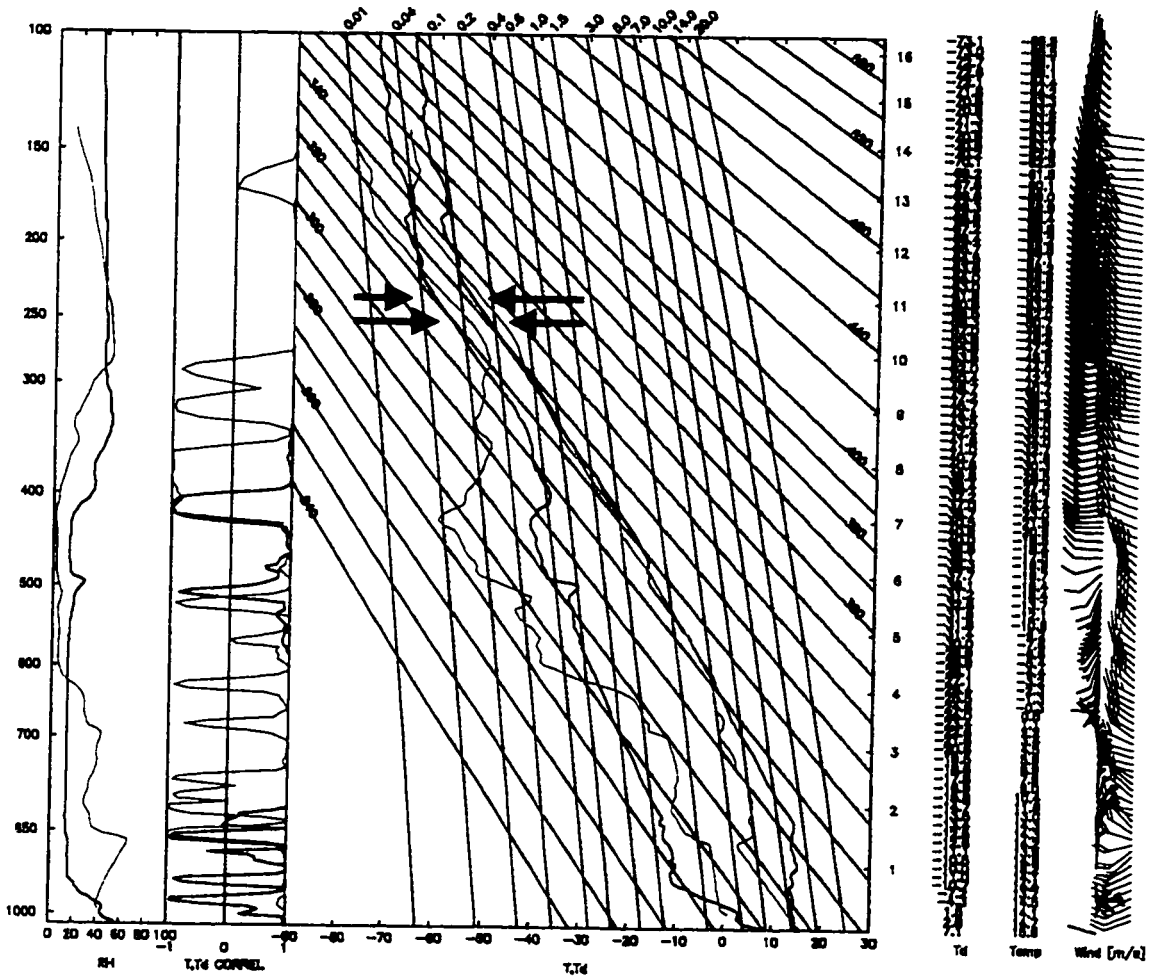

**Fig. 21:** Stuve diagram of radiosonde data at Oakland, CA (OAK) for 2301 UTC 4 December 1991 (bold black lines) and at COF for 2045 UTC 5 December 1991 (magenta lines). OAK represents the approximate origin of the 21-h, 250-mb COF trajectory. The layer between the thick black arrows represents the region of air moving nearly zonally, W-E from 241 - 250 mb.

**Fig. 22:** GOES water vapor imagery for 02/06.

We conclude that the back-trajectories, combined with the radiosonde data, provide sufficient evidence to show that the mid-tropospheric air over COF at 21/05 originated upstream in the northwestern U.S. and that the upper-tropospheric cirrus was advected from the west and southwest towards COF at around 250 mb. A look into the actual dynamics of the air parcels now gives more insight into this case study.

## 4.2 Dynamics

A series of MM4 diagnostics at 18/05 and 21/05 are given to show several dynamical footprints of the tropopause fold that is observed over COF at 21/05. Figures 23a, 23b show the progression of a 50 m $s^{-1}$ jet streak at 250 mb towards COF at 18/05 and 21/05, respectively. This jet streak originates upstream in the lee of the Rockies over northeastern Colorado (not shown). Recall that the trajectory path ending at COF at both 18/05 and 21/05 are westerly around COF (Figs. 23a, 23b). By 21/05 the jet is elongated with a distinct jet entrance region located in west-central KS, as evidenced by the large wind gradient.

Figure 24a shows a cross section of potential vorticity, winds, and potential temperature along the jet streak at 18/05. A lobe of 1 PVU extends down to just below 10 km to the west-northwest of COF (located at the right most point in the cross section), indicating the beginnings of a tropopause fold. Notice the tightening of the potential

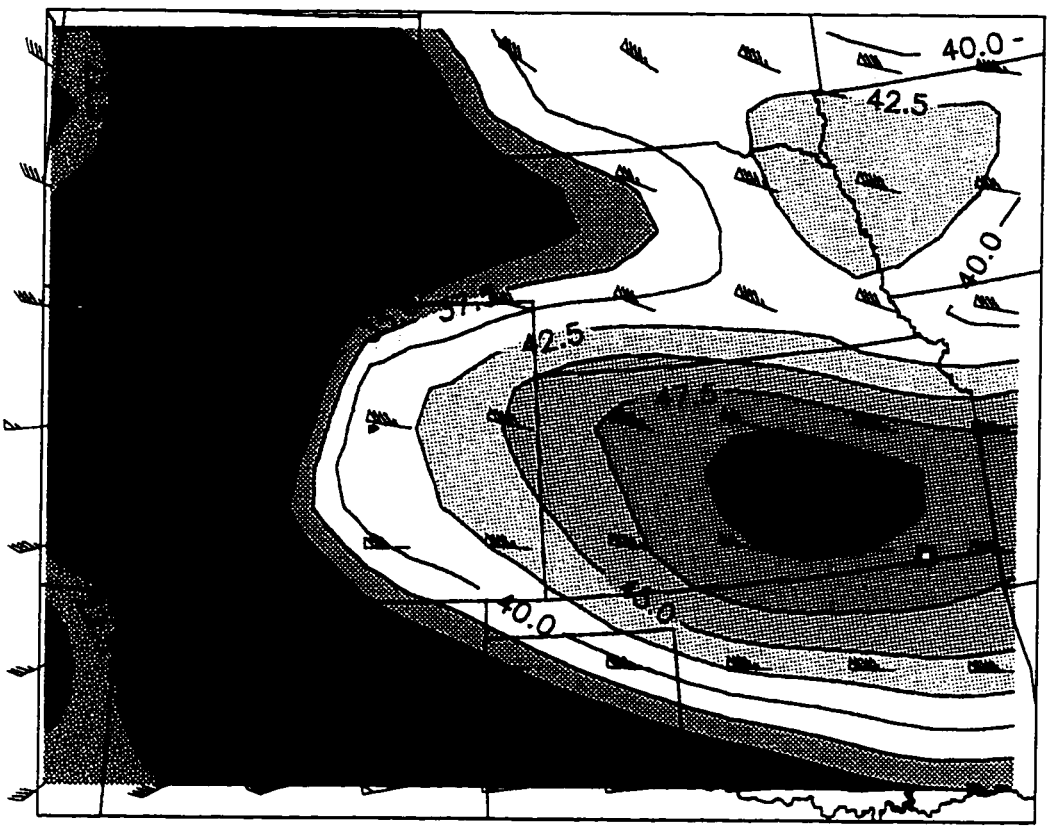


**Fig. 23a:** 250-mb MM4 horizontal winds (m $s^{-1}$; black lines separated by shaded areas, kts; red wind barbs) at 18/05 near the vicinity of COF.

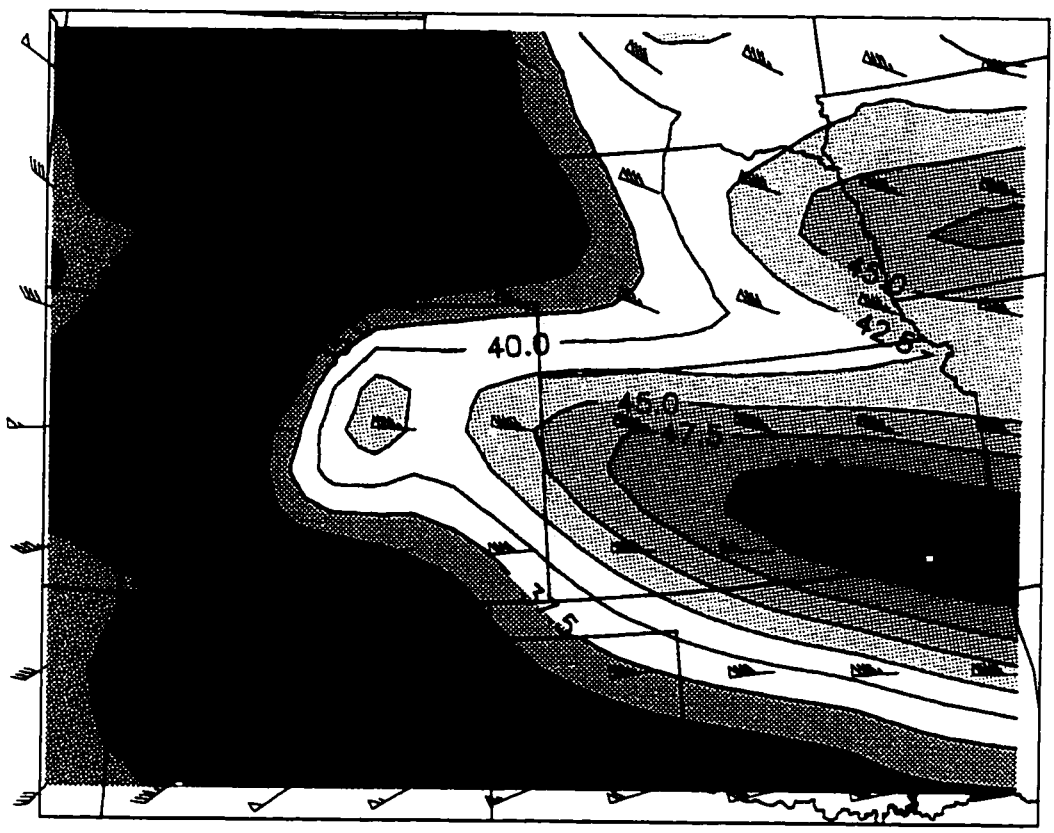


**Fig. 23 (cont.) b:** Same as in Fig. 23a except for 21/05.

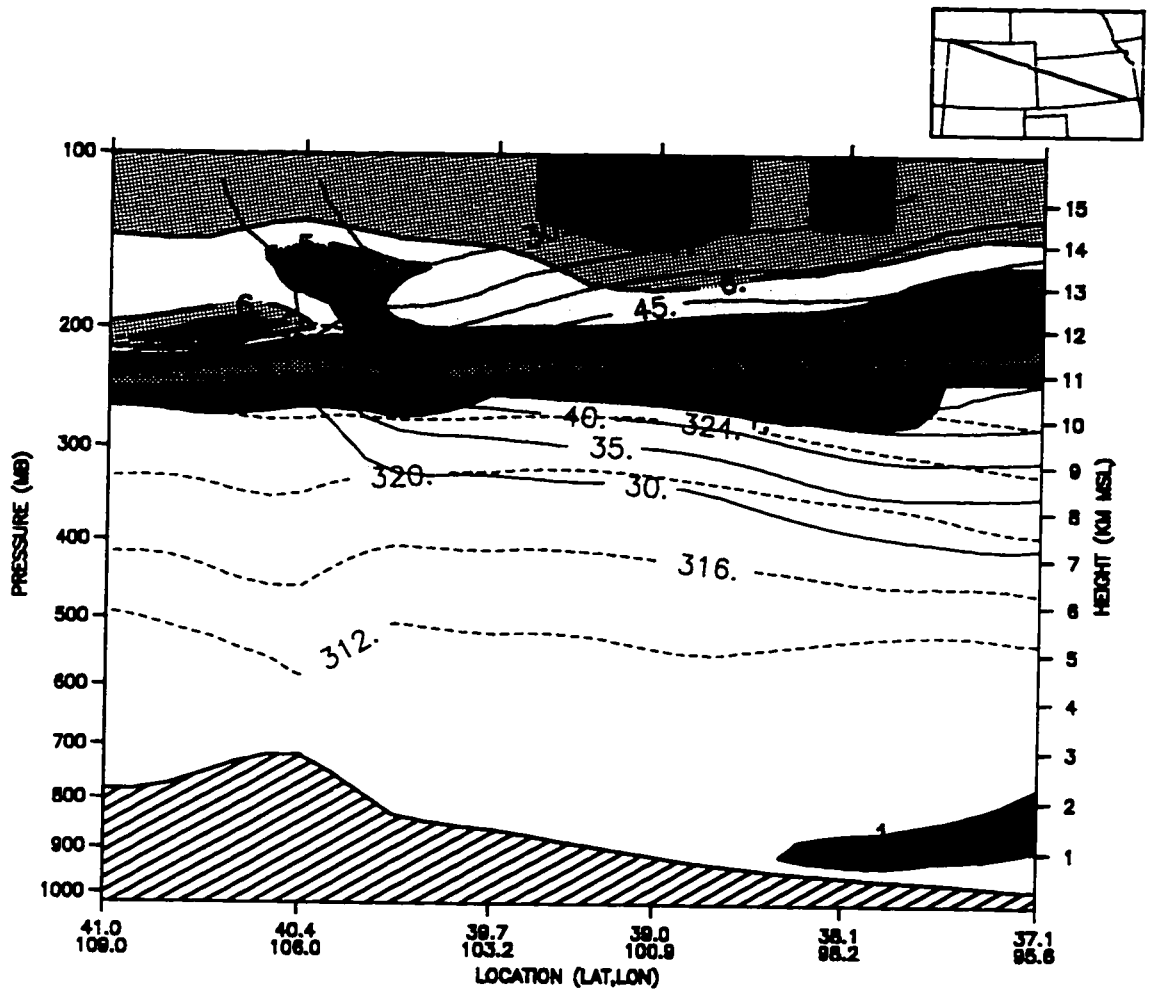


**Fig. 24a:** WNW-ESE cross section of MM4 potential vorticity (PVU; solid black lines separated by shaded areas), horizontal winds (m $s^{-1}$; solid red lines) and potential temperature (K; dashed red lines contoured only from 312 to 340 K) at 18/05 along the line depicted in the upper right-hand map. This cross section is along the jet axis shown in Figs. 23a, 23b.

temperature gradient in this region between 324 K and 328 K. This is a statically stable stratospheric layer beginning to descend into the troposphere. As Eq. (2.1) indicates, where we see larger potential temperature gradients we will see larger potential vorticity. This is easily seen in Fig. 24a by looking at the very stable layers above 332 K and their associated high potential vorticity values of 4 - 8 PVU. By 21/05 (Fig. 24b), we see that the lobe of 1 PVU is now elongated and has descended to 9 km at COF. Notice how the potential vorticity extrusion wraps around the 50 m $s^{-1}$ jet streak in the cross section. This is much like the classic tropopause fold shown in Fig. 8.

In order for a stratospheric extrusion to take place, one would expect to see strong sinking motion somewhere along the jet streak. Figures 25a, 25b show a cross section of vertical velocity along the jet streak at 18/05 and 21/05, respectively. In the atmospheric layers near COF, beneath the 1 PVU area, the vertical velocity pattern is downward or negative. In order for the 1 PVU area to descend 1 km in 3 hours (as was the case from 18/05 to 21/05) the downward vertical velocity would have to average 9 - 10 cm $s^{-1}$. At these two instances in time, the downward vertical velocities are between 5 - 10 cm $s^{-1}$. This indicates that the vertical velocity patterns look consistent with the amount of potential vorticity being extruded.

We see that the dynamics are in place at the expected time to cause the tropopause fold, and that the primary signature of a tropopause fold, an extrusion of potential

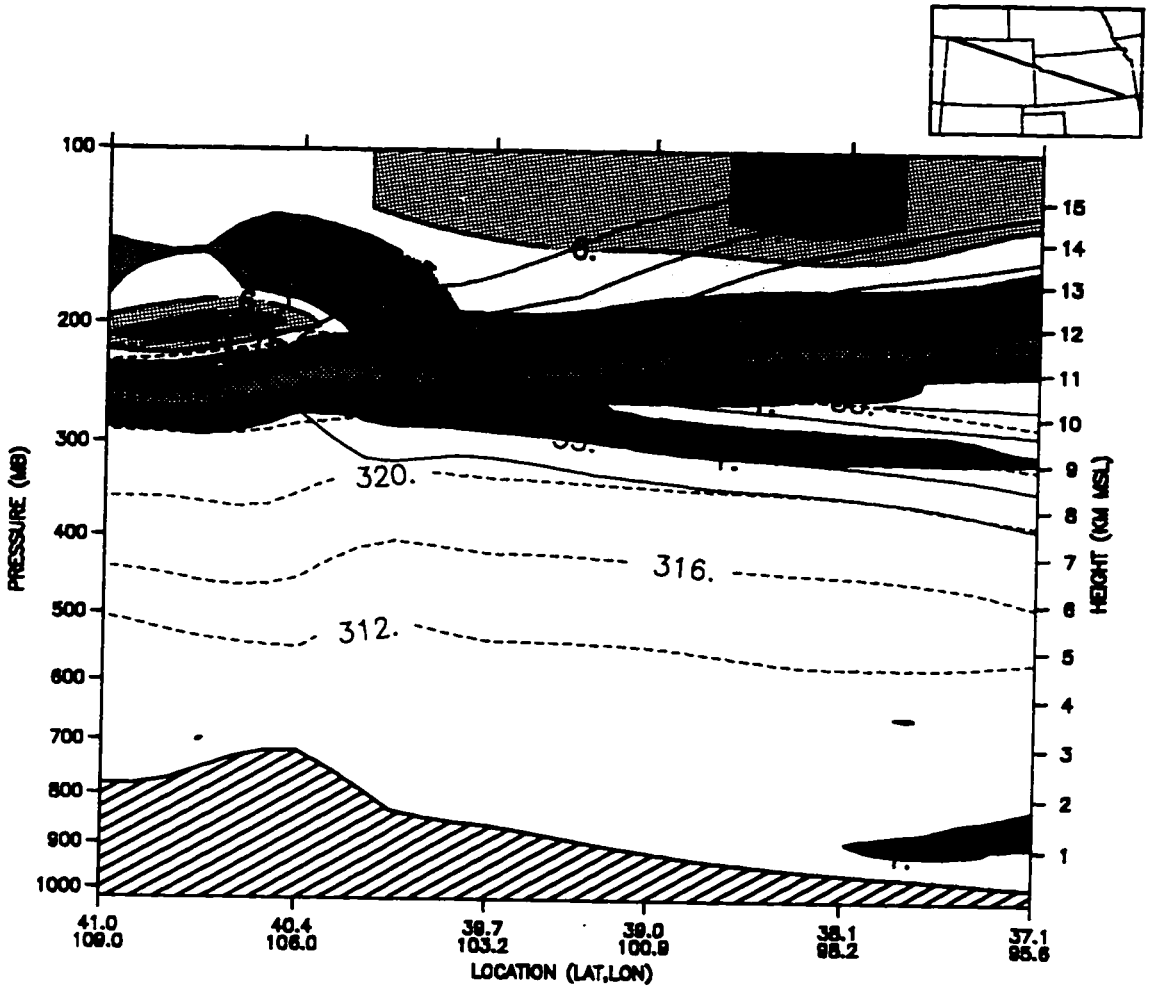


**Fig. 24 (cont.) b:** Same as in Fig. 24a except for 21/05.

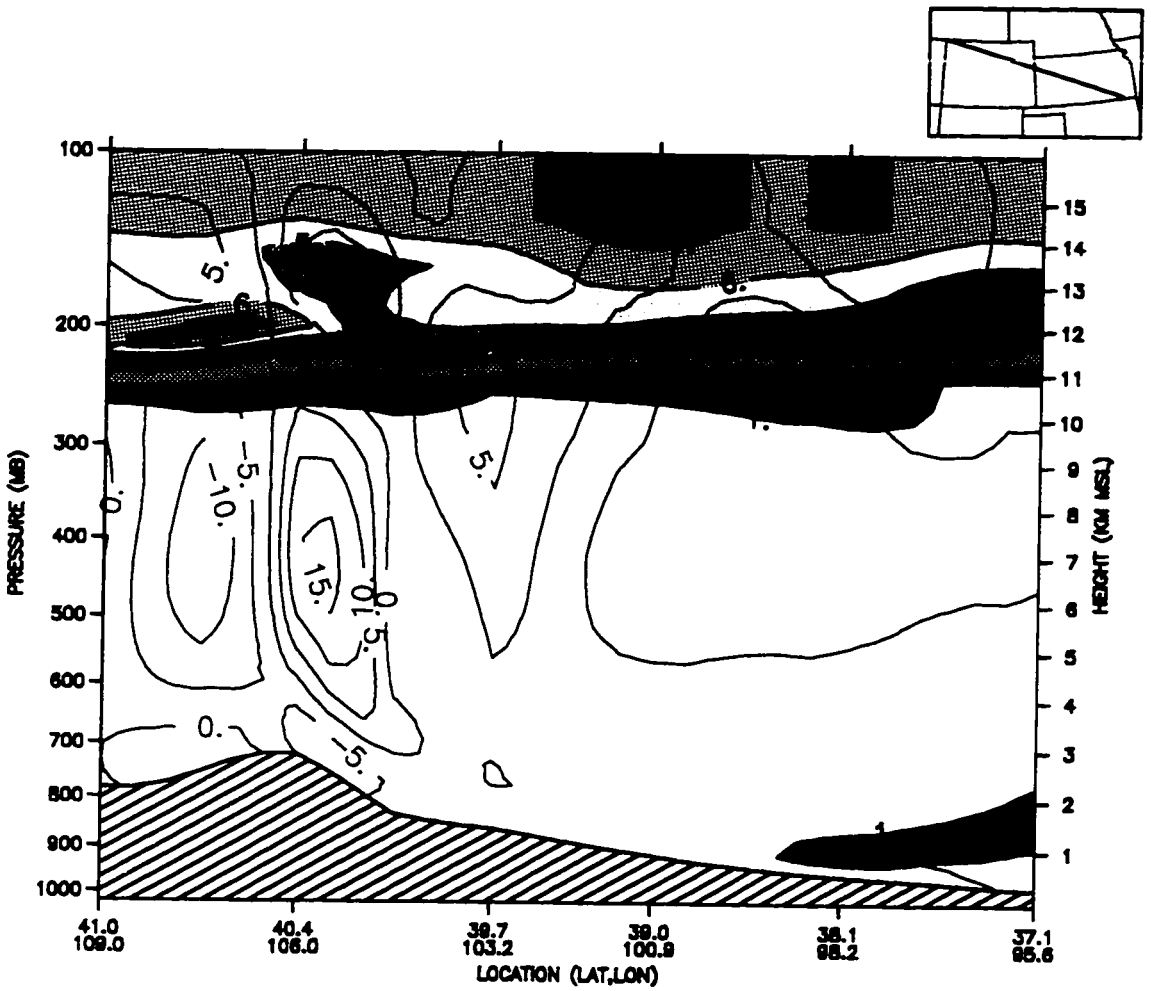


**Fig. 25a:** WNW-ESE cross section of MM4 potential vorticity (PVU; solid black lines separated by shaded areas) and vertical velocity (cm $s^{-1}$; solid red lines) at 18/05 along the line depicted in the upper right-hand map.

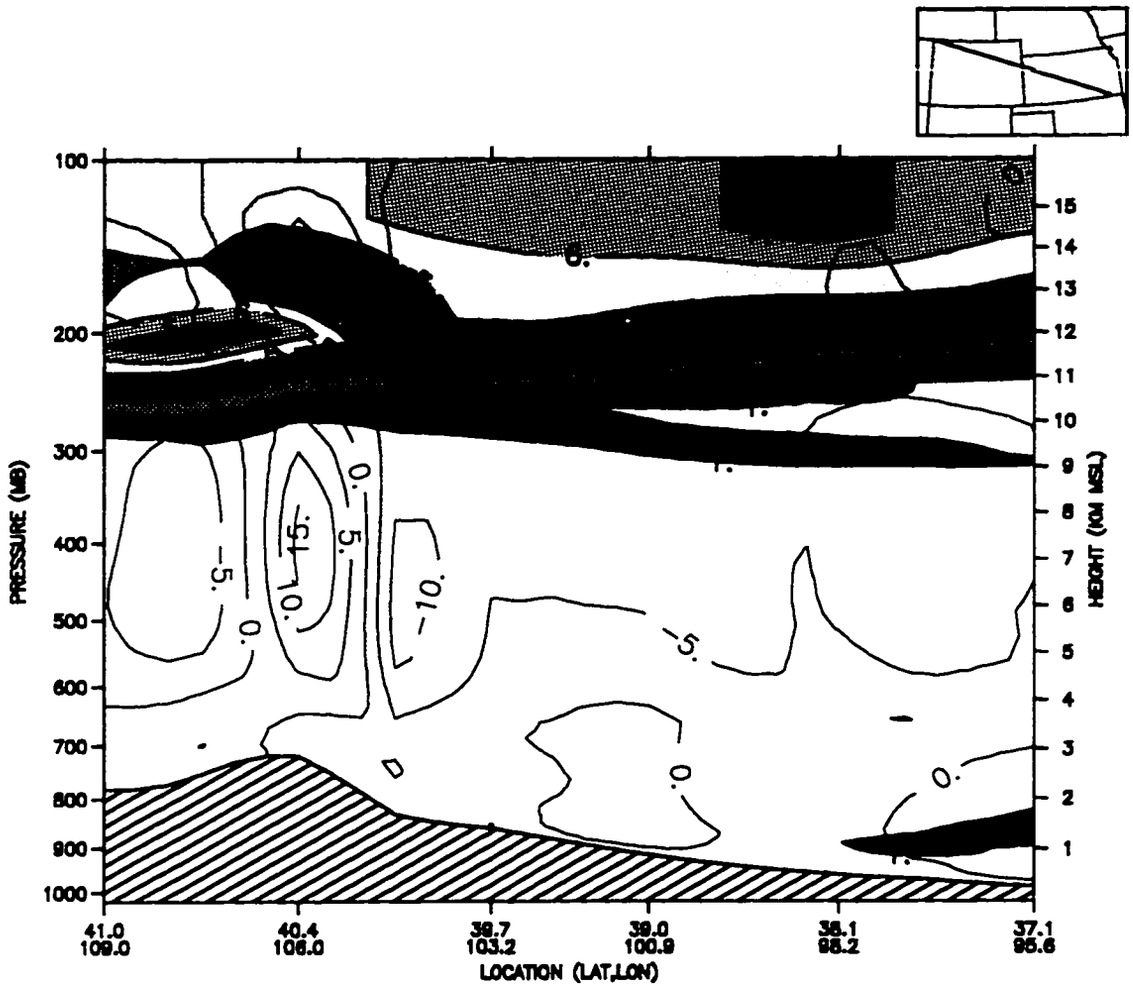


**Fig. 25 (cont.) b:** Same as in Fig. 25a except for 21/05.

vorticity, did exist. The quasi-geostrophically induced vertical motions are now examined to see how they compare with the vertical velocity fields. This provides an opportunity to see the exact location of jet streak-induced sinking and rising motions that lead to tropospheric folds.

Figure 23b shows that the jet streak is primarily from west to east at 21/05 and is essentially straight. Recall that Barnes and Colman (1993) said that one could analyze the vertical motions around a straight jet streak by diagnosing the divergence of **Q**-vectors. Figures 26a, 26b show the divergence of the **Q**-vector pattern around the jet entrance region over the KS/OK area at 18/05 and 21/05, respectively. An area of sinking motion is seen just to the left of the jet entrance region in north-central KS during this time frame. Correlating the QG-induced vertical motion with the vertical velocity, Fig. 27 shows a cross section of vertical velocity across the jet streak. Note that to the left in Fig. 27 (which is north of the jet streak), the downward vertical velocity is roughly 6 - 10 cm $s^{-1}$ at jet level, while to the right (which is south of the jet streak), the vertical velocity is upward between 1 - 6 cm $s^{-1}$ . This shows that the QG-induced vertical motion is positively correlated with the vertical velocity field. Recall that the QG-induced vertical motion is due to geostrophic forcing alone. One would expect to see this positive correlation; however, this QG approach alone does not show all vertical motion activity. In order to diagnose the vertical motion due to ageostrophic forcing, the Sawyer-Eliassen approach discussed by Keyser and Shapiro (1986) could be used.

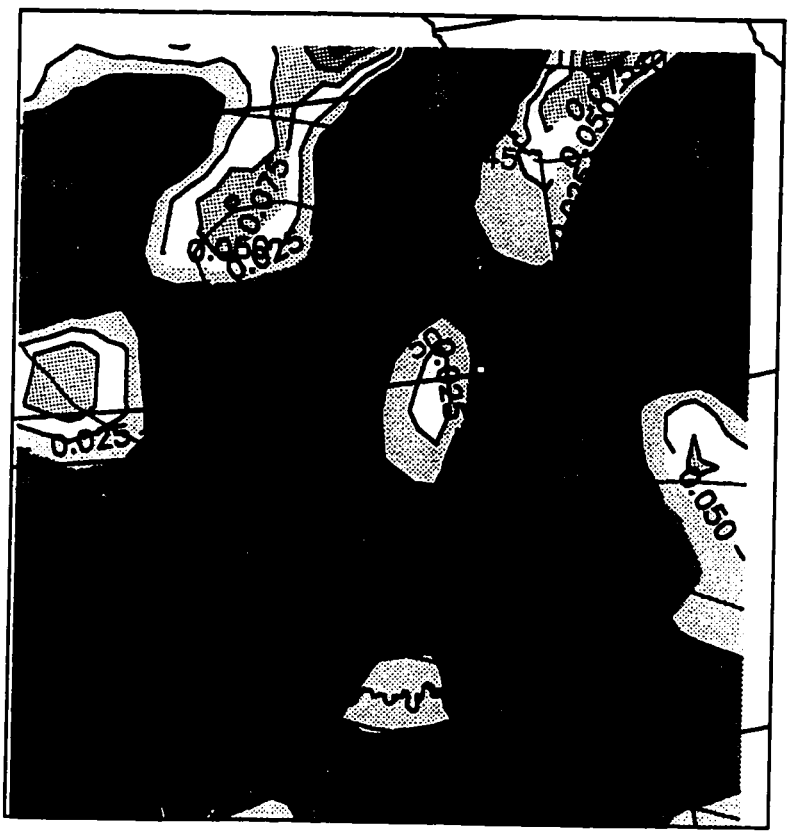

**Fig. 26a:** 250-mb MM4 divergence of geostrophic **Q**-vector ($10^{-15}$ m kg$^{-1}$ s$^{-1}$; solid black lines separated by shaded areas; positive/negative [yellow/blue-green] values represent sinking/rising motion) and horizontal winds (m s$^{-1}$; solid red lines) at 18/05 near the vicinity of COF.

**Fig. 26 (cont.) b:** Same as in Fig. 26a except for 21/05.

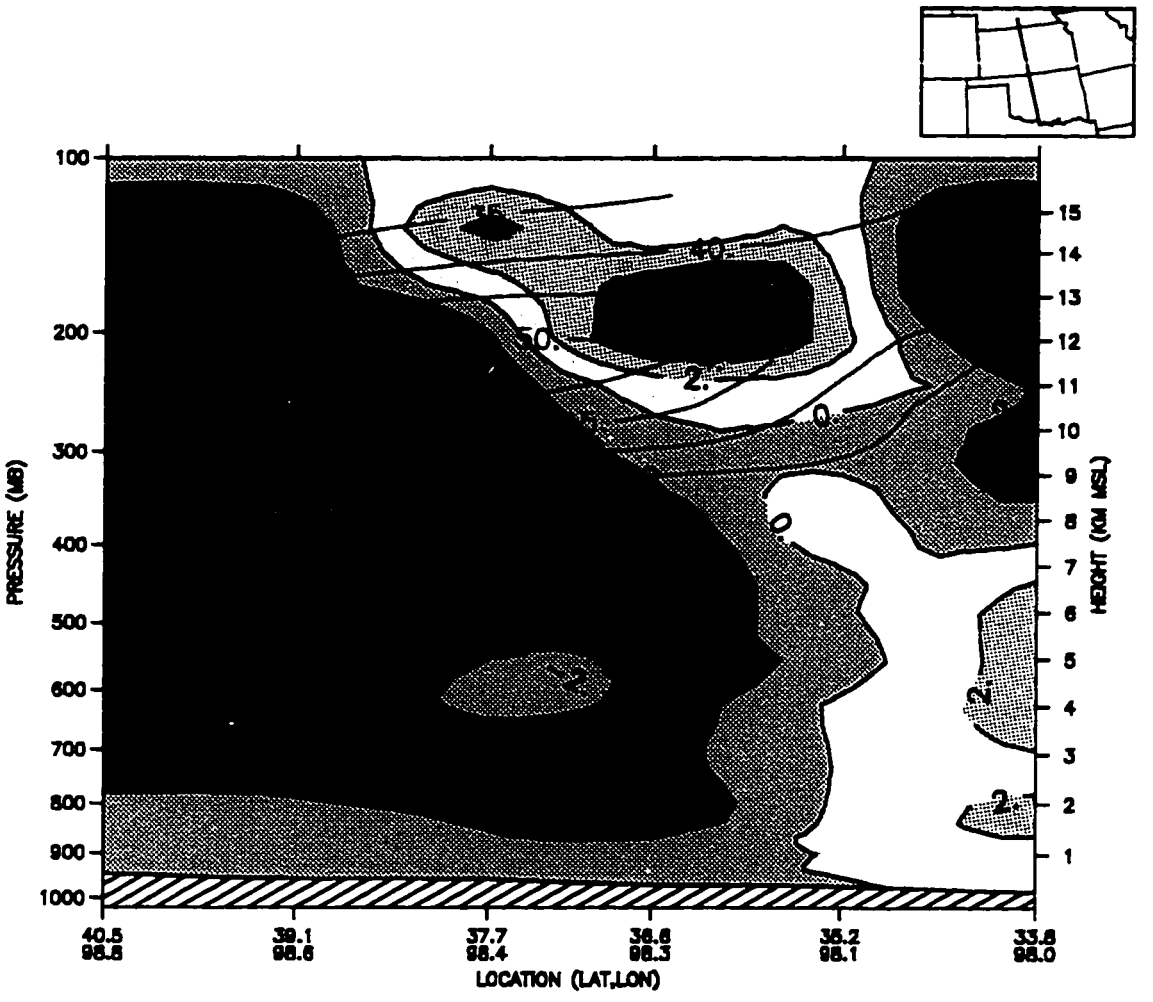


**Fig. 27:** N-S cross section of MM4 vertical velocity (cm $s^{-1}$; solid black lines separated by shaded areas) and horizontal winds (m $s^{-1}$; solid red lines) at 18/05 along the line depicted in the upper right-hand map.

It is concluded that the MM4 simulation is producing realistic motion fields, and that the fold was induced by this weak jet streak. Therefore, Sassen *et al. 's* (1995) claim that stratospheric ozone and aerosols were mixed down into the troposphere along a tropopause fold is substantiated with this MM4 simulation initialized with MAPS data. We will now examine the extent of the mass exchange during this fold event and extrapolate the global effects of ST mass exchange based upon our results.

## 4.3 Mass Exchange

As was the case for diagnosing the dynamics of this case study, the same MM4 simulation is used to diagnose the mass exchange associated with this fold event. ST mass exchange associated with the tropopause fold in this case study is expected to have begun northwest and west of the COF area based upon the back-trajectories shown in Fig. 16 and Fig. 19, respectively. The MM4 simulation of mean upper-tropospheric humidity (UTH; averaged over a layer between 200 and 500 mb) substantiates this claim. Figure 28 shows that between 09/05 and 15/05, UTH values dropped up to 35% across most of NB and northern KS, showing that drier air advected over the area from the north and west. Low UTH values (20-40%; also averaged over a layer between 200 and 500 mb) from Soden (1991), and shown in Figs. 29a, 29b, 29c, and 29d, lend further support to this theory by showing that between 15/05 and 00/06 dry stratospheric air advected from southwest NB

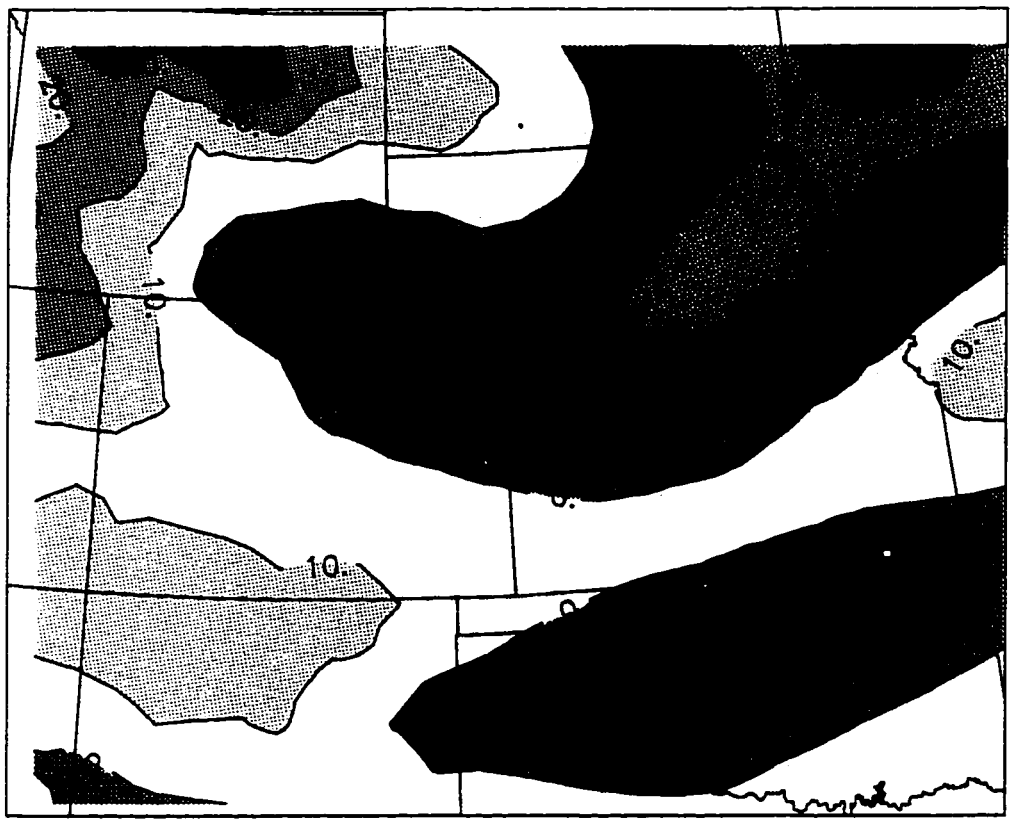


**Fig. 28:** Differences (%) of MM4 UTH between 15/05 and 09/05.

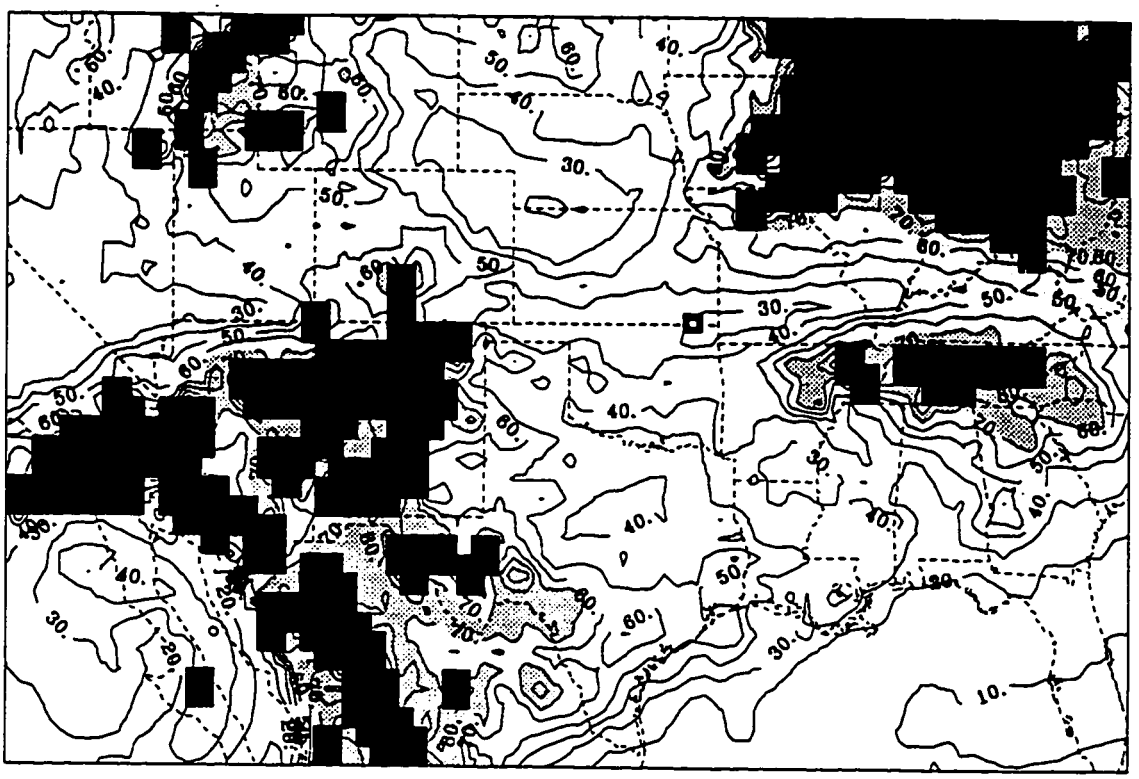

**Fig. 29a:** GOES-derived UTH (%) for 15/05. (From Soden, 1991).

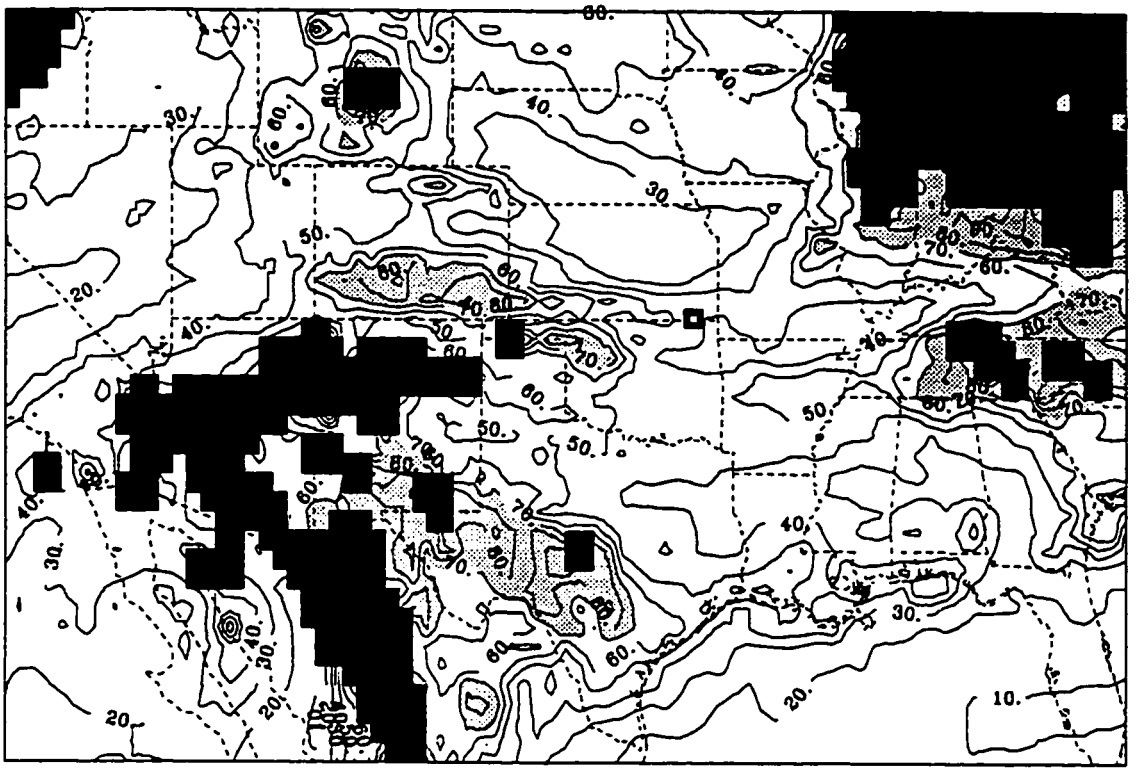

**Fig. 29 (cont.) b:** Same as in Fig. 29a except for 18/05.

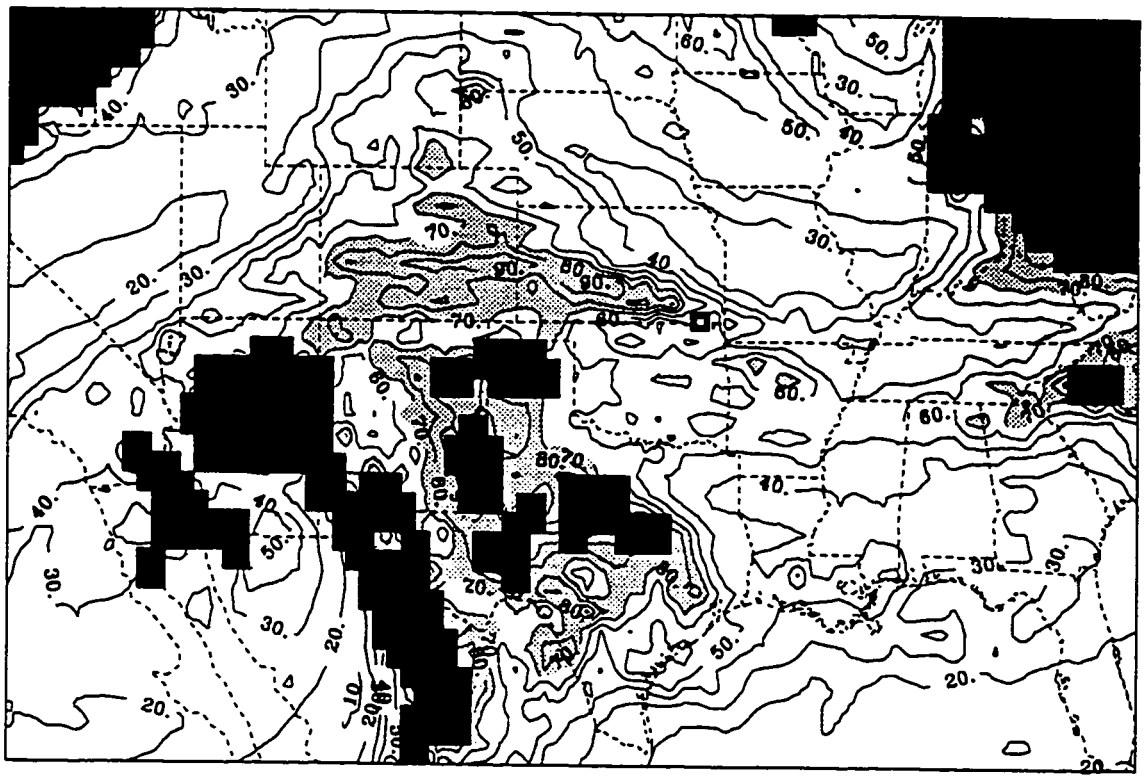

**Fig. 29 (cont.) c:** Same as in Fig. 29a except for 21/05.

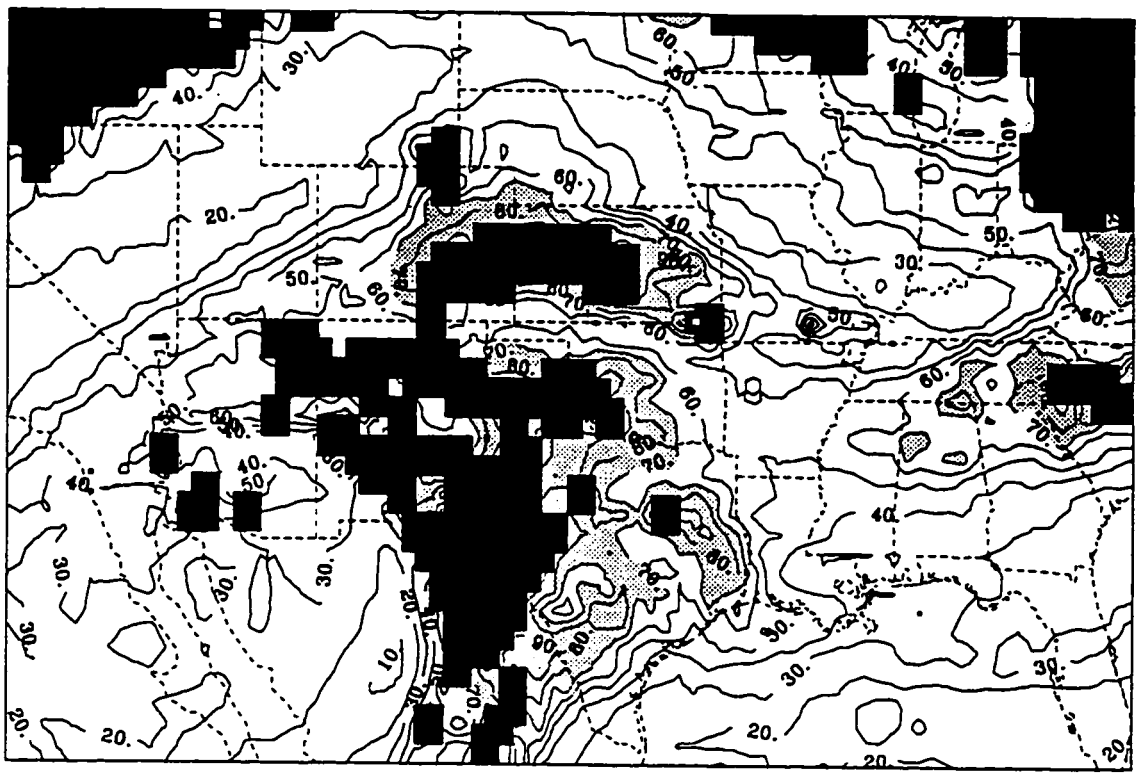

**Fig. 29 (cont.) d:** Same as in Fig. 29a except for 00/06.

over northern KS and then to the east. Recall that radiosonde data (Fig. 18), showed that the air ending at 250 mb at COF had descended nearly 2.5 km in 21 hours. This sinking motion occurred along a path through the NB/KS area, and is well correlated with the drier air advecting over the area.

Figures 30a, 30b, 30c, and 30d show successive 3-hourly contours of positive ST mass flux (kg $m^{-2}$ $s^{-1}$) and winds (m $s^{-1}$) in the COF vicinity from 15/05 through 00/06. For comparison purposes, the vertical level shown in Figs. 30a, 30b, 30c, and 30d is the one of closest proximity to the 250-mb pressure level shown in Figs. 23a, 23b, as evidenced by the similarity in the jet streaks at like times. The area of positive ST mass flux of interest to this study is contained within the thick black-boxed outline primarily along the cyclonic side of the jet in Figs. 30a, 30b, 30c, and 30d. This result correlates positively with the findings of Ebel *et al.* (1991), where in their model simulation, the intrusion of stratospheric air occurs mainly through the lateral northern boundary of the fold. The core area of mass flux moves southeastward into KS at 18/05 and 21/05 and then begins to move east of KS by 00/06. This area of ST mass flux is positively correlated with the dry area seen in the Soden (1991) UTH data (Figs. 29a, 29b, 29c, and 29d), and the MM4 simulation (Fig. 28).

The total mass exchange associated with this fold event is estimated by using Eq. (2.12). First, the instantaneous fluxes at 18/05 - 00/06 are determined by numerically

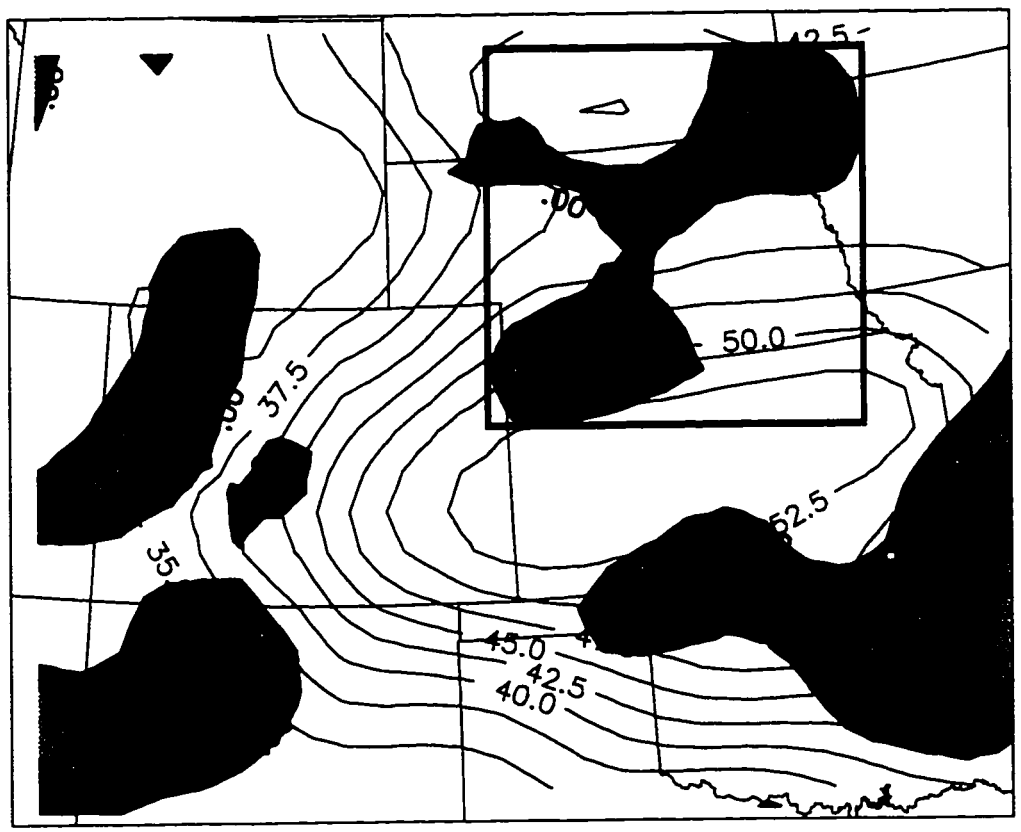


**Fig. 30a:** MM4 positive ST mass flux (kg $m^{-2}$ $s^{-1}$; black lines separated by shaded areas) and horizontal winds (m $s^{-1}$; solid red lines) at 15/05 near the vicinity of COF. The thick black box represents the area of mass flux associated with the tropopause fold being studied.

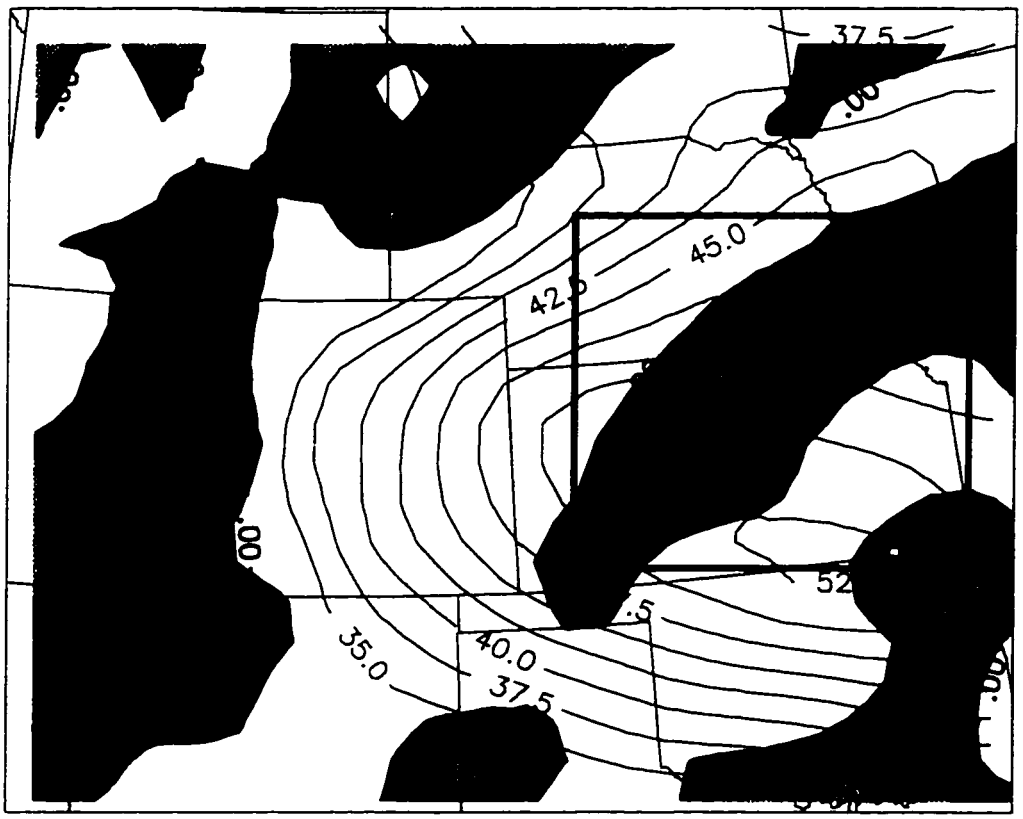


**Fig. 30 (cont.) b:** Same as in Fig. 30a except for 18/05.

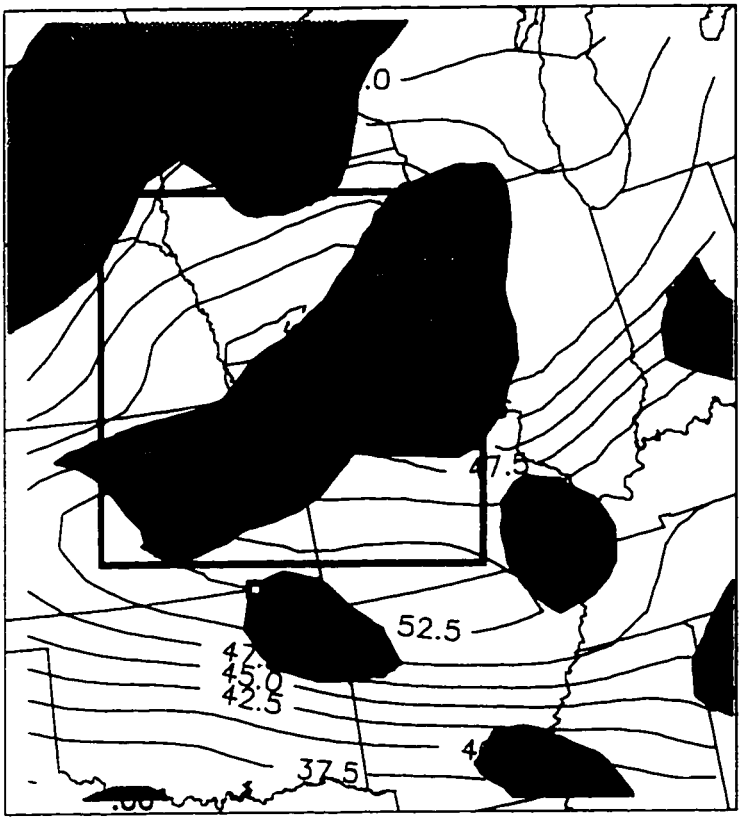


**Fig. 30 (cont.) c:** Same as in Fig. 30a except for 21/05.

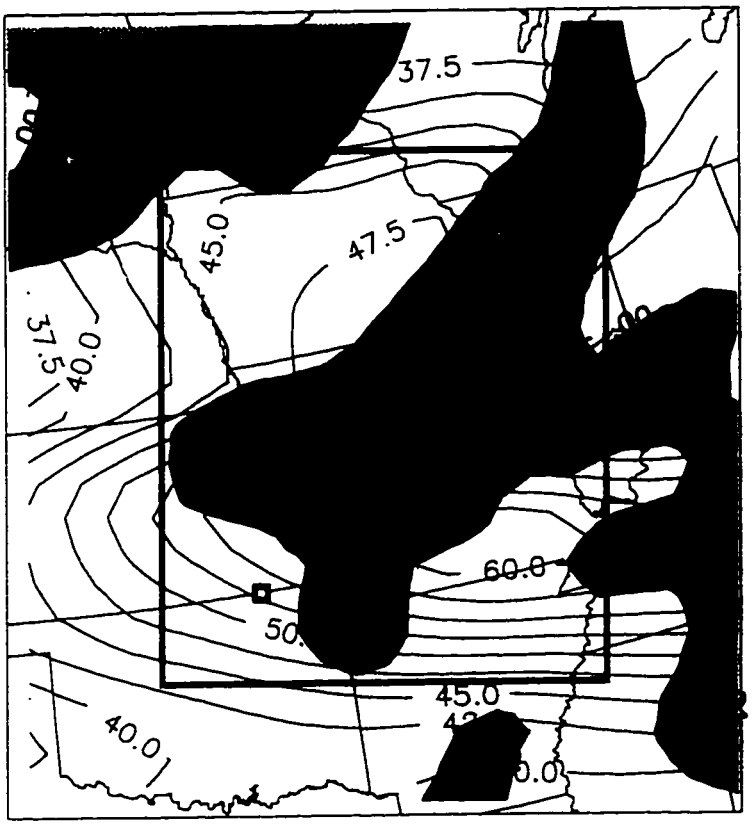


**Fig. 30 (cont.) d:** Same as in Fig. 30a except for 00/06.

integrating $F(\rho)da$ over the area of positive exchange within the thick black box in Figs. 30a, 30b, 30c, and 30d. Note that the box does not perfectly enclose the area of positive exchange. This error is assumed to be insignificant in the calculation of the overall mass exchange associated with this tropopause fold. Second, assuming a constant mass flux equal to these instantaneous values over a 3-h interval, the total ST mass exchange is estimated to be $1.13 \times 10^{14}$ kg over a 12-h period. Results are summarized in Table 3. Multiplying this result by $2000 \pm 500$ (the estimate of the number of weak baroclinic waves associated with weak tropopause fold events over the Northern Hemisphere per year), yields estimated annual mass exchange results ranging from $1.70 \times 10^{17}$ to $2.83 \times 10^{17}$ kg. Table 4 shows how these results compare with other recent studies involving stronger tropospheric fold events. The wide range of estimates illustrates the relatively limited knowledge of the ST mass exchange process.

These results, based on a single case study, indicate weak tropopause folds may have a substantial effect on the ST mass exchange process. The results also indicate that they are worthy of continued research in order to fully understand their impact on microphysical cloud processes, as elaborated on in the introduction to this thesis.

**Table 3:** MM4 simulated 3-h ST mass exchange (kg) associated with the tropopause fold near the vicinity of COF between 15/05 and 00/06, except as noted.

| Model Time | Exchange Rate ($10^9$ kg $s^{-1}$) $\int_A F(\rho)da$ | Time ($10^4$ s) ($t$) | Total Mass Exchange ($10^{13}$ kg) $= TME$ |
|---|---|---|---|
| 15/05 | 1.03 | 1.08 | 1.11 |
| 18/05 | 2.68 | 1.08 | 2.89 |
| 21/05 | 2.41 | 1.08 | 2.60 |
| 00/06 | 4.35 | 1.08 | 4.70 |
| Total | | | 11.3 |
| 06/03* | 3.60 | | |

*Exchange rate for tropopause fold case study over Texas at 06/03.

**Table 4:** Annual mid-latitude cross-tropopause mass flux estimates for the Northern Hemisphere, except as noted. Adapted from Follows (1992).

| Source of estimate | Basis of estimate | Mass Flux ($10^{17}$ kg $yr^{-1}$) |
|---|---|---|
| Reiter (1975) | Analysis of the mean meridional circulation and extrapolation from observations of tropopause fold events | 2.3 |
| Danielsen and Mohnen (1977) | Extrapolation from observations of tropopause folding events | 3.7 |
| Holton (1990) | Calculation via the "downward control" method using data from Oort (1983) | 1.33 |
| Rosenlof and Holton (1993) | Revision of Holton (1990) using United Kingdom Meteorological Organization data with more data levels in the stratosphere than Oort (1983) | 1.53 |
| Hoerling *et al.* (1993) | Calculation via both a thermal and dynamic tropopause boundary using mass flux theory from Wei (1987) | 0.6* |
| This paper (1996) | Extrapolation from MM4 model output based on MAPS input data using a thermal tropopause boundary | 1.7 - 2.8 |

* Estimate for January 1979 only, 25-50°N.

## 4.4 Evolution of the Potential Vorticity Extrusion

As Danielsen (1968) discussed, the primary signature of a tropopause fold, a potential vorticity extrusion, should be seen wrapping underneath the cyclonic side of a jet streak. Figures 31a, 31b, 31c, and 31d show potential vorticity and winds at 3-h intervals between 15/05 and 00/06 in a cross section across the jet streak area shown in Figs. 30a, 30b, 30c, and 30d, respectively. Notice at 15/05 and 18/05 the 1 PVU area extends down to below 300 mb, but it is not until 21/05 and 00/06 that the extrusion takes on the tongue-shaped signature of a tropopause fold and wraps underneath the 50 - 60 m $s^{-1}$ jet streak. In combination with the results just shown, it appears that the mass exchange occurs upstream to the west-northwest of where the primary fold signature is seen. Recall that the mass exchange is defined at a tropopause boundary when a certain critical stability is reached. Any mass sinking below this boundary accounts for ST mass exchange. The lag that is seen between the mass exchange and the primary signature of the fold indicates that a sufficient amount of time and downward motion is required before the potential vorticity extrusion forms its characteristic shape.

These results show that the ST mass exchange took place to the west-northwest of the where the tropopause fold occurred approximately 3-6 hours before the potential vorticity extrusion became obvious over the COF area. Additionally, the mass exchange results were significant in magnitude when compared with previous studies. This research

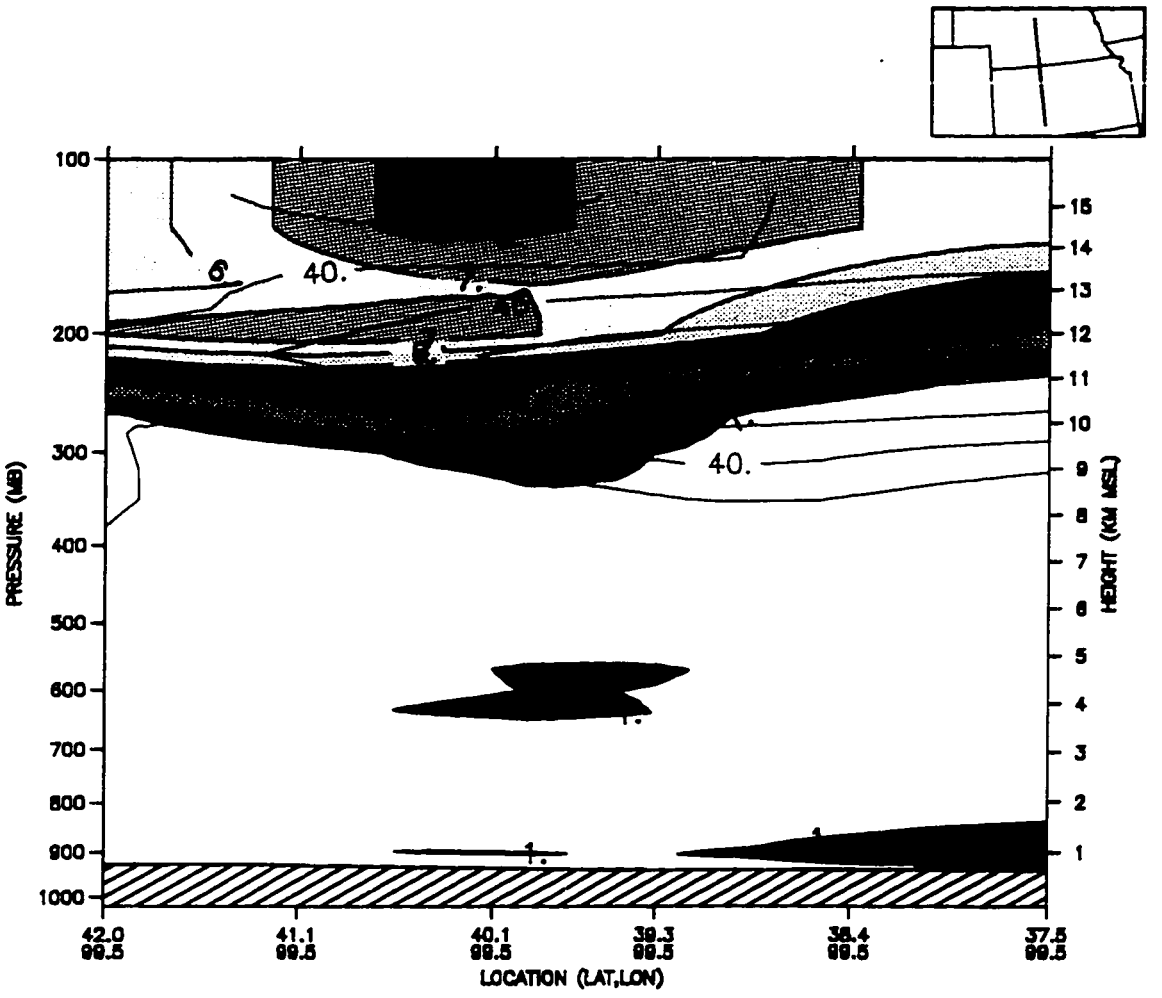


**Fig. 31a:** N-S cross section of MM4 potential vorticity (PVU; solid black lines separated by shaded areas) and horizontal winds (m $s^{-1}$; solid red lines) at 15/05 along the line depicted in the upper right-hand map.

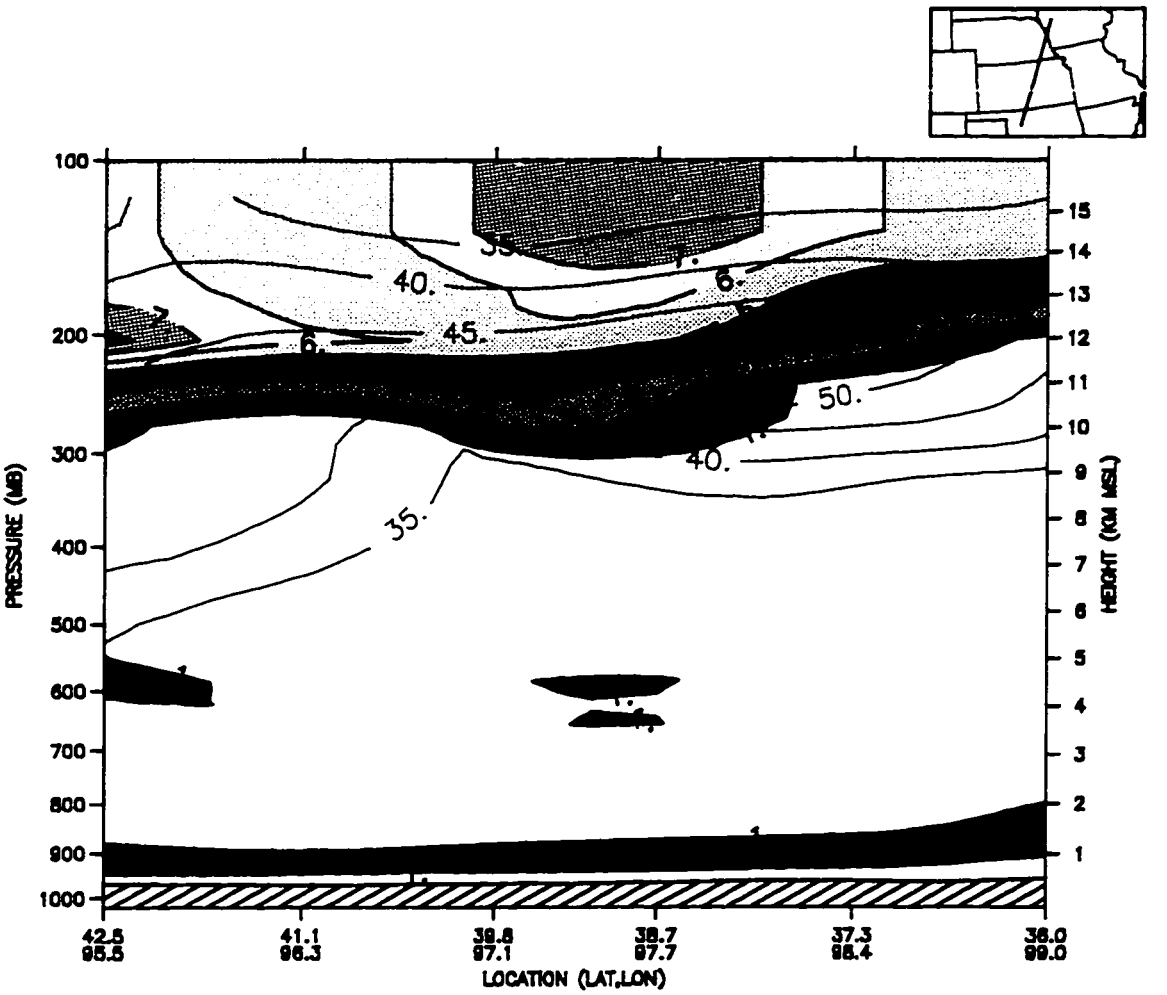


**Fig. 31 (cont.) b:** Same as in Fig. 31a except for 18/05.

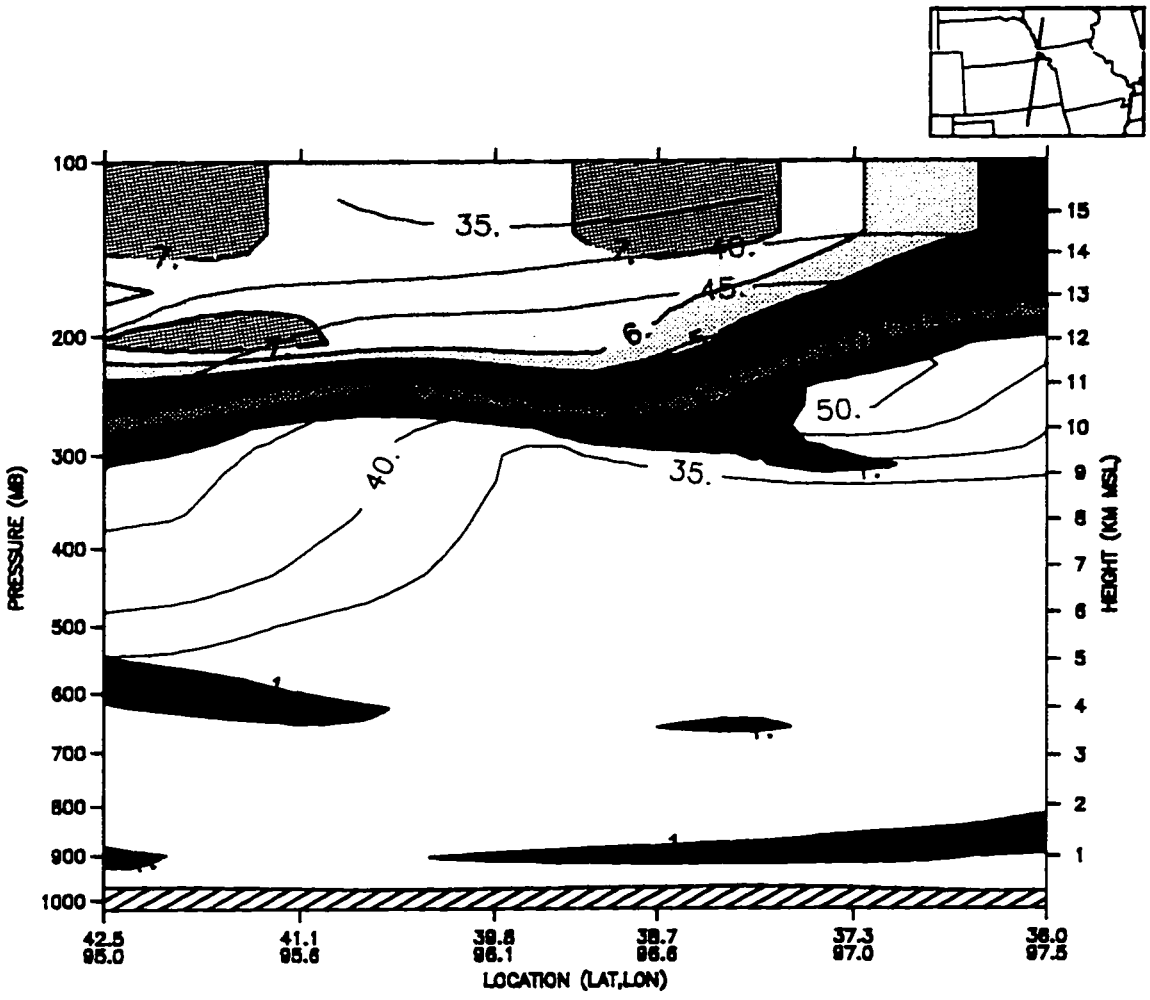


**Fig. 31 (cont.) c:** Same as in Fig. 31a except for 21/05.

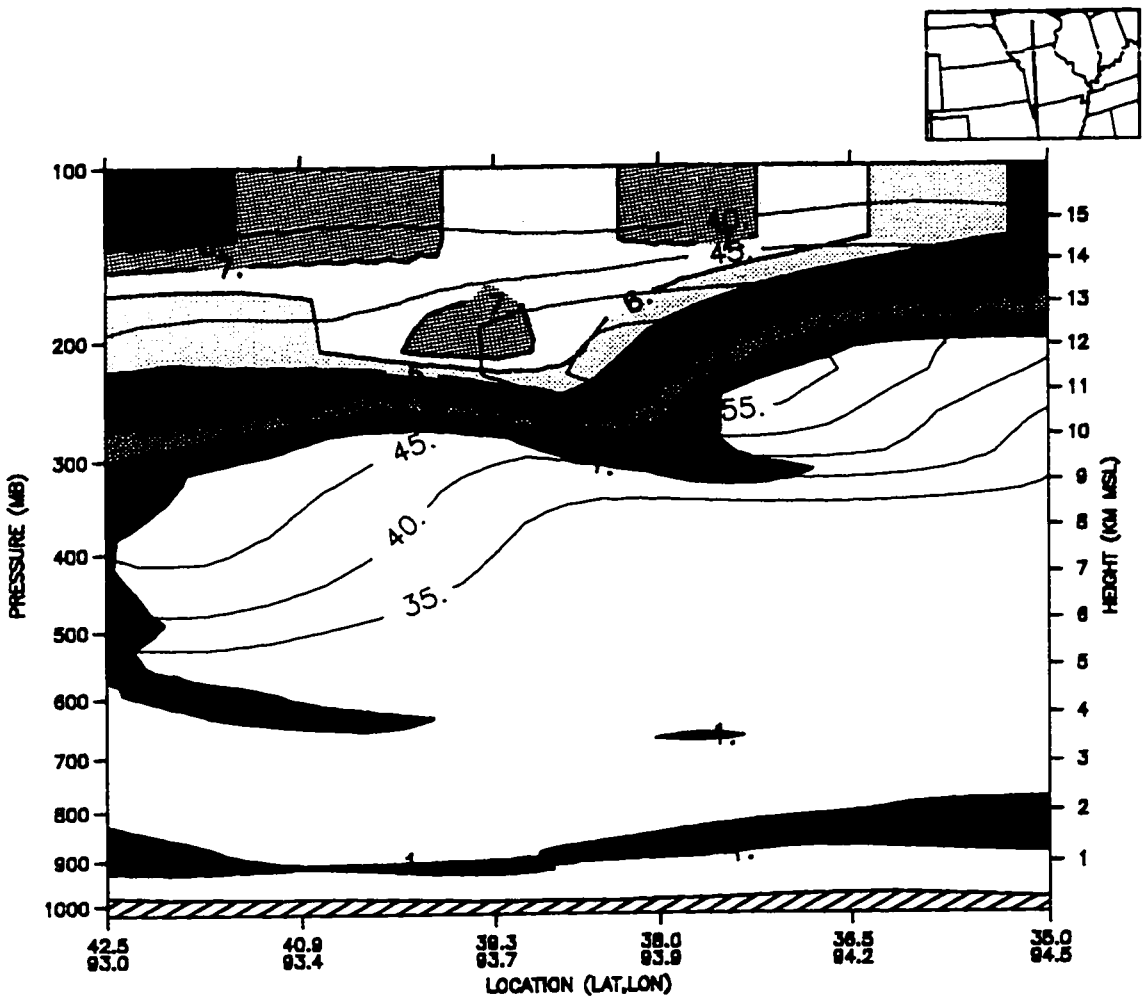


**Fig. 31 (cont.) d:** Same as in Fig. 31a except for 00/06.

solidifies and substantiates previous research by Sassen *et al.*(1995), and demonstrates a diagnostic approach that could be used to study other fold events in order to further understand the dynamics associated with tropopause folds.

## 4.5 Tropopause Fold Case Study 06/03

Recall from the synoptic overview discussed previously, a large trough/ridge disturbance existed over the central U.S. at 00/03, as shown in Fig. 1a. Eastern Texas is located in the center of a jet entrance region at this time. This region is similar to the jet entrance region over COF at 00/06 (Fig. 1d), and can be used to see how the dynamics associated with large baroclinic waves compare with smaller ones. A MAPS analysis at 06/03 is used to perform the comparison between the two fold events since an MM4 simulation was not run. This comparison helps to quantify the importance of weak tropopause folds.

Figure 32 shows a 70 m $s^{-1}$ jet streak extending from a SW-NE path through eastern TX at 06/03. This jet streak is nearly 20 m $s^{-1}$ greater than in the weak tropopause fold case study over KS. Figure 33 shows vertical velocity and winds in a cross section across the jet streak at 06/03. Downward vertical velocities beneath the cyclonic side of the jet are very similar in magnitude, but cover a broader area compared to those shown in Fig. 27 for the weak tropopause fold case study. In contrast, downward vertical velocities above the cyclonic side of the jet are approximately 6 cm $s^{-1}$ greater than in the previous

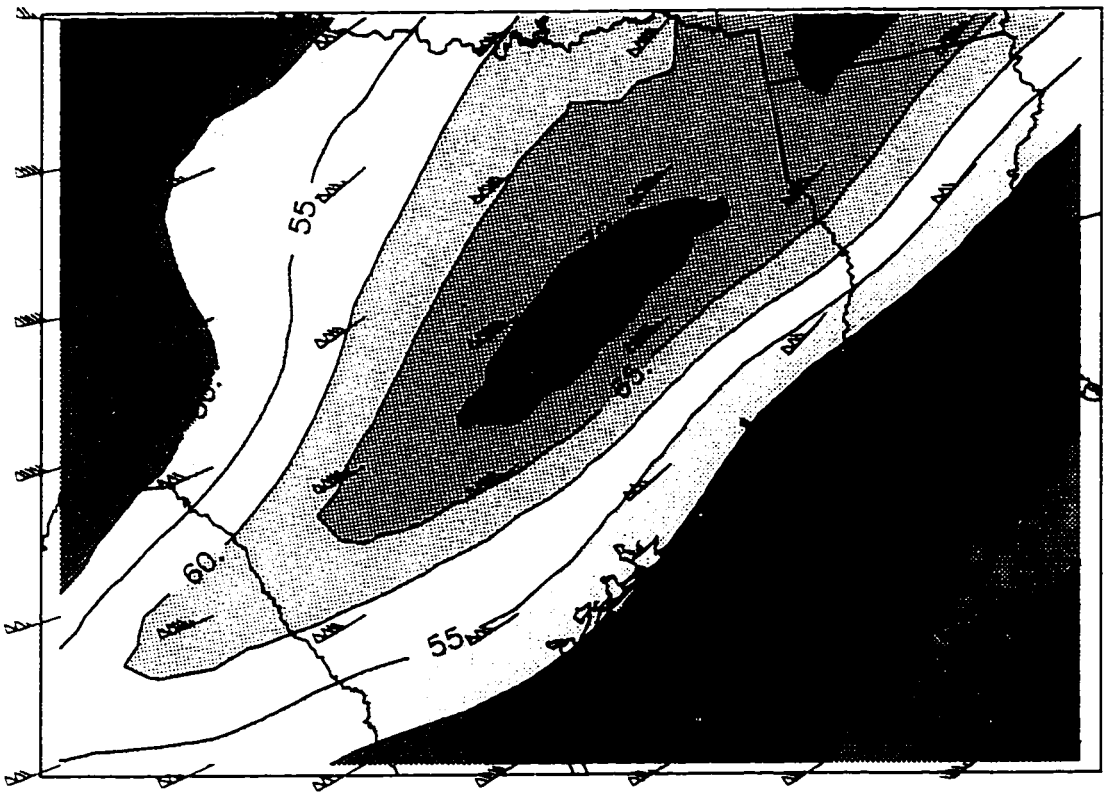


**Fig. 32:** 250-mb MAPS horizontal winds (m $s^{-1}$; black lines separated by shaded areas, kts; red wind barbs) at 06/03 over eastern Texas.

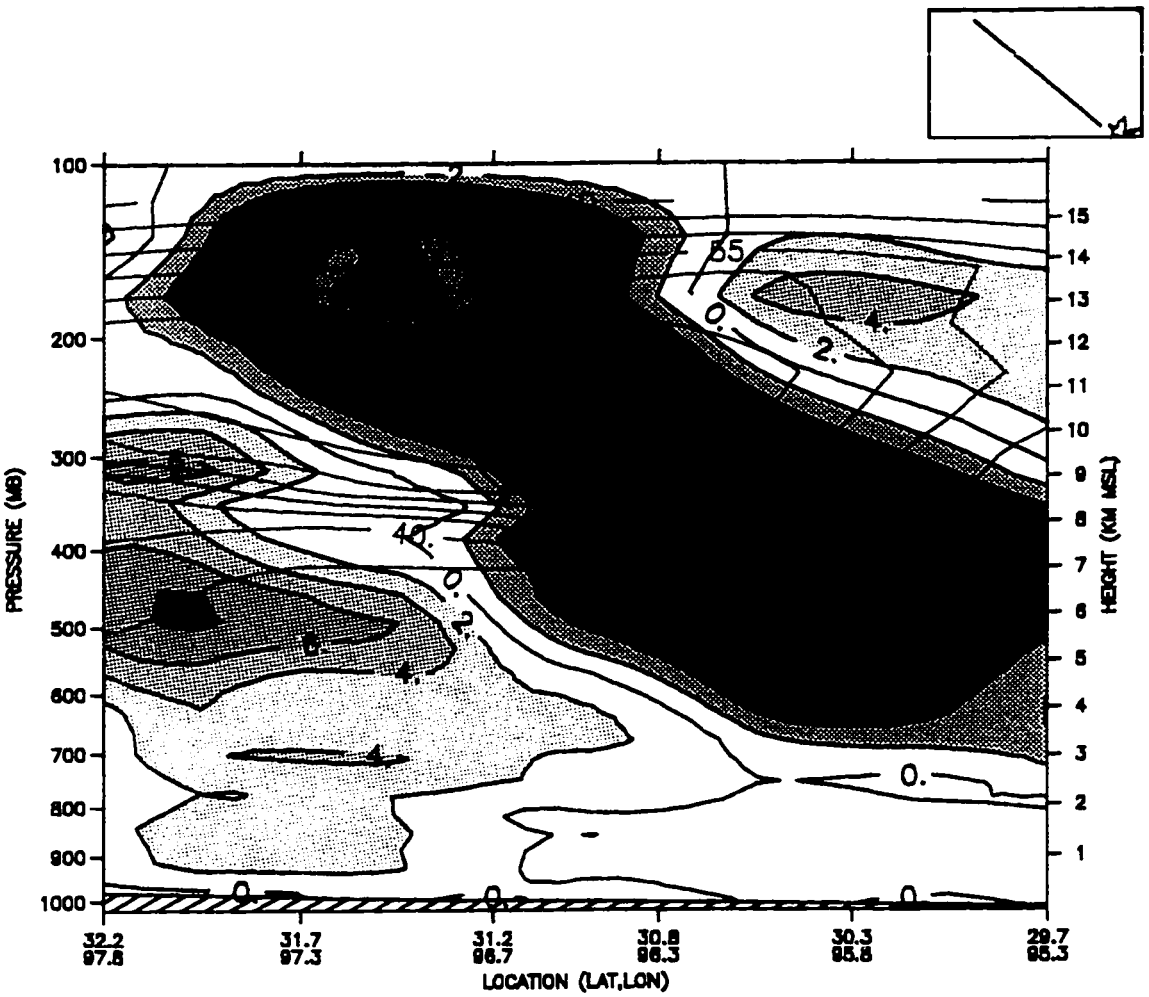


**Fig. 33:** WNW-ESE cross section of MAPS vertical velocity (cm $s^{-1}$; solid black lines separated by shaded areas) and horizontal winds (m $s^{-1}$; solid red lines) at 06/03 along the line in eastern Texas depicted in the upper right-hand map.

case study. This indicates that as the jet streak becomes stronger the dynamics associated with it become stronger as well. Figure 34 shows the instantaneous mass flux at 06/03. This is approximately 25% greater in magnitude (Table 3), compared to the weak tropopause fold case study at 18/05 shown in Fig. 30b. It appears that the stronger downward motion associated with a stronger jet streak leads to stronger cross-tropopause mass flux at an instant in time. Finally, Fig. 35 shows the potential vorticity extrusion around the jet streak at 06/03. This shows that the potential vorticity signature is nearly 3 km deeper at 06/03 than with the weak tropopause fold case study shown in Fig. 31d. This difference is consistent with the stronger jet streak, vertical velocities, and mass exchange results.

Overall, the general patterns of sinking motion on the cyclonic side of the jet, ST mass exchange on the cyclonic side of the jet, and a potential vorticity signature wrapping underneath the cyclonic side of the jet streak, are found in both weak and strong tropopause fold case studies. As the diagnostics show, the dynamics are moderately stronger during the fold event on 06/03. This does not lessen the importance of weak tropopause fold events, and is included here as a comparison.

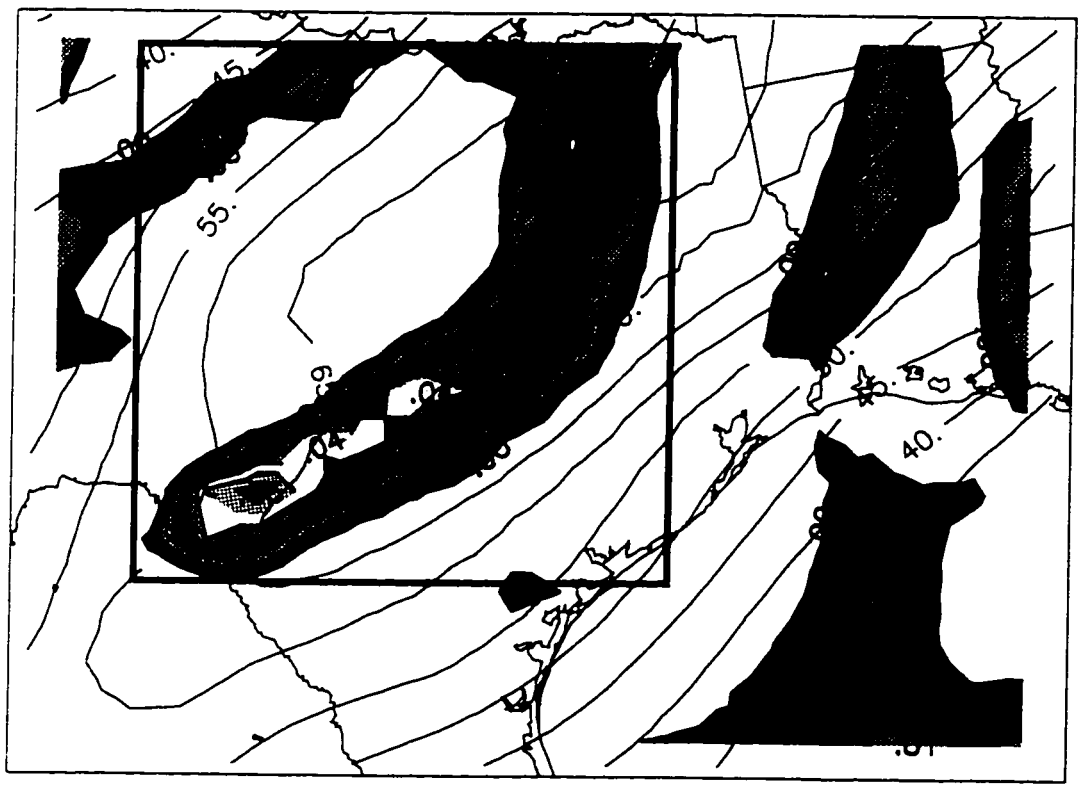


**Fig. 34:** MAPS positive ST mass flux (kg $m^{-2}$ $s^{-1}$; black lines separated by shaded areas) and horizontal winds (m $s^{-1}$; solid red lines) at 06/03 over eastern Texas. The thick black box represents the area of mass flux associated with the tropopause fold being studied.

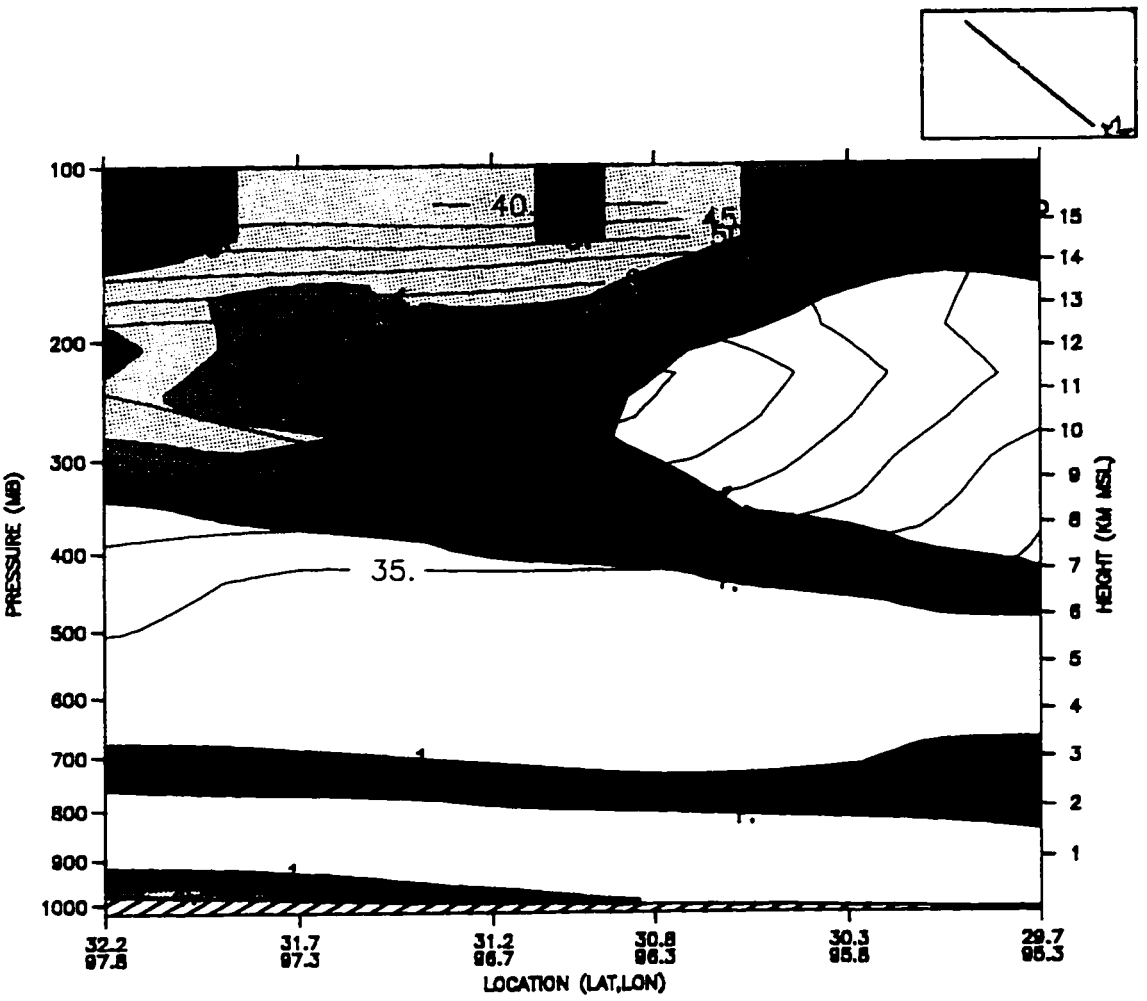


**Fig. 35:** WNW-ESE cross section of MAPS potential vorticity (PVU; solid black lines separated by shaded areas) and horizontal winds (m $s^{-1}$; solid red lines) at 06/03 along the line in eastern Texas depicted in the upper right-hand map.

# Chapter 5

# Conclusion

It has been shown that on 5 - 6 December 1991 a weak tropopause fold moved over the COF area and that sufficient mass exchange took place upstream of the event to support the claims of Sassen *et al.* (1995). Recall that they concluded that a tropopause fold existed near COF by interpreting ozone and radioactive samplings between 8.5 - 13 km. Given that they found high concentrations of ozone and radioactive elements (typically found in the stratosphere) deep into the troposphere, they concluded that some type of extrusion from the stratosphere to the troposphere must have taken place.

Our research has built upon the results of Sassen *et al.* (1995) by using a diagnostic approach to answer three specific questions: Where did the tropopause fold originate? What was the dynamical forcing that led to the fold? What was the magnitude

of the fold? A brief summary of the answers to these questions is now presented, followed by some final suggestions on future research on weak tropopause folds and their overall climatic effects.

In answering the first question, the back-trajectory analyses (Figs. 19, 16) have determined the origin of the air parcels that ended at COF at 250 mb and 400 mb, respectively. Cross sections along the air parcel trajectory path (Figs. 17a, 17b) indicated that air descended roughly 2.5 km from the northwestern U.S., approximately along isentropic surfaces until it reached COF at 21/05. The cirrus seen over COF at 21/05 advected WSW-ENE from the upper-level low over the Baja CA area. This air mixed with the air from the northwest U.S. and led to the unusual cirrus over COF during the case study period as defined by Sassen *et al.* (1995).

In answering the second question, the passage of the 50 m $s^{-1}$ jet streak (Figs. 23a, 23b), in combination with the geostrophic and ageostrophic circulations around the jet streak, led to the fold. Various cross sections along and across the jet streak have shown that there was sufficient downward motion through time on the cyclonic side of the jet to cause stratospheric air to be extruded down into the troposphere. This finding was further supported by the divergence field of the geostrophic **Q**-vector which showed downward motion to the left of the jet entrance region (Figs. 26a, 26b). Additionally, the primary signature of a tropopause fold, a potential vorticity extrusion, was evident around the time

of the fold (Fig. 25b). Each one of these diagnostics alone would not necessarily support the claims of Sassen *et al.* (1995). However, in combination, they support the fact that a tropopause fold moved through the COF area on 5 - 6 December 1991.

In answering the third question, mass exchange calculations showed that the total ST mass exchange was $1.13 \times 10^{14}$ kg over the duration of this tropopause fold event. Extrapolating a Northern Hemispheric annual ST mass exchange based upon this result showed that our estimates compared favorably to other recent studies (Table 4). This result was significant because these other studies were based upon stronger tropopause fold events than the one presented in this thesis.

Several uncertainties exist with the results given in this thesis. First, we looked at essentially one case study. Additional case studies would likely lead to a better understanding of weak tropopause fold events. Second, the annual number of weak tropopause folds was estimated, based upon an estimate of large baroclinic disturbances. More knowledge surrounding the number of weak tropopause folds would lead to more accurate results. Third, we looked at purely ST mass exchange, and did not address the reverse process, troposphere-to-stratosphere mass exchange. Some research has shown that over time, up to 50% of ST mass exchange ends up back in the stratosphere.

There are several areas where this research could be improved with future work. Most of the improvements could be made with better initial data, finer MM4 model resolution, or more sophisticated and theoretical mathematical formulations. During the analysis of the MAPS data we found that the UTH pattern was poorly resolved when compared with the GOES UTH data (Soden, 1991). Better resolved MAPS and MM4 simulated UTH data would facilitate both the analysis and comparison of the formation and enhancement of cirrus with the research done by Sassen *et al.* (1995). A finer resolution MM4 model would improve the path of the trajectory analysis, as well as resolving features associated with the fold process, i.e. especially analyzing jet streak dynamics near the top of the model. Additionally, a purely isentropic model would facilitate better resolution of upper-level advective features such as mass exchange and potential vorticity extrusions. Usage of the Sawyer-Eliassen approach to diagnose the ageostrophic forcing terms associated with confluence and shear around the jet would provide greater insight into the tropospheric fold process. These are just a few of the improvements or differences that could be made to enhance future work in diagnosing and interpreting dynamics related to tropopause folds.

This research has proven that the fold that Sassen *et al.* (1995) believed took place near the COF area, did indeed occur. This diagnostic case study can be used as the basis for future numerical modeling of fold events that impact cirrus clouds and other microphysical cloud processes.

I leave you with a quote that I found during my journey that best describes this thesis, and I think meteorology as a science, by Peter Chaston (1994), a National Weather Service meteorologist: *"Meteorology is the study of the redistribution of air"*.

# References


Ancellet, G., J. Pelon, M. Beekmann, A. Papayannis, and G. Megie, 1991: Ground-based lidar studies of ozone exchanges between the stratosphere and the troposphere. *J. Geophys. Res.*, **96**, 22401-22421.

Andrews, D. G., J. R. Holton, and C. B. Leovy, 1987: *Middle Atmospheric Dynamics*. Academic Press, 489 pp.

Anthes, R. A., E.-Y. Hsie, and Y.-H. Kuo, 1987: Description of the Penn State/NCAR Mesoscale Model Version 4 (MM4). NCAR Technical Note, NCAR/-TN-282+STR, National Center for Atmospheric Research, P.O. Box 3000, Boulder, CO 80307.

Barnes, S. L., and B. R. Colman, 1993: Quasigeostrophic diagnosis of cyclogenesis associated with a cutoff extratropical cyclone - The Christmas 1987 storm. *Mon. Wea. Rev.*, **121**, 1613-1634.

Benjamin, S. G., 1989: An isentropic mesoα-scale analysis system and its sensitivity to aircraft and surface observations. *Mon. Wea. Rev.*, **117**, 1586-1603.

Benjamin, S. G., K. A. Brewster, R. Brummer, B. Jewett, T. W. Schalatter, T. L. Smith, and P. A. Stamus, 1991: An isentropic three-hourly data assimilation system using ACARS aircraft observations. *Mon. Wea. Rev.*, **119**, 888-906.

Bluestein, H.B., 1986: Fronts and jet streaks: A theoretical perspective. *Mesoscale Meteorology and Forecasting*, P. S. Ray, Ed., Amer. Meteor. Soc., 173-215.

Chaston, P., 1994: Graphical Guidance. 9th ed. National Weather Service Training Center, Kansas City, MO.

Danielsen, E. F., 1959: The laminar structure of the atmosphere and its relation to the concept of a tropopause. *Arch. Meteor. Geophys. Bioklim.*, **A11**, 293-332.

____, 1964: Project Springfield Rep., Washington, D. C., Defense Atomic Support Agency Rep., DASA 1517, 97 pp.

____, 1968: Stratospheric-tropospheric exchange based on radioactivity, ozone, and potential vorticity. *J. Atmos. Sci.*, **25**, 502-518.

____, and V. A. Mohnen, 1977: Project Duststorm report: Ozone transport, in situ measurements, and meteorological analyses of tropopause folding. *J. Geophys. Res.*, **82**, 5867-5877.

____, and R. S. Hipskind, 1980: Stratospheric-tropospheric exchange at polar latitudes in summer. *J. Geophys. Res.*, **85**, 393-400.

____, R. S. Hipskind, S. E. Gaines, G. W. Sasche, G. L. Gregory, and G. F. Hill, 1987: Three-dimensional analysis of potential vorticity associated with tropopause folds and observed variations of ozone and carbon monoxide. *J. Geophys. Res.*, **92**, 2103-2111.

Ebel, A., H. Hass, H. J. Jakobs, M. Laure, M. Memmesheimer, A. Oberreuter, H. Geiss, and Y.-H. Kuo, 1991: Simulation of ozone intrusion caused by a tropopause fold and cut-off low. *Atmos. Environ.*, **25A**, 2131-2144.

Follows, M. J., 1992: On the cross-tropopause exchange of air. *J. Atmos. Sci.*, **49**, 879-882.

Hoerling, M. P., T. K. Schaack, A. J. Lenzen, 1993: A Global Analysis of Stratospheric-tropospheric exchange during northern winter. *Mon. Wea. Rev.*, **121**, 162-172.

Holton, J. R., 1990: On the global exchange of mass between the stratosphere and the troposphere. *J. Atmos. Sci.*, **47**, 392-395.

____, 1992: *An Introduction to Dynamic Meteorology*. 3d ed. Int. Geophys. Ser., Vol. 48.

Hoskins, B. J., M. E. McIntyre, and A. W. Robertson, 1985: On the use and significance of isentropic potential vorticity maps. *Quart. J. Roy. Meteor. Soc.*, **111**, 877-946.

Keyser, D. and M. J. Pecnick, 1985: Diagnosis of ageostrophic circulations in a two-dimensional primitive equation model of frontogenesis. *J. Atmos. Sci.*, **42**, 1283-1305.

Keyser, D., and M. A. Shapiro, 1986: A review of the structure and dynamics of upper-level frontal zones. *Mon. Wea. Rev.*, **114**, 452-499.

Lester, P. F., 1993: *Turbulence - A New Perspective for Pilots.* 1st ed. Jeppesen Sanderson, Inc., pp. 7-5.

Mace, G. G., D. O'C Starr, T. P. Ackerman, P. Minnis, 1995: Examination of coupling between an upper-tropospheric cloud system and synoptic-scale dynamics diagnosed from wind profiler and radiosonde data. *J. Atmos. Sci.*, **52**, 4094-4127.

Mattocks, C. and R. Bleck, 1986: Jet streak dynamics and geostrophic adjustment processes during the initial stages of lee cyclogenesis. *Mon. Wea. Rev.*, **114**, 2033-2056.

Oort, A. H., 1983: *Global Atmospheric Circulation Statistics*. U.S. Dept. of Commerce, National Oceanic and Atmospheric Administration.

Reed, R. J., 1955: A study of a characteristic type of upper-level frontogenesis. *J. Meteor.*, **12**, 226-237.

____, and E. F. Danielsen, 1959: Fronts in the vicinity of the tropopause. *Arch. Meteor. Geophys. Bioklim.*, **A11**, 1-17.

Reiter, E. R., and J. D. Mahlman, 1965: Heavy radioactive fallout over the southern United States, November 1962. *J. Geophys. Res.*, **70**(18), 4501-4520.

Reiter, E. R., 1975: Stratospheric-tropospheric exchange processes. *Rev. Geophys. Space Phys.*, **13**, 459-474.

Riegel, C. A., 1992: *Fundamentals of Atmospheric Dynamics and Thermodynamics*. 1st ed. Editor, A. F. C. Bridger. Publisher, World Scientific Pub. Co. Pte. Ltd., pp. 180.

Rosenlof, K. H. and J. R. Holton, 1993: Estimates of the stratospheric residual circulation using the downward control principle. *J. Geophys. Res.*, **98**, 10,465-10,479.

Rossby, C.-G., 1937: On the mutual adjustment of pressure and velocity distributions in certain simple current systems, 1. *J. Mar. Res.*, **1**, 15-28.

Sassen, K., D. O'C. Starr, G. Mace, M. Poellot, S. H. Melfi, W. L. Eberhard, J. D. Spinhirne, E. W. Eloranta, D. E. Hagen, and J. Hallett, 1995: The 5-6 December 1991 FIRE IFO II jet stream cirrus case study: Possible influences of volcanic aerosols. *J. Atmos. Sci.*, **52**, 97-123.

Shapiro, M. A. and P. J. Kennedy, 1981: Research aircraft measurements of jet stream geostrophic and ageostrophic winds. *J. Atmos. Sci.*, **38**, 2642-2652.

Soden, B. J., 1991: Upper tropospheric humidity graphical data supplied on-line.

Vaughan, G., J. D. Price, A. Howells, 1994: Transport into the troposphere in a tropopause fold. *Quart. J. Roy. Meteor. Soc.*, **120**, 1085-1103.

Wei, M., 1987: A new formulation of the exchange of mass and trace constituents between the stratosphere and troposphere. *J. Atmos. Sci.*, **44**, 3079-3086.

Wirth, V., 1995: Comments on "A new formulation of the exchange of mass and trace constituents between stratosphere and troposphere". *J. Atmos. Sci.*, **52**, 2491-2493.

# Appendix A

# Symbols

| | |
|---|---|
| $a$ | Area |
| $f$ | Coriolis force |
| $g$ | Gravitational constant |
| $\tilde{k}$ | Unit vector in the z-direction |
| $p$ | Atmospheric pressure |
| $p_s$ | Surface pressure |
| $p_t$ | Atmospheric pressure at the model top |
| $p_*$ | Surface pressure minus atmospheric pressure at the model top |

$t$ Time

$x$ x-coordinate (increases eastward)

$y$ y-coordinate (increases northward)

$z$ z-coordinate (increases upward)

$A$ Area

$F(\rho)$ Mass flux

$J_\theta$ Magnitude of the partial change in height with respect to potential temperature

$P_\theta$ Potential vorticity in isentropic coordinates

$\tilde{Q}$ **Q**-vector

$\tilde{Q}_1$ i-component of the Q-vector

$\tilde{Q}_2$ j-component of the Q-vector

$R$ Gas constant for dry air

$T$ Temperature

$T_L$ Duration of time for tropopause fold event

$TME$ Total mass exchange

$\tilde{U}_\sigma$ Horizontal wind vector on a sigma surface

$\tilde{U}_\theta$ Horizontal wind vector on an isentropic surface

$\tilde{V}_{ag}$ Ageostrophic wind vector

$\tilde{V}_g$ Geostrophic wind vector

$\tilde{V}_H$ Horizontal wind vector

$\tilde{V}_T$ Thermal wind vector

$Z_0$ Critical stability threshold

$\theta$ Potential temperature

$\theta_B$ Isentropic coordinate tropopause boundary

$\rho$ Density

$\sigma$ Vertical coordinate in sigma coordinate system

$\dot{\sigma}$ Vertical velocity in sigma coordinates

$\sigma_B$ Sigma coordinate tropopause boundary

$\omega$ Vertical velocity in isobaric coordinates

$\zeta_\theta$ Relative vorticity on isentropic coordinates

$\nabla$ Del-operator in a horizontal plane